ADDITIVE MANUFACTURING WITH CARBON NANOTUBE ENRICHED ACRYLONITRILE BUTADIENE STYRENE

By

DOMINIC THALER

A thesis submitted in partial fulfillment of
the requirements for the degree of

MASTER OF SCIENCE IN MECHANICAL ENGINEERING

WASHINGTON STATE UNIVERSITY
School of Engineering and Applied Sciences

MAY 2018

To the Faculty of Washington State University:

The members of the Committee appointed to examine the thesis of DOMINIC THALER find it satisfactory and recommend that it be accepted.

_____

Amir Ameli, Ph.D., Chair

_____

Christof Brändli, Ph.D., Co-Chair

_____

Joseph Iannelli, Ph.D.

_____

Mohammed Noor-A-Alam, Ph.D.

_____

Marcello Righi, Ph.D.

ACKNOWLEDGMENTS

I would like to thank my advisor, Dr. Amir Ameli, for his support, advice, and sharing of his expertise throughout this thesis. Many thanks also to my fellow lab-mates Nahal Aliheidari, Ahmed Saib Naji, and Cameron Hohimer for their assistance. I would like to acknowledge my committee members from Washington State University Tri-Cities in the US, Dr. Joseph Iannelli and Dr. Mohammed Noor-A-Alam, and the committee members from Zurich University of Applied Sciences in Switzerland, Dr. Christof Brändli and Dr. Marcello Righi. Special thanks go to Dr. Joseph Iannelli for supporting me during this year abroad and arranging everything needed as first student of the international double master's degree program.

ADDITIVE MANUFACTURING WITH CARBON NANOTUBE ENRICHED ACRYLONITRILE BUTADIENE STYRENE

Abstract

by Dominic Thaler, M.S.
Washington State University
May 2018

Chair: Amir Ameli

Additive manufacturing, also known as 3D printing is an emerging method to produce customized parts with functional materials without big investments. Fused filament fabrication (FFF) uses thermoplastic-based feedstock and has recently been adapted to fabricate composite materials. Acrylonitrile butadiene styrene (ABS) is a very common engineering plastic which is commonly used as FFF feedstock. Carbon nanotubes (CNT) are attractive fillers because of their high aspect ratio, high conductivity and excellent mechanical and physical properties. Therefore, a nanocomposite of these two materials can potentially be electrically conductive with enhanced mechanical properties that is compatible with FFF printing.

This work focuses on the investigation of the relationships between the FFF process, CNT concentration and the electrical, tensile, piezoresistive, and fracture properties of the printed ABS/CNT nanocomposites.

Nanocomposite filament with CNT concentrations up to 10 wt% were produced for the FFF process using a twin-screw extruder. The feedstock was pellets from a masterbatch containing 15 wt% multi-walled CNT. For the electrical conductivity tests, the effects of the FFF process parameters such as layer orientation, layer thickness, and nozzle size were analyzed. The tensile properties were analyzed together with the piezoresistivity for different CNT concentrations by measuring the resistance while straining the printed tensile specimen. Compression-molded samples were also prepared as the bulk baselines for electrical and tensile tests. With the fracture tests, the influence of CNT on the layer-to-layer bonding strength in the printed parts were quantified.

At the proper amount and dispersion of CNT, ABS becomes an electrically conductive nanocomposite. The results showed that the CNT orientation during FFF process produces different in-layer and through-layer conductivity. ABS/CNT shows piezoresistivity and higher sensitivity with lower CNT concentrations. With 5 wt% CNT, the Gauge factor is about 5. The stiffness of 3D printed ABS could be enhanced by 100% with 3 wt% CNT but dropped with higher CNT percentages. Up to 5 wt% CNT, the increase in strength is about 25%. The fracture toughness of nanocomposites up to 3 wt% CNT is slightly higher than pure ABS and decreases after 5 wt% CNT.

TABLE OF CONTENTS

Page

LIST OF TABLES

Page

LIST OF FIGURES

Page

1. INTRODUCTION AND LITERATURE REVIEW

Additive manufacturing (AM) is an emerging manufacturing method, which has a huge potential in many areas. Compared to conventional fabrication techniques, it allows to produce more complex parts, but also functional components. Acrylonitrile-butadiene-styrene (ABS) is a widely used engineering plastic for fused filament fabrication AM process. In this thesis, it will be analyzed how the properties change when ABS is enriched with multiwalled carbon nanotubes (CNT) and what effects the 3D printing process and CNT content have on the electrical, mechanical and electromechanical properties.

1.1. Polymer nanocomposite production

Carbon Nanotubes

There are two main types of CNT. Single-walled carbon nanotubes (SWCNT) and multi-walled carbon nanotubes (MWCNT). The nanotubes are rolled sheets of graphene. SWCNT has only one tube with a diameter of about 1nm and lengths up to centimeters and the MWCNT has several tubes within each other and can have diameters up to 100nm and lengths of tens of microns. CNT are most commonly produced with chemical vapor deposition. This is not the best method as the nanotubes have many defects, but it is the cheapest way to produce large quantities. The mechanical properties of CNT are outstanding. The Young's modulus is close to 1TPa. This makes them very interesting to use for composites [1] [2]. CNT has also very interesting electrical properties. The electrical resistance is very low because of their one-dimensional shape. Electrons are not easily scattered because of the huge aspect ratio. Prior to CNT, diamond was the best thermal conductor, now it is CNT which has a thermal conductivity that is twice as that of diamond [3].

Acrylonitrile-Butadiene-Styrene (ABS)

ABS is a very commonly used engineering thermoplastic. It is tough, has good impact resistance, dimensional stability and it is resistant to many chemicals. It is a copolymer consisting of acrylonitrile, butadiene, and styrene. The nitrile groups bind neighboring molecular chains together which makes ABS stronger than pure polystyrene. The butadiene phase is rubbery and improves the toughness of ABS. ABS is used for many applications in different industries. Enhancing the properties of ABS to open new application fields is important for the competitiveness of ABS [4] [5]. Tiganis et al. investigated the thermal degradation of ABS [6].

Solution processing

In this method, the carbon nanotube powder and the polymer are mixed in a suitable solvent. With this technique, a very good dispersion can be achieved and it hinders forming of agglomerations. The agitation within the mixture can be provided by either magnetic stirring or ultrasonication. The choice of the solvent is based on the solubility of the polymer, but pristine CNT usually do not disperse very well in most solvents. To overcome this problem, surfactants can be used to disperse the CNTs before mixing them with the polymer solution [1].

Melt processing

Melt processing involves the heating of material and is limited to thermoplastic polymers, but can be used for polymers which are not soluble. Its advantages are simplicity, high speed and the fact that standard industrial techniques can be used. Polymer pellets are melted to form a viscous liquid to which CNT can be mixed. With shear mixing in the extruder, the CNTs can be dispersed and subsequently the composite is extruded or injected into a mold. The melt processing conditions need to be optimized for a given CNT-polymer composite. A better dispersion can be

achieved with higher mixing energy (increasing residence time / mixing speed) at the expense of nanotube breakage [1]. On the example of polylactic acid/multi-walled carbon nanotubes composite, intensive research was done on maximizing the dispersion of CNT with a twin-screw extruder [7].

Literature review of ABS/CNT

S. Kapoor et al. prepared ABS/MWCNT nanocomposites using solvent mixing technique with chloroform as the solvent. The ABS polymer and the CNT were separately dispersed in the solvent followed by magnetic stirring for 2-3 hours and sonication for 2-3 hours. Both solutions were mixed together and stirred again and sonicated for another 2-3 hours. The nanocomposite solution was then poured into petri dishes. After 24 hours, they were dried in a vacuum oven at around 70°C for 3-4 hours. The thin films were then fabricated using compression molding. The dispersion was analyzed using a Field Emission Scanning Electron Microscope [8].

Table 1.1: Distribution of CNT in polymer matrix [8]

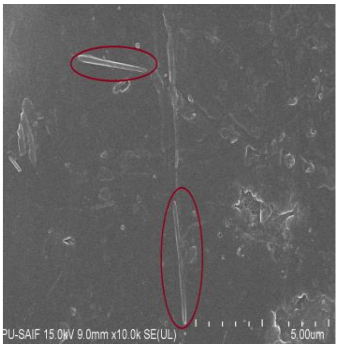

1 wt% CNT

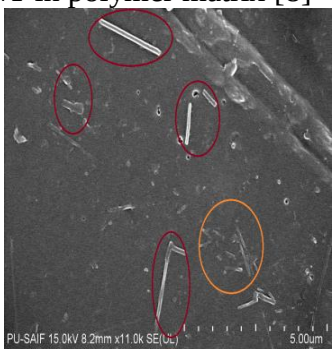

5 wt% CNT

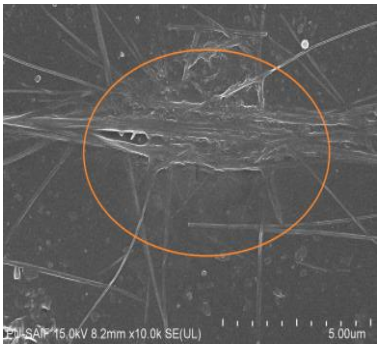

10 wt% CNT

The images in Table 1.1 compare the distribution of CNT within ABS at three different CNT percentages. The red encircled regions show stand-alone CNTs and the orange circles denote the

bundles of CNT. The conclusion was that the dispersion at lower CNT content is good, but at higher contents, the dispersion is not uniform and agglomerations form [8].

M. H. Al-Saleh et al. studied the dispersibility of CNT in four different solvents. Chloroform showed the best dispersion ability for CNT. The CNT suspension was ultrasonicated for 10 minutes and then added to the ABS solution and sonicated for another 10 minutes. After drying at room temperature and in the vacuum oven, rectangular samples were made with a hot press. With a Transmission Electron Microscope, the morphology of the nanocomposites was investigated, and no CNT aggregates could be observed. A very low electrical percolation threshold of 0.06 vol% CNT was obtained. The good dispersion of the CNT within the ABS polymer matrix can be attributed to the low viscosity environment, the proper solvent, and the good compatibility with the SAN phase of the polymer matrix [9].

Melt mixing of ABS/CNT has also been reported in the literature. P. Jindal et al. prepared ABS/CNT composite by melt mixing using a co-rotating twin-screw extruder with back flow channel followed by micro injection molding. Because of the back-flow channel and the optimized mixing of 3 minutes at 265°C and 100 rpm, the CNT could be dispersed uniformly in the polymer [10].

M. H. Al-Saleh et al. also used a small batch mixer to prepare ABS/CNT nanocomposites by melt mixing. The polymer was melted at 220 °C and 100 rpm for 3 minutes before the CNT were added. The compounding of the nanofiller/polymer was done for 10 minutes. The mixed nanocomposite was then fed to a compression molding machine to produce tensile test specimen. The microstructure of the fractured surface was investigated with a Scanning Electron Microscope. When analyzing the ABS, they differentiate the rubbery poly-butadiene particles (PB) which are dispersed in a styrene-acrylonitrile (SAN) matrix. They reported that the CNT particles are

localized within the SAN phase. As the PB phase is cross-linked, the nanotubes cannot penetrate into this phase easily. They reported good dispersion results for CNT contents up to 10 wt% [5].

Table 1.2: CNT dispersion in ABS matrix [5]

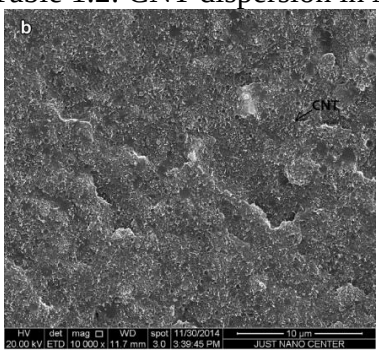

5 wt% CNT, low magnific.

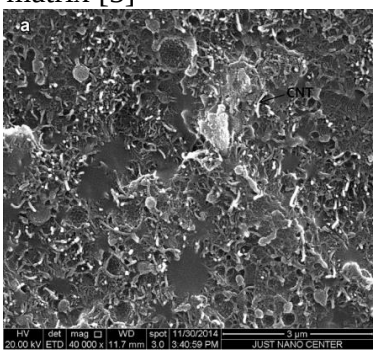

5 wt% CNT, medium magnific.

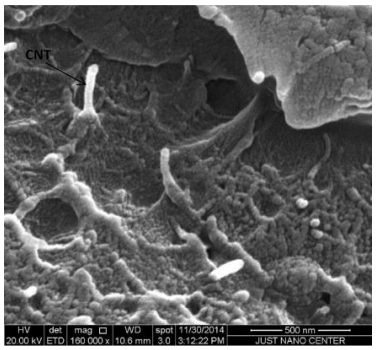

5 wt% CNT, high magnific.

The images of Table 1.2 show that the CNTs are well embedded within the SAN matrix. The CNT diameters visible here are higher than those of the pristine ones because they are wrapped with layers of SAN. Due to this wrapping, the adhesion is good between the CNTs and the matrix and thus the mechanical properties of ABS can be significantly increased with the implementation of CNT (increase in the tensile strength and Young's modulus of 72% and 107%, respectively with 10 wt% CNT) [5].

A. Dorigato et al. used a masterbatch of ABS with 15 wt% CNT and mixed it with pure ABS by melt compounding (190 °C, 15 min, 90 rpm). Thin sheets of composite samples were then produced with compression molding. Some of them were mechanically grinded to feed a twin-screw extruder to produce filament, which can be used for FFF 3D printing. They reported a good dispersion and selective localization of CNT in the SAN phase. A percolation threshold of only 0.6 wt% was achieved [11].

A good dispersion of CNT can be achieved with both methods, solution processing and melt processing. Chloroform is a very good solvent for ABS and CNT system. It appears that

ultrasonication gives better dispersions than magnetic stirring. When preparing the nanocomposite with melt mixing, long mixing times and therefore higher mixing energy can lead to good results. However, this method seems to reduce the average nanotube length more significantly.

Jyoti et al. studied the rheology of multiwall carbon nanotube-reinforced ABS composite. They described the increase in the dynamic moduli, viscosity and shear stress with the addition of MWCNT in ABS in a systematic way [12]. A mechanical spectroscopy analysis to investigate the glass transition temperature of ABS/CNT was also done by D. Mari and R. Schaller [13].

Another way to fabricate ABS/CNT nanocomposite is in situ polymerization. A very good dispersion of CNT can be achieved with in situ co-polymerization. Shrivastava et al. achieved a percolation threshold of only 0.2 vol% CNT with this method [14].

1.2. Additive Manufacturing

Additive Manufacturing is a generative production method. With this method, it is possible to directly manufacture physical effigy out of a 3D-CAD model. Solid models created in CAD first need to be stored as STL (surface tessellation language) files. The surface of the model is divided into numerous triangular facets. The smaller the size of the facets, the closer is the convergence to the model with an expense of the file size. In the next step, the model is cut in slices. This procedure is called slicing and appropriate software is needed for this process. It is then defined how every single layer is built. This information is saved in the G-Code. After transmitting the code to the machine, the part is created layer by layer. Different machines and processes are used to 3D print parts. Some well-known manufacturing methods are stereolithography, selective laser melting, material jetting, and fused filament fabrication (FFF). FFF is also known as fused deposition modeling (FDM™, trademark from Stratysys Inc.) and it is probably the most common 3D printing method. FFF will be used in this thesis.

Fused filament fabrication

FFF is a type of additive manufacturing where thermoplastics are melted and applied layer by layer. The structure of an FFF printer is shown in Figure 1.1. The base material is usually a polymer filament. FFF Filaments are commercially available with a diameter of 2.85 mm or 1.75 mm. It is wound on a spool and is fed into a heated nozzle section at the printing head. The nozzle is heated and a polymer strand is extruded. The nozzle diameter of the extruder varies typically between 0.35 mm to 0.8 mm, but they can also be smaller or bigger. The part is built on a heated platform. The heating is required for a proper adhesion of the part to the build platform, but also to prevent excessive cooling and shrinking of the part. Because of the residual thermal

stresses, sometimes the ends of a printed part dissociate from the build platform and the part bends upward, which is called warpage. This problem can be mitigated with a heated printing chamber. A recent work has dealt with the modeling of the warpage during fused filament fabrication [15]. For better adhesion of the deposited material to the platform, Kapton tape and/or hairspray can be applied on the platform surface. A disadvantage of FFF process is the anisotropy of the printed parts. Because the lines of the extruded material are deposited in the horizontal plane, strength is usually lower in the vertical direction. The adhesion of the layers is obtained by the passive fusion of extruded lines.

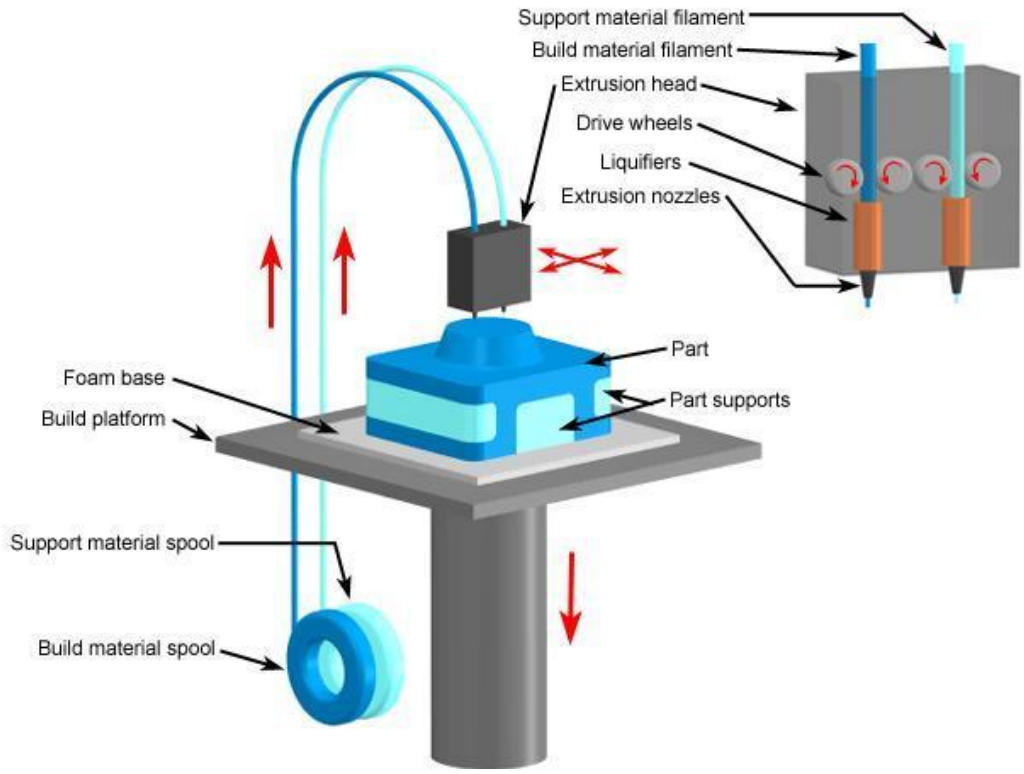

Figure 1.1: Structure of an FFF printer [16]

FFF with ABS/CNT

FFF printers use thermoplastic filament as feedstock. The processing of the material is simply extrusion through a small nozzle located on the printing head. Because of the simplicity and the few requirements of the filament, the feedstock can be any material that exhibits proper viscoelastic properties at high temperatures, including composites. Commercially available filament composites include carbon fibers, and wood and metal particles. In this thesis, carbon nanotubes are chosen as the fillers. Many researchers have used polymer-carbon nanotube composites as feedstock for FFF printers [11] [17] [18] [19] [20].

Zhang et al. found out that a faster printing speed leads to larger porosity and higher residual stresses and shrinkage after thermal treatment of the specimen (heating for 1 h at 180°C). Raster angle has shown even bigger influence on specimen shrinkage and porosity. ABS/CNT printed parts had much less shrinkage compared to pure ABS but the voids were a little bigger [21].

FFF printing process has also been used with graphite-reinforced, carbon fiber-reinforced [22], and graphene-reinforced ABS [23].

1.3. Electrical conductivity of ABS/CNT

ABS is an electrically insulating polymer. On the other hand, Carbon nanotubes are very conductive. They are attractive fillers because of the high aspect ratio, and their 1D structure with low electron scattering. They have an electrical resistivity of only 10^{-4} Ω.cm. A proper compound of these two materials gives a nanocomposite with a wide range of conductivity. The conductivity depends on the amount of dispersed CNT and their orientation. Once a network of inter-connected CNTs is formed, the nanocomposite becomes conductive. This point is called the percolation threshold.

Al-Saleh et al. investigated the conductivity and EMI shielding properties of ABS/CNT. They prepared the ABS/CNT samples with melt mixing and subsequent compression molding. They achieved a percolation threshold of around 0.75 wt% CNT. Table 1.3 lists the conductivity values for the composites having various CNT contents [24].

Table 1.3: Conductivity results of melt processed ABS/CNT from Al-Saleh et al. [24]

Wt% CNT	0.75	1	1.5	2	3	5	10	15
σ [S/cm]	$4\cdot10^{-7}$	$1\cdot10^{-2}$	$6\cdot10^{-2}$	$1.3\cdot10^{-1}$	$4\cdot10^{-1}$	$1.2\cdot10^{0}$	$2.5\cdot10^{0}$	$5.2\cdot10^{0}$

Al-Saleh et al. also studied the impedance characteristics of ABS/CNT in the frequency range of 10^0 Hz - 10^6 Hz. The samples were prepared by solution processing for their study. For up to 4 wt% CNT, the nanocomposites showed a frequency independent plateau of conductivity at lower frequencies which is indicating a segregated network of CNT. At higher frequencies, the conductivity increases due to tunneling in addition to the conductive network. With more than 7 wt% CNT, the nanocomposites are totally frequency independent [25].

Wen-yi Wang et al. studied the electrical and thermal properties of ABS/CNT. They used solution blending and achieved an electrical percolation threshold of 1-2 wt% CNT [26].

In another work, Al-Saleh et al. studied the AC and DC conductivity of ABS filled with different carbon fillers (MWCNT, carbon nanofibers, and high structure carbon black nanoparticles). The nanocomposites were produced with solution processing and the samples produced with compression molding. They achieved an electrical percolation of 0.5 wt% CNT. They showed that only for samples with a DC conductivity below 1 S/m, the AC conductivity is remarkably higher than the DC conductivity. Table 1.4 summarizes the AC conductivity of ABS/CNT deduced from a graph of [27].

Table 1.4: AC conductivity results of solution processed ABS/CNT from Al-Saleh et al. [27]

Wt% CNT	0.5	1	2	3	5	10	15
σ_{AC} [S/cm]	$4 \cdot 10^{-2}$	$1.2 \cdot 10^{-1}$	$2.2 \cdot 10^{-1}$	$2.8 \cdot 10^{-1}$	$5 \cdot 10^{-1}$	$7 \cdot 10^{-1}$	$1.4 \cdot 10^{0}$

There are also some other works published about the electrical properties of ABS/CNT [9] [28] [29] [30] and a blend of ABS with PC, enriched with MWCNT [31]. Some paper have also focused on how the electrical properties can be improved with changes in the phase morphology, for example with segregated structures [32] [33].

Du et al. investigated the effect of alignment of 1D fillers with high aspect ratio on the conductivity in nanocomposites. There are two different percolation thresholds. With increasing the filler loading, the concentration percolation threshold can be achieved. If the fillers are very much aligned, the alignment percolation threshold can be achieved with increasing isotropy. At low filler contents, there are significant changes in conductivity with small variations of alignment. With higher loadings, the alignment percolation threshold shifts to more anisotropy, meaning that a material with high filler content is only not conductive if the fillers are all oriented in the same direction. By orienting the fillers a bit more randomly the alignment percolation threshold is reached. Near the concentration threshold, the best conductivity values are not obtained with

isotropy, but rather with slightly anisotropic material. The difference between highest conductivity in anisotropic conditions versus the isotropic conditions decreases with increasing filler content. All these findings from experiments could be proven with 2D Monte Carlo simulations [34].

Chang et al. studied the effect of uniaxial and biaxial strains on the fiber alignment and percolation threshold with 3D Monte Carlo simulations. Through controlled application of strain, an optimum percolation threshold may be achieved invariant to the aspect ratio of the fibers. This effect is stronger with lower concentrations of fibers. If the strains are too high (resulting in excessive alignment), the percolation threshold increases in all directions [35].

Electrical conductivity of FFF printed ABS/CNT

Few works have analyzed the electrical resistivity of FFF printed ABS/CNT parts. They observed changes in the resistance depending on the printing direction. Higher conductivity values are reported in the printing direction. Printed samples generally exhibit lower conductivity values than their bulk counterparts [11] [17].

1.4. Tensile testing of ABS/CNT

Tensile testing is a basic engineering and materials science test. For uniaxial tensile tests, a sample is clamped between two grips, which pull the sample vertically apart. The tension in the sample increases until it fails. Ultimate tensile strength, Young's modulus, and the elongation at break are the material properties that can be measured using a tensile test. With the stress-strain plots, also strain hardening and toughness characteristics can be analyzed.

Significant amount of research work is available in the literature about the mechanical properties of ABS/CNT nanocomposites. Riddick et al. studied the tensile properties of 3D printed ABS in depth. They printed tensile test samples with FFF method with different raster angles and studied the fracture surfaces [36]. Increasing strength and stiffness values with increasing CNT content have been reported. The range of CNT content in these publications varies, but in general, the ultimate tensile strength declines at high CNT contents around 10 wt% because of the formation of CNT agglomerations [5] [8] [11] [28] [37] [38] [39] [40]. Some authors report heavy embrittlement and a loss of ductility with increasing CNT content [11] [28]. One paper reports a drop in stiffness already at 0.5 vol% CNT [41]. Several papers mention that the CNT are located in the styrene-acrylonitrile (SAN) phase rather than in the polybutadiene phase. The adhesion of the CNT to the SAN phase is very good, which promises good mechanical properties of this nanocomposite [5] [41]. An increase in stiffness was also shown with atomic force microscopy method [42]. Using nano-indentation, an enhancement in the hardness and elastic modulus of ABS is reported once CNT is incorporated. Dynamic mechanical analysis up to 200 Hz have shown that the storage modulus can be increased by 50 % with 10 wt% CNT [10].

Jyoti et al. studied the reinforcement of ABS with double filler, graphene oxide and carbon nanotube. They observed better static and dynamic mechanical properties of graphene oxide-

carbon nanotube hybrid material compared to the ABS/CNT. Because of higher dispersion in the hybrid material, it overcomes the problem of CNT agglomeration [43].

Tensile testing of FFF printed ABS/CNT

In general, the FFF printing process introduces a loss of ductility. This is especially the case if the tension direction is normal to the printing direction. The best properties are obtained if the deposited filament lines are parallel to the applied load direction. In this case, the reinforcing effect of the CNT is maximized [11] [17] [18]. The printability of ABS can be increased at lower CNT concentrations due to the decreased warpage of the printed nanocomposites, but the printability decreases at high CNT concentrations due to the chance of extrusion nozzle clogging [19] [21]. Gardea et al. conducted a dynamic mechanical analysis of FFF printed ABS/CNT nanocomposite. They showed that CNTs have the potential to alter the energy dissipation mechanisms present in AM structures to control structural damping [20].

1.5. Piezoresistivity of polymer nanocomposites

Great interest has been generated in the last years for nanocomposite-based strain sensors. CNTs are interesting fillers because of their high electrical conductivity and their ability to form a conductive network within a polymer matrix at relatively low contents. CNT are also interesting because of their mechanical reinforcement effects. Polymer/CNT nanocomposites can be applied toward piezoresistive strain sensors, as well as electromagnetic interference shields and high dielectric charge storage materials. The size, shape, aspect ratio, and electrical conductivity of the filler particles have an influence on the sensor piezoresistivity. A change in resistance while straining a sample can be explained through different mechanisms; by variation of conductive networks through loss of contact among CNTs, through resistance change by electron tunneling when the distance between CNTs change, and by the piezoresistivity of the CNT themselves when they are deformed. The latest is expected to have a very small effect due to the very high stiffness of CNTs [44]. Under small strains, the tunneling effect between neighboring CNTs is considered to be the principal mechanism of strain sensing. The highest sensitivity can be achieved if the volume fraction of CNT is close to the percolation threshold [45]. CNT can be used for a wide range of nanoscale sensors and actuators [46]. It is noted that in the CNT nanocomposites, the sensing capability is integrated within the material itself (self-sensing) and no external sensors are needed e.g., for structural health monitoring.

Piezoresistivity of polymer/carbon nanotube composites has been the subject of intense research in recent years [47]. Some of the studied polymer matrices are epoxy [48], thermoplastic polyurethane (TPU) [49] [50], polycarbonate (PC) [51].

FFF printed strain sensors have also been reported using thermoplastic polyurethane (TPU) [52] [53] [54], polydimethylsiloxane (PDMS) [55], and other 3D printed sensors [56]. The reported

properties allow the use of these nanocomposites in a very wide field of applications. Structural health monitoring for example is an interesting application, which finds an increasing demand in the industry. With 3D printing, it is possible to work with multiple materials within the same structure. With this technique, parts can be built partially sensitive, have integrated conductive paths or can be heated locally by applying a current. With highly elastic polymers as matrix, it would be possible to measure strains for a wider range of displacement than with traditional metal-based sensors.

However, to the best of the authors' knowledge, no publications about the piezoresistivity of ABS/CNT nanocomposites, especially in the FFF printed form are available. One of the objectives of this work is to investigate the strain sensing capability of printed ABS/CNT nanocomposites.

1.6. Fracture behavior of polymers

Fracture toughness is a property, which describes the resistance of a material to crack growth during fracture. Pre-cracked samples are used to analyze the crack initiation and growth. If the yield area at the crack tip compared to the rest of the specimen cross section is small, linear-elastic fracture mechanics (LEFM) can be used for fracture analysis. If the yield area at the crack tip is large and a large portion of the cross section is plasticized, LEFM is not accurate and elastic-plastic fracture models (EPFM) must be used.

The mode I critical strain energy release rate, G_{Ic} and the critical stress intensity factor K_{Ic} are fracture resistance measures, which quantify the resistance of a cracked material to opening loads. To have a material characteristic independent of geometry, K_{Ic} is usually measured under plane strain condition.

There are three different fracture modes. Mode-I is the opening or tensile mode, mode-II is the sliding or shear mode, and mode-III is the tearing mode. The fracture mechanics concepts behind all three modes are essentially the same but the loading configurations are different, resulting in different fracture resistance values at different modes. The simplest and most widely reported type is mode-I [57].

Oskui et al. investigated the fracture toughness of pure ABS with a new loading device which allows to measure any combination of mode-I and mode-II. For mode-I, they reported an average fracture toughness value of K_{Ic} = 4.32 MPa $m^{1/2}$ [58].

Fracture behavior of polymer/CNT nanocomposites

The effect of CNT on the fracture toughness is reported for an epoxy nanocomposite. When untreated CNTs are used, a decrease in K_{Ic} values was discovered due to a bad dispersion and

agglomeration formation of CNTs. The dispersion of CNT and the K_{Ic} values were enhanced with silane functionalized CNTs until 0.5 wt% CNT. With higher CNT contents, the fracture toughness did not increase because agglomerations formed [59].

Zhao et al. and Liu et al. reported that CNT can increase the toughness of the polymer matrix only if they are oriented in a way to serve as a bridge at the crack mouth to suspend crack development [60] [61]. Gorga et al. showed an increase in the fracture toughness due to bridging effects of crazes and micro-cracks by drawing the nanocomposite to orient the CNT in a desired direction [62].

Grimmer et al. added CNT to the matrix of glass-fiber composites. They reported a significant increase of the inter-laminar fracture toughness. This improvement are explained through the effects of crack bridging, nanotube fracture, and nanotube pull-out [63].

Fracture properties of FFF printed ABS

ABS is the most widely used polymer for FFF. Its microstructure makes it stiff and tough and causes complex failure mechanisms such as cavitation, crazing, localized shear yielding, and void coalescence [64] [65] [66]. Most of the studies about the mechanical properties of additively manufactured ABS parts with investigations in infill density, build orientation, layer thickness, line width, raster orientation, and printing temperatures were conducted with tensile tests. In general, FFF printed parts have worse mechanical properties compared to bulk materials due to the porosity and imperfect weld-lines. The fusion of the layers during FFF process is its weakness. The reason is because molten plastic is deposited on a cooler layer which makes it hard for polymer chains to flow and entangle across the interface. Fracture tests provide a valuable means to investigate the inter-layer bonding. Recently, Hart et al. studied the fracture toughness of 3D

printed ABS with single edge notch bend (SENB) specimens. The interlayer fracture resistance (crack grows between the layers) is approximately one order of magnitude lower than the intralayer fracture resistance (crack grows through the layers) [67]. Gardan et al. changed the G-code to deposit the threads along the principal stress directions. With this method, the fracture results of compact tension specimen could be increased by 20 % [68]. Aliheidari et al. studied the fracture resistance and interlayer adhesion of FDM printed ABS specimen. They reported an increase in interlayer bonding with higher printing temperatures [69]. Young et al. studied the influence of carbon fibers in FFF printed ABS parts. The findings are that the inclusion of fibers decreases the interlayer fracture toughness approximately by a factor of 5. This was explained through little evidence of fiber pull-out or bridging and bad adhesion between the fibers and the ABS matrix [70].

The literature covers the fracture toughness of pure ABS in bulk or FFF printed form. Also, the effect of carbon fibers on the fracture behavior of printed parts is briefly reported. In a few publications, the effect of CNT on the fracture toughness of polymer matrix are analyzed for some polymers in the bulk form. However, to the best of the authors' knowledge, no studies have been conducted about the influence of CNT on the fracture toughness of ABS. Although mechanical properties of ABS/CNT have been intensively studied, its fracture toughness has been neglected so far, even though it is an important property for many engineering applications. Especially for FFF printed parts where the inter-layer bonding is the most critical factor, the influence of CNT on the fracture toughness must be known. This was one of the main objectives of this study.

2. FILAMENT FABRICATION

2.1. Introduction

This chapter describes how the ABS/CNT filament was prepared which is later used for printing with the FFF method. An extruder with counter-rotating twin screws is used. Its specification and screw profile are listed in the appendix.

2.2. Feedstock

The most important material used in this thesis was Plasticyl ABS1501, which is a conductive masterbatch based on ABS resin loaded with 15 wt% of Nanocyl's multi-walled carbon nanotubes (MWCNT) NC7000™ with an average diameter of 9.5 nm and an average length of 1.5 μm. To decrease the CNT content, pure ABS pellets (MAGNUM™ 3404 Styron) were used which is the same ABS resin as used from Nanocyl in ABS1501. No plasticizer or surfactants were added to the composition.

2.3. Primary extrusion process

In this work, a melt process was used to fabricate the filament feedstock, as shown in Figure 2.1. Before extrusion the polymer pellets were dried in a vacuum oven at 70°C for at least 3 hours. The first fabricated filament was pure ABS. This step was relatively straightforward and the filament could be collected quickly. The temperature profile of the extrusion barrel, the speed of the twin screws and the resulting torque for all the filaments are listed in Table 2.1.

For 1 wt% CNT, the masterbatch pellets and pure ABS pellets needed to be mixed. 9 g of the masterbatch and 126 g of the pure ABS were measured using an analytical balance. The pellets were then physically mixed by shaking in a sealed plastic bag and transferred to a beaker, ready to

fill the hopper of the extrusion machine. Seven beakers were prepared to have almost a full spool (~ 1 kg) of the filament at the end of the extrusion process. The pellets were fed from the hopper to the barrel, where the material travels through several different zones, including feeding, plastification, mixing, and compaction zones. A circular die with a nominal diameter of 1.75 mm was used at the end. The filament was collected with a spool-winding device. To faster cool the extrudate before winding, it was hovered over a layer of ice and blown with a fan, as seen in Figure 2.1. The filament diameter could be adjusted by varying the distance between the die exit and the winding device as well as the speed of winding. A constant filament diameter is important to obtain quality prints without extrusion flow rate fluctuations at the nozzle output.

Figure 2.1: Filament fabrication process

Table 2.1: Extrusion parameters for different CNT concentrations

wt% CNT	RPM	Max Torque [%]	Temperature Zone 1 [°C]	Temperature Zone 2 [°C]	Temperature Zone 3 [°C]	Temperature Zone 4 [°C]	Temperature Die [°C]
0, pure ABS	30	55	214	249	251	243	214
1	25	55	215	250	251	243	215
2	15	60	216	244	251	244	219
3	15	65	229	269	244	242	222
5	15	75	238	272	251	248	229
10	19	90	254	284	271	266	247

For ABS with 1 wt% and 2 wt% CNT, the temperature profile of the barrel was almost the same as for the pure ABS production, except slightly higher temperature levels were used. It is a rise in the temperature until the middle of the barrel where nanocomposite mixing occurs, followed by a gradual decrease in the temperature towards the die. Different screw rotation speeds were tried and the resulting filaments were analyzed. The filaments were analyzed by braking them and looking at their fracture surface. Sometimes it showed many chunks of dark masterbatch phases and the dispersion of CNT was therefore not good. For 3 wt% CNT, a new strategy was introduced. High temperatures were set in the beginning after the hopper to assure complete melting of the masterbatch that had higher viscosity, compared to the pure ABS. Then, the temperatures were lowered again where the mixing takes place to have higher shear (Table 2.1). In general, relatively low screw speeds were chosen to give the polymer melt more residence time and more time for mixing.

The filament obtained with the new strategy appeared to be less brittle and had less masterbatch chunks. 5 wt% CNT nanocomposite was also fabricated in this manner.

The Extrusion of ABS with 10 wt% CNT filler content was tough. The temperatures were much higher than those for the other nanocomposites and the torque was very close to the maximum capacity of the extrusion machine. Although a higher speed of the screws was used, the

outflow of filament was very slow (ca. 10 mm in 3 seconds). In 2 hours, only one beaker of material could be fed through the machine.

To examine if the filament overall quality was good, different samples with filaments having up to 3 wt% CNT were printed and tested. The electrical conductivity tests showed that none of the compositions are conductive, even ABS with 3 wt% CNT. In the literature, different authors have already reached the percolation threshold under 1 wt% CNT content. Tensile test samples were tested for ABS with 1 wt%, 2 wt%, and 3 wt% CNT. The samples did not deform much plastically. The samples with even only 1 wt% CNT were quite brittle. This could be explained with the chunks of the masterbatch, which were not well-mixed with the pure ABS and cause early fracture. Because of these poor mixing results, it was decided to pelletize all the filaments (except 10 wt% CNT) and extrude it again. This way the material could be mixed again and the residence time inside the barrel could be doubled. In the secondary extrusion, no big pellets of the masterbatch were needed to melt and mix with pure ABS. This time, the mixing started with finer masterbatch chunks (as opposed to pellets), which should have helped for a better dispersion of the CNTs. A simple feeding system was designed and used in a drilling machine to pelletize the filaments. With automatic feeding of the filament, the material could be processed fast and the resulting pellets had a constant size as seen in Figure 2.2.

Figure 2.2: Pelletized filament with constant size

2.4. Secondary extrusion process

In Table 2.2, the process parameters of the secondary extrusion process are given for each nanocomposite composition. The temperature profiles did not include anymore the high temperatures at the beginning of the barrel. The filament produced in the second run appeared to be less brittle and chunks of the masterbatch are reduced significantly.

Table 2.2: Extrusion parameters for the secondary extrusion

wt% CNT	RPM	Max Torque [%]	Temperature Zone 1 [°C]	Temperature Zone 2 [°C]	Temperature Zone 3 [°C]	Temperature Zone 4 [°C]	Temperature Die [°C]
1	20	81	219	249	251	243	211
2	20	82	218	247	248	243	213
3	20	85	224	253	254	247	222
5	15	85	242	268	262	256	243

2.5. Comparison of samples before and after 2nd extrusion

The conductivity of printed samples was out of the measurable range before and after the secondary extrusion. Therefore, this test did not give any information about a change in the CNT dispersion. With the tensile tests, the improvement through secondary extrusion can be shown better. The results of the samples with 1 wt% CNT are compared. Before the secondary extrusion, the tensile test results were 26.4 MPa of ultimate tensile strength, 789 MPa of Young's modulus, and 5.3 % of strain at break. For the ABS/1 wt% CNT samples printed with the secondary filament, the tensile results were 31.14 MPa of ultimate tensile strength, 2630 MPa of Young's modulus, and 7.6 % of strain at break. The comparison of these results show a clear improvement in all the mechanical properties through the secondary extrusion process. Also, visual inspection revealed that the samples with secondary extrusion process experienced more color change, indicating that they underwent more crazing and plastic deformation before the final failure.

3. ELECTRICAL CONDUCTIVITY

3.1. Introduction

This chapter focuses on the influence of additive manufacturing on the electrical conductivity. When the filament is extruded through the nozzle of the printer, it is likely that the carbon nanotubes are aligned in the extrusion direction. The orientation of the CNT has an influence on forming the electrical network [34] [35]. The layer-to-layer bonding may also affect the electrical conductivity in the printed samples. To better understand the influences of the printing process on the electrical conductivity of the ABS/CNT nanocomposites, different types of samples were produced.

3.2. Experimental

The starting point to produce different samples was the filament, which was produced with a twin-screw extruder as described in the previous chapter. For all different sample preparation methods, at least three samples were produced and tested.

3D printing of through-layer samples, 1st version

In the first attempt, round disc samples with a diameter of 15 mm and a thickness of 1 mm were printed with a Felix Pro 2 printer (printer specification in appendix). The nozzle temperature was set to 260°C and the printing bed was kept at 100°C. A nozzle of 0.35 mm diameter was used, and the layer thickness was set to 0.2 mm. The printing speed of the rectilinear infill was 32 mm/s. ABS with 10 wt% CNT content couldn't be printed with these settings. The viscosity of the material was too high even with 275°C at the nozzle.

3D printing of through-layer samples, 2nd version

The second version of printed samples were square with a length of 15 mm and a thickness of 1 mm. The nozzle was changed to a diameter of 0.8 mm and heated up to 275°C. The bed temperature was raised to 105°C, but the rest of the settings were kept the same as the 1st version. The ratio of nozzle diameter to layer thickness could be increased to four with which a better layer adhesion can be expected.

3D printing of in-layer samples

To perform in-layer direction measurements, cuboid samples were printed. The printing conditions were the same as for the second version of the through-layer samples. The cuboid's dimensions were 30x8x8 mm^3. Small discs with a thickness between 1 and 2 mm were cut from the cuboids and the cut surfaces were grinded. In Figure 3.1 the through-layer and in-layer measurement directions of printed parts are illustrated.

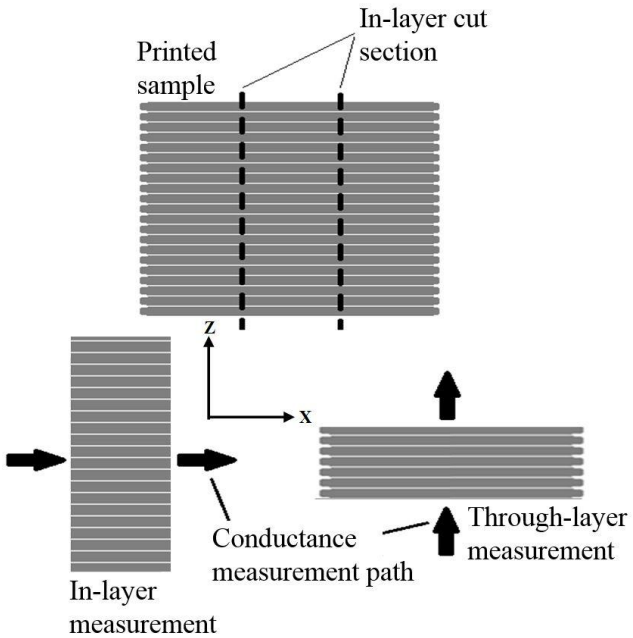

Figure 3.1: Schematic illustration of conductance measurements in through-layer and in-layer direction of 3D printed specimen, z is in build direction and x in printing line direction

Hot pressed samples

Compression molded samples were also produced with a Carver hot press (hot press specification in appendix) for each composition to be used as the baselines for the electrical properties of the bulk nanocomposites. The upper and lower plate of the hot press were set to 260°C. The mold was filled with pelletized filament and heated up between the plates in the hot press for 2 minutes. The top plate of the mold was added and the mold was put back in the hot press. Slowly a pressure of 11 metric tons (8000 psi, 24,000 pounds) was applied to give time for the air between the pellets to escape and prevent voids in the samples. After reaching the set pressure, the mold was left in the press for another 2 minutes. Then the mold was taken out to cool down with a fan and weights were placed on top of the mold. With this manufacturing method, the masterbatch pellets could also be pressed to obtain samples with 15 wt% CNT for the analysis.

Impedance test

Before the samples were tested with the impedance analyzer (Impedance analyzer specification in appendix), a thin layer of silver epoxy (MG Chemicals Silver Epoxy Adhesive, 4 hr. working time, Electrical resistivity: 0.006 Ω·cm) was applied on both sides of the samples to ensure the good contact to the electrodes of the analyzer and to overcome the surface resistivity. The output data of the impedance analyzer was the impedance $|Z|$ and the phase angle θ. With these two values, the thickness of the sample t, and the sensor area A, the conductivity σ is calculated with the following formula:

$$\sigma = \frac{t}{|Z| \cdot \cos\theta \cdot A}$$

3.3. Results and Discussion

Hot pressed samples

The compression molded ABS/CNT samples achieved the best electrical conductivity results. The percolation threshold was about 1 wt% CNT, which is in the range of the published literature for the melt processed ABS/CNT nanocomposites [11] [24]. This agreement indicates that the CNT dispersion state was comparable to what is available in the literature. In the compression molded samples, the CNT are relatively randomly oriented, which makes it easier to form a conductive network. The results shown in Figure 3.2 show the AC conductivity over broad band of frequencies. If an electrical network is formed the impedance and conductivity shows a frequency independent plateau.

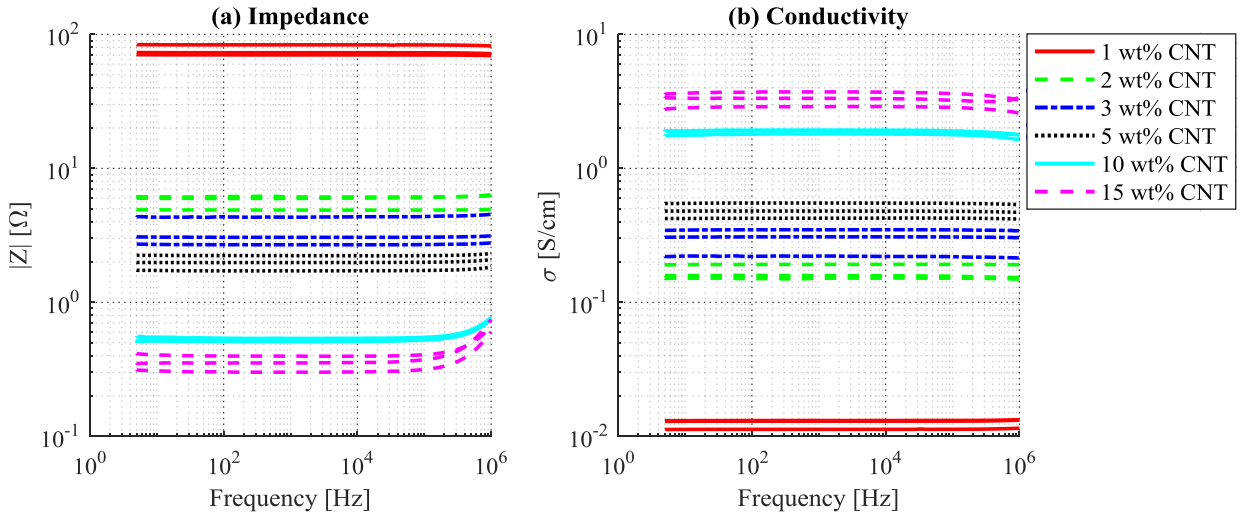

Figure 3.2: Broadband impedance (a) and electrical conductivity (b) of compression molded ABS/CNT nanocomposites

Printed samples through-layer, 1st version

The first printed samples were only conductive with a CNT content of 5 wt% or higher. They are significantly less conductive than the hot-pressed ones. There are several possible reasons

for that. One reason is the bonds between layers. If the layers are not well fused together, or if the CNT do not connect to each other at the interlayer, not a good conductive network can be obtained. Another reason is the orientation of the CNTs. During the extrusion, which includes the flow through the nozzle, but also the deposition of the layer, the CNT are aligned in the layer deposition direction, which is normal to the conduction measurement direction. For aligned CNTs, it is more difficult to form a conductive network, particularly in the direction normal to the alignment direction. With 5 wt% CNT, the impedance is only frequency independent at low frequencies. At higher frequencies the impedance decreases due to electron tunneling in addition to the conductive network.

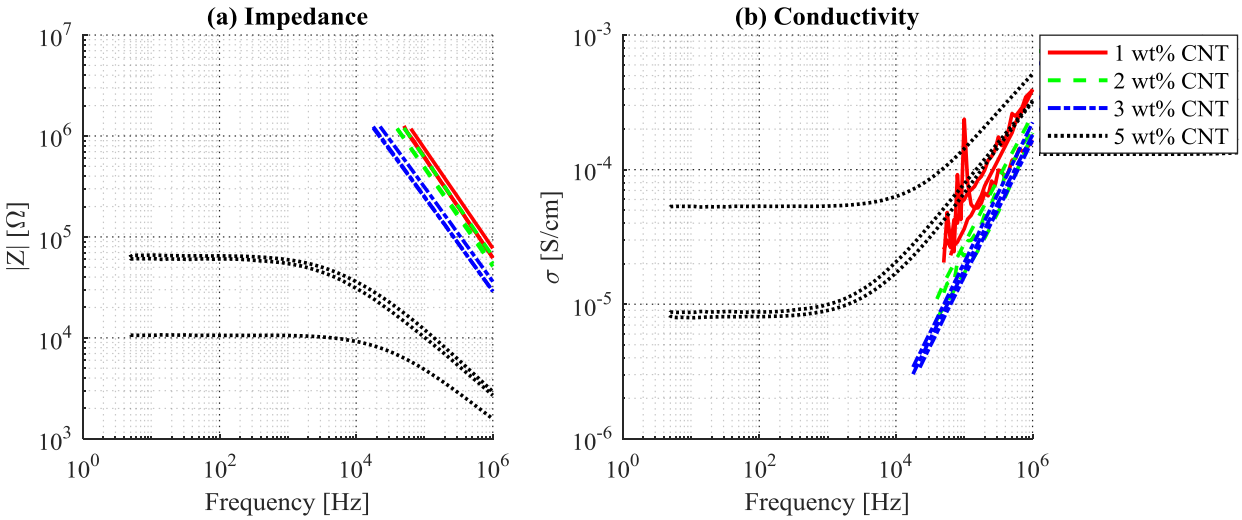

Figure 3.3: Broadband through-layer impedance (a) and electrical conductivity (b) of printed ABS/CNT samples 1st version

Printed samples through-layer, 2nd version

The results of the second version of the printed samples were better than the first version. In this case, ABS with 3 wt% CNT became conductive (Figure 3.4). With the 0.8 mm nozzle diameter, it was possible to also print ABS with 10 wt% CNT. In this case, the greater nozzle

diameter with the same layer thickness as first version implies that more squeezing should be applied to the deposited material to reduce the 0.8 mm diameter to 0.2 mm thickness. More squeezing results in higher compressive forces between the deposited layer and the underneath layer, providing a better contact and wetting between them and consequently a better interlayer bond can be formed. In addition, the nozzle temperature was also higher in the 2nd version, which provides a better fusion between the layers. Overall, a better interlayer bond enhances the chance of through-layer CNT interconnection. Moreover, with a bigger nozzle, it is plausible to assume that the CNTs align less as the shear stresses reduces on the viscoelastic material passing through the nozzle. Reduced alignment in the layer direction means the higher probability of CNT interconnection in the normal direction, which is the direction of conduction measurement. Therefore, the through-layer conductivity of the 2nd version samples were significantly better than those of 1st version.

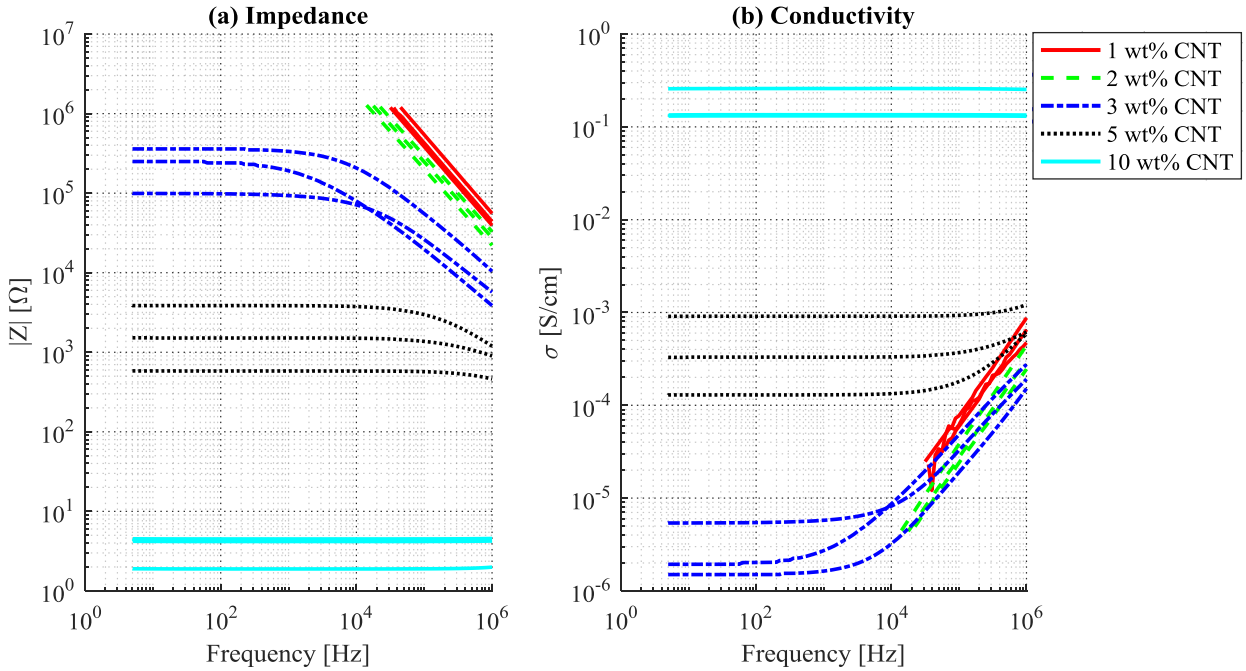

Figure 3.4: Broadband through-layer impedance (a) and electrical conductivity (b) of printed ABS/CNT samples 2nd version

Printed samples in-layer

It is also important to characterize the in-layer conductivity of printed samples. This provides information on the isotropy of the conductivity and helps in better inferring the results in terms of the CNT alignment and interlayer bonding effects. In-layer conduction should be minimally affected by the CNT alignment, as the alignment direction and conduction measurement direction are the same. Also, the in-layer conduction does not necessarily need layer-layer CNT interconnection. These differences should be manifested by the comparison of the through-layer and in-layer conductivities. The conductivity of ABS with 3 wt% and 5 wt% CNT increased by two orders of magnitude (Figure 3.5). Also, 2 out of 5 samples of ABS with 2 wt% CNT achieved a measurable conductivity. The printing parameters for these samples were the same as those for through-layer samples. Therefore, the only difference is the orientation of the layers. The higher in-layer conductivity values can thus be related to the less influence of the layer-to-layer bonding and CNT alignment in that direction compared to the through-layer direction.

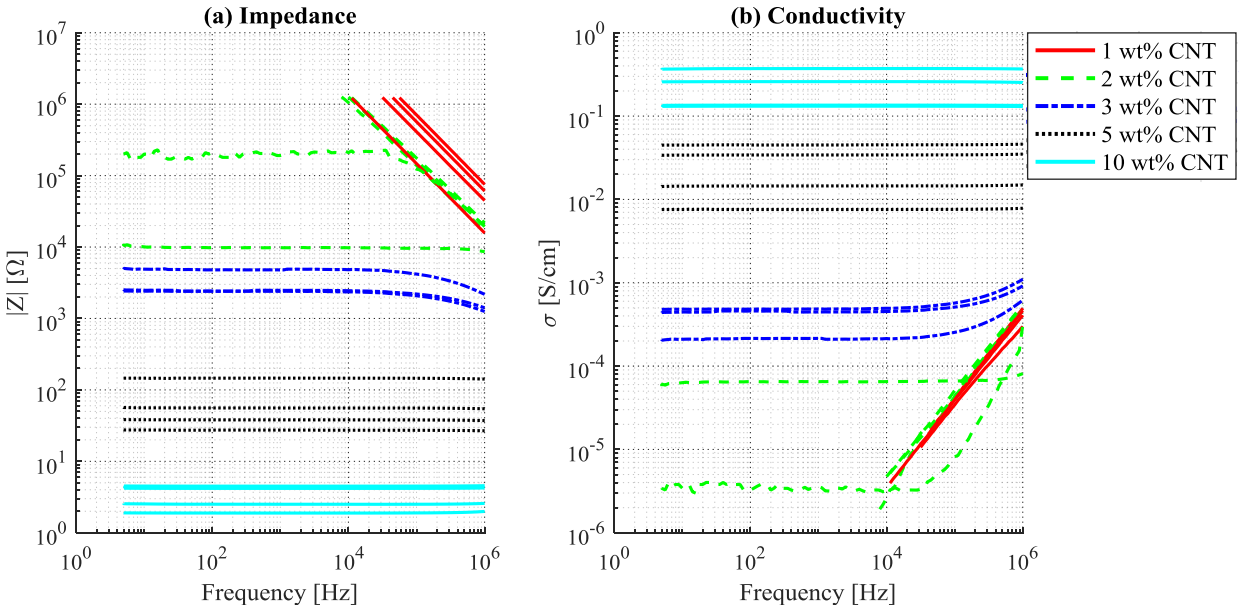

Figure 3.5: Broadband in-layer impedance (a) and electrical conductivity (b) of printed ABS/CNT samples

3.4. Comparison

In order to provide a better comparison, the mean of the conductivity at frequencies below 50 Hz was calculated and plotted in Figure 3.6. It is apparent that the conductivity increases with increasing CNT content. The percolation threshold for the compression molded samples would be around 1 wt% CNT or lower. Unlike the compression molded samples, the printed samples appear not to exhibit a sharp insulation-conduction transition. Both through-layer and in-layer conductivities of the printed samples slowly rise as the CNT content increases. This is a characteristic of nanocomposites with alighted CNTs, similar to injection-molded samples. At high CNT contents (10 wt%), the through-layer and in-layer conductivities became the same, indicating that the layer orientation doesn't matter anymore. This is due to the formation of a sufficient number of CNT networks, which can provide electron transfer paths independent of the CNT alignment and bond quality. The through-layer conductivity of the printed samples could be increased with higher temperatures and a bigger nozzle. With changes in the printing parameters, the overall percolation threshold may be enhanced.

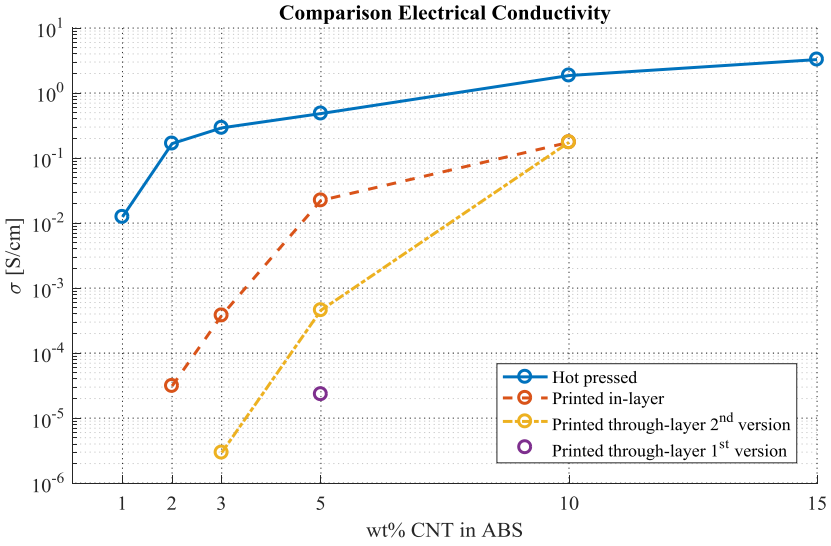

Figure 3.6: Conductivity vs. CNT content for printed and compression molded ABS/CNT nanocomposites

Here, the conductivity results of the compression molded samples are compared with the literature (chapter 1.3). The conductivity results of this work are summarized in Table 3.1. Compared with the melt processed samples of Al-Saleh et al. (Table 3.2), the samples in this work achieved very similar results. Only at 5 wt% CNT, some notable difference is found.

Solution processed samples are better at very low CNT concentrations. At 1 wt%, the difference is about one magnitude as shown in Table 3.3. It is interesting that at higher percentages, the properties of melt processed samples exceed the solution processed ones. At 10 wt% CNT, the result of this work is 1.2 S/cm, which is greater than 0.7 S/cm for the solution case. This is maybe because at higher concentrations, CNTs form agglomerations more easily in the solution compared to the molten state.

Table 3.1: Results of electrical conductivity

Wt% CNT	1	2	3	5	10	15
	Conductivity σ [S/cm]					
Hot Presses	$1.2 \cdot 10^{-2}$	$1.7 \cdot 10^{-1}$	$2.9 \cdot 10^{-1}$	$4.8 \cdot 10^{-1}$	$1.9 \cdot 10^{0}$	$3.3 \cdot 10^{0}$
Printed in-layer	-	$3.1 \cdot 10^{-5}$	$3.8 \cdot 10^{-4}$	$2.2 \cdot 10^{-2}$	$1.7 \cdot 10^{-1}$	-
Printed 2nd version	-	-	$2.9 \cdot 10^{-6}$	$4.6 \cdot 10^{-4}$	$1.7 \cdot 10^{-1}$	-
Printed 1st version	-	-	-	$2.3 \cdot 10^{-5}$	-	-

Table 3.2: Conductivity results of melt processed samples form from Al-Saleh et al. [24]

Wt% CNT	0.75	1	1.5	2	3	5	10	15
σ [S/cm]	$4 \cdot 10^{-7}$	$1 \cdot 10^{-2}$	$6 \cdot 10^{-2}$	$1.3 \cdot 10^{-1}$	$4 \cdot 10^{-1}$	$1.2 \cdot 10^{0}$	$2.5 \cdot 10^{0}$	$5.2 \cdot 10^{0}$

Table 3.3: AC conductivity results of solution processed samples from Al-Saleh et al. [27]

Wt% CNT	0.5	1	2	3	5	10	15
σ_{AC} [S/cm]	$4 \cdot 10^{-2}$	$1.2 \cdot 10^{-1}$	$2.2 \cdot 10^{-1}$	$2.8 \cdot 10^{-1}$	$5 \cdot 10^{-1}$	$7 \cdot 10^{-1}$	$1.4 \cdot 10^{0}$

3.5. Further experiments

Influence of nozzle size for through-layer samples

To investigate the influence of the nozzle size on the electrical properties of printed samples, an additional experiment was conducted. The closest concentration of CNT to the percolation (i.e., 3 wt% CNT) and therefore the most sensitive one was analyzed. The printing parameters were the same as for the 2nd version of the printed through-layer samples. When looking at the results of Figure 3.7, it is clearly visible that the conductivity decreases with smaller nozzle sizes. Most likely this is due to the higher alignment of the CNT within the nozzle, as discussed before. Another reason can be the worse adhesion, because the ratio of nozzle to layer thickness and therefore also the pressure decreases. A third reason can be the increase of lines relative to the measured area with smaller nozzles. It is assumed that the first reason has the biggest influence although it is not known for sure. To have more conclusive results, it would be interesting to do the same experiment also for higher percentages of CNT.

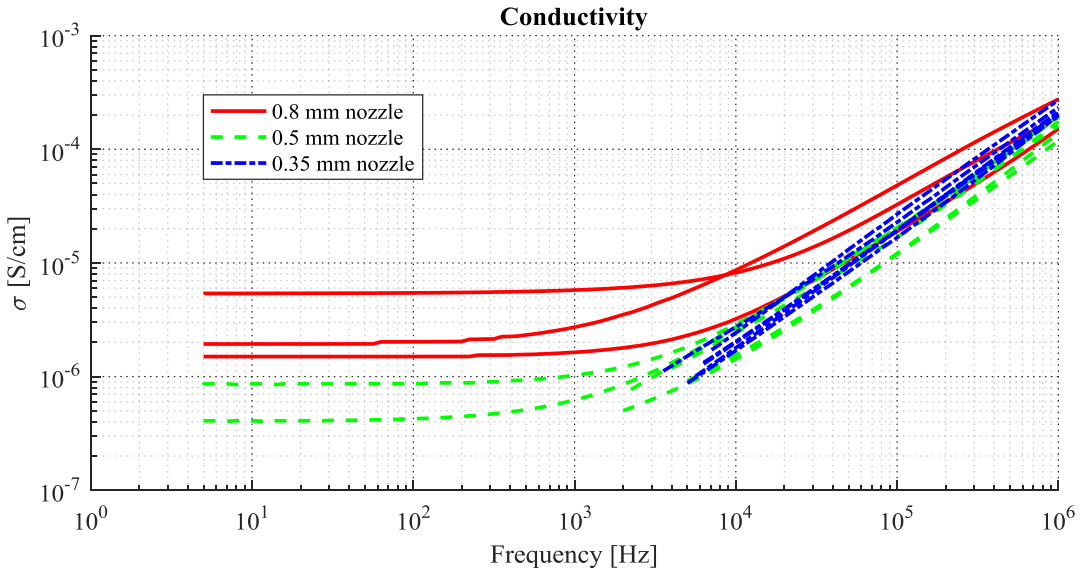

Figure 3.7: Influence of nozzle diameter size on the through-layer conductivity of ABS/3 wt% CNT samples

Influence of layer thickness for in-layer samples

To further analyze the impact of the alignment of the CNTs, an additional experiment was conducted. Randomly oriented CNT are more likely to form a conductive network. With a higher layer thickness, the shear in depositing a layer of polymer is smaller and therefore there should be less alignment of CNT. More samples for the most sensitive concentration with 2 wt% CNT were printed with layer thicknesses of 0.4 mm and 0.8 mm. The rest of the printing parameters stayed the same. The results (Figure 3.8) vary a lot and the repeatability is not good, but the trend is that with higher layer thicknesses, more samples are conductive, and two of the 0.8 mm samples are much higher relative to the others and even more than 3 wt% CNT samples. With the higher layer thickness, we may have more randomly oriented CNT which could be the cause of the slightly increased conductivity. But because the scatter is so high, it is safer to make no conclusions from this experiment. The high scatter could be because the CNT concentration is very close to the percolation threshold. It would be interesting to repeat this experiment for 3 wt% and 5 wt% CNT.

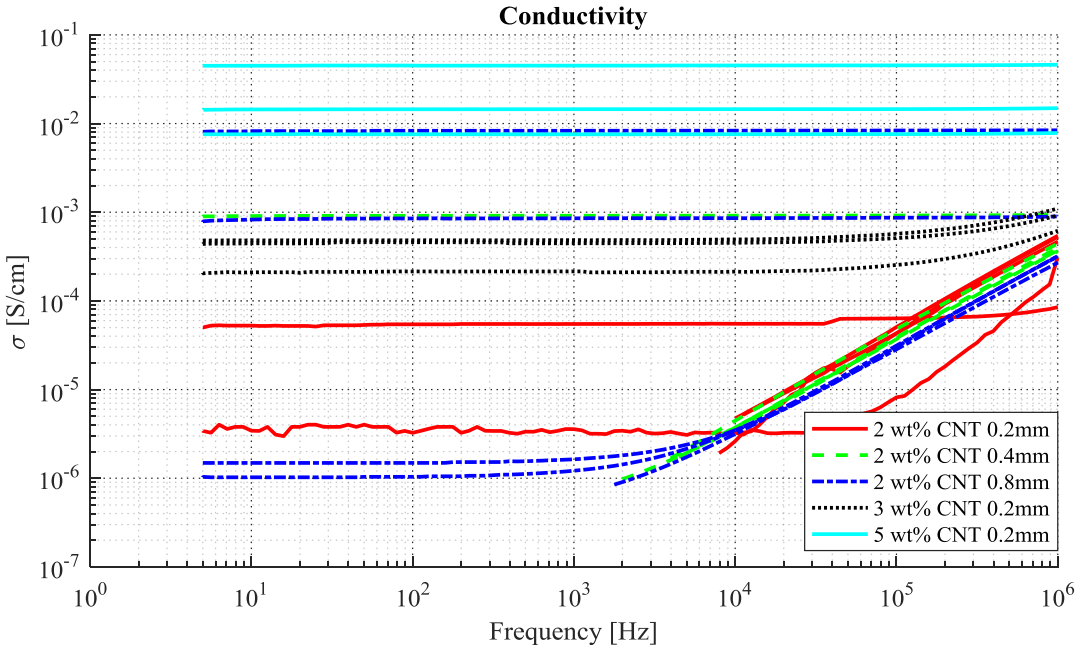

Figure 3.8: Influence of layer thickness on the in-layer conductivity of ABS/CNT samples

4. TENSILE TESTS

4.1. Introduction

This chapter focuses on the effects of CNT in a nanocomposite with ABS on basic mechanical properties. In the first step, the pure ABS samples were produced via compression molding to evaluate the bulk material properties. Then pure ABS samples were printed to assess the influence of additive manufacturing on the mechanical properties of the polymer matrix. In the next step, the ABS/CNT nanocomposite samples with different contents of CNT were printed and tested.

4.2. Experimental

The starting point to produce different samples was the filament which was produced with a twin-screw extruder as described in chapter 2. The tensile tests were conducted following the ASTM D 638 standard. This test method covers the determination of the tensile properties of unreinforced and reinforced plastics in the form of standard dumbbell-shaped test specimens under defined conditions. The Type V specimen geometry was chosen to save material and printing time. The gauge length of this sample is 7.626±0.25 mm at a width of 3.18±0.5 mm with a thickness below 4 mm. At least 5 samples need to be tested at room temperature (23 ± 2 °C) and at a speed of 1 mm/min (0.02 mm/s).

Hot pressed ABS samples

To get the basic mechanical properties of pure ABS without any influences of the printing, compression molded samples were produced (hot press specification in appendix). The upper and lower plate of the hot press were set to 170°C. The mold was filled with dried pure ABS pellets

and heated up between the plates in the hot press for 8 minutes. The top plate of the mold was added and the mold was put back in the hot press and warmed up for 1 minute. Slowly a pressure of 11 metric tons (8000 psi, 24,000 pounds) was applied to give the air between the pellets time to escape and prevent voids in the samples. After reaching the set pressure, the mold was left pressed for another 2 minutes. Then, the mold was taken out to cool down with some weights on top of it.

Because the mold shape was not perfect, the samples were altered with a file in the gauge section to guarantee that they break at the gauge section, not at the transition to the clamping section where the width changed too drastically.

3D printing of ABS/CNT samples

Before printing the final samples, a small parameter study was conducted with ABS/1 wt% CNT samples. The optimal nozzle diameter and line width needed to be evaluated. The samples were printed with a nozzle temperature of 275 °C and a bed temperature of 105 °C. The layer thickness was set to 0.2 mm to build samples with 1 mm thickness. The printing speed of the outline and the rectilinear infill was 24 mm/s and 32 mm/s, respectively. The outline overlap was set to 50 percent to prevent gaps in areas with a small difference in the angle between the outline and the infill-lines. These settings stayed the same for all the tensile test samples, irrespective of CNT content. A Felix Pro 2 printer was used (printer specification in appendix).

Three different combinations of nozzle diameter and line width were analyzed. With a 0.8 mm nozzle and a line width of 0.35 mm, the adhesion of the first layer to the printing bed was very problematic. To print a line which is smaller than the nozzle diameter, the extrudate is drawn and hovers over the bed. With a decreased distance between the nozzle tip and the bed for the first layer, this problem could be circumvented. The printing was easier with a 0.8 mm nozzle and

0.53 mm line width. Also, the combination of a 0.5 mm nozzle and 0.35 mm line width performed well. The bigger the line width, the more the properties should shift toward the bulk ones. To analyze properties specific to additive manufacturing, a smaller line width of 0.35 mm is preferable which works better together with a 0.5 mm nozzle. The nanocomposites containing 0, 1, 2, 3, 5, and 10 wt% CNT were then printed using the above conditions. Although the nozzle temperature of 275 °C is very high for pure ABS, it was still used to have the same conditions for all the printed samples for better comparison.

Tensile testing

A home-made load frame was used in this study, which suffered from some excessive compliance. A rigid metal piece was first clamped in the grips and loaded to test the deformation of the machine. Figure 4.1 shows the result of this test. Above 100 Newton, which is about 27 MPa with the average cross section at the gauge section of the printed dumbbell-shaped samples, the machine showed some serious deformation.

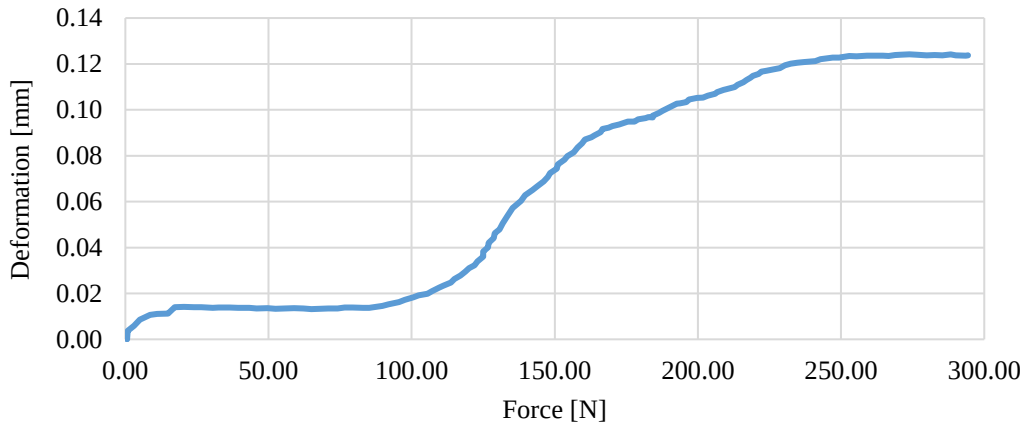

Figure 4.1: Deformation test of the home-made tensile test machine

The displacement was measured over the whole machine instead of only in the gauge length of the sample. For the modulus of elasticity measurements, ASTM recommends using an extensometer with a maximum strain error of 0.0002 mm/mm. An extensometer classified by Practice E 83 as fulfilling the requirements of a B-2 classification within the range of use for modulus measurements meets this requirement. This requirement was not met in the current test, due to the machine compliance. Because of this, all the results of the Young's modulus need to be treated with caution. But, they should be still valid for comparative purposes.

Analyzing the data

The output of the load cell and the displacement sensor of the tensile test machine are in Volts. The data was recorded with Personal Daq and saved as .txt file. To analyze the data, a Matlab script was written to automatize the processing of the data. (It is findable in the appendix.) After the Voltage values were converted into force and displacement, together with the cross section of the sample in the gauge section, the strain and stress could be calculated. The next step was to cut off the data points in the beginning where the sample settling occurs and at the end after the sample broke. These alterations of the graph are shown in Figure 4.2. The end was cut when the difference between two following stress data points was greater than 1 MPa. To smoothen the graph, a mean over 5 points was calculated. The increase in stress which triggers the loading of the sample is detected by exceeding a slope of 300 MPa. The slope is calculated over 20 data points. The next step was to fit a line to the elastic region. The fitting of the polynomial of first order includes the points with stress values between 3 and 15 MPa. The slope of this line corresponds to the Young's modulus and the intersection with the zero-stress axis sets the zero-

strain point. Therefore, the graph is shifted slightly to the left in the final stress-strain plot, as seen in Figure 4.2.

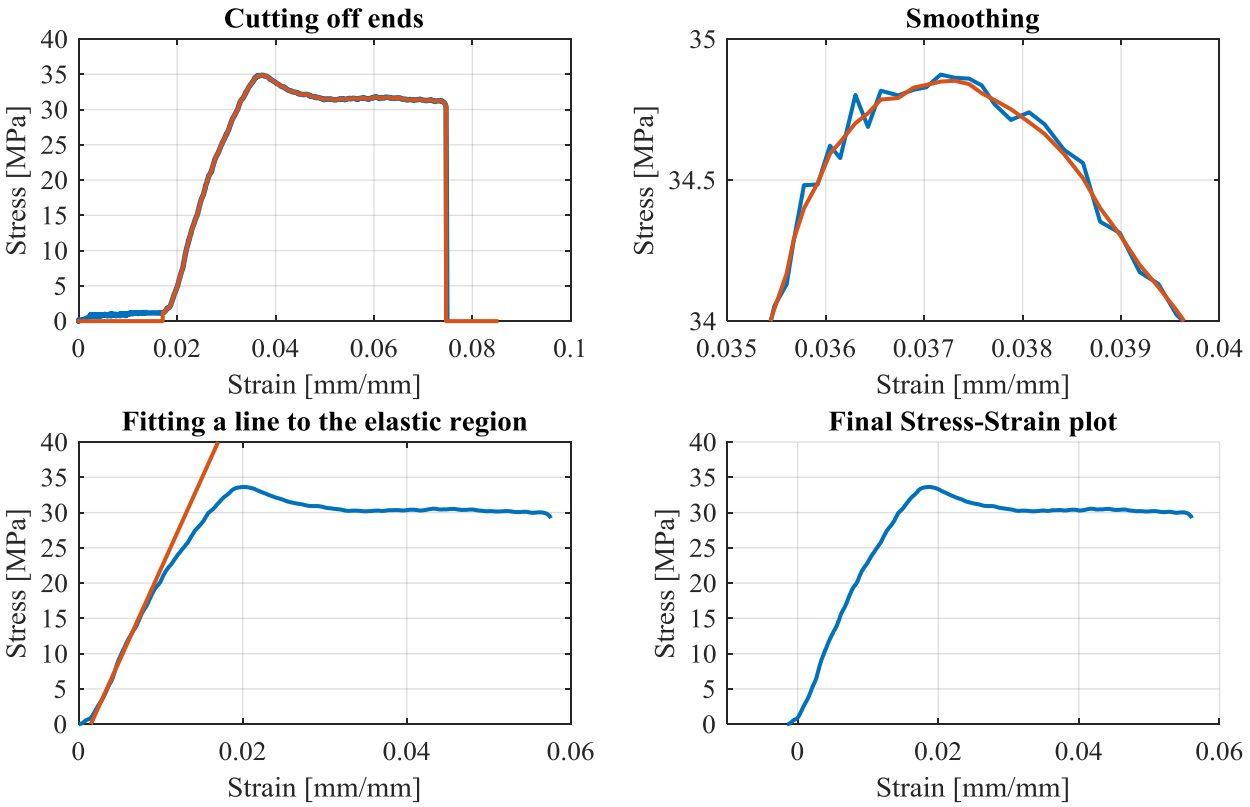

Figure 4.2: Alterations and analysis of the stress-strain graphs

4.3. Results and Discussion

Nozzle size and line width comparison

In this section, the mechanical properties of printed ABS/CNT are reported as a function of nozzle size and line width. With these changes, the print quality also changed, which probably had the biggest impact on the mechanical propeorties. Figure 4.3 shows the broken tensile samples printed using different nozzle size and line width combinations. None of the samples printed with a 0.8 mm nozzle diameter and 0.53 mm line width broke at the gauge section. Because of the small number of infill lines, a small gap was created between the outline and the end of the infill line at the fillet, where geometry changes. The fracture surface of the gauge section is given in Figure 4.4 for this case (fractured under liquid nitrogen with a starting crack). The pictures were taken with a Leica stereo microscope (specification in appendix). The print quality and the density of the samples appeared acceptable, but the gaps at the fillet region were the problem.

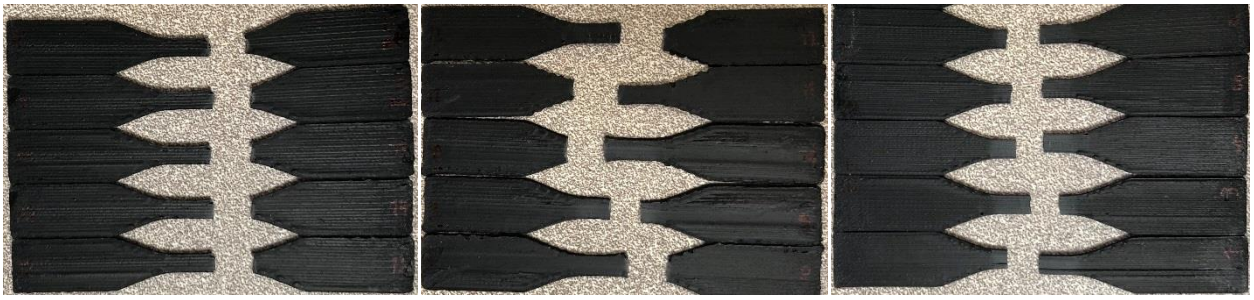

0.8 nozzle, 0.53 mm line width 0.8 nozzle, 0.35 mm line width 0.5 nozzle, 0.35 mm line width

Figure 4.3: Broken tensile test samples printed with different nozzle sizes and line widths

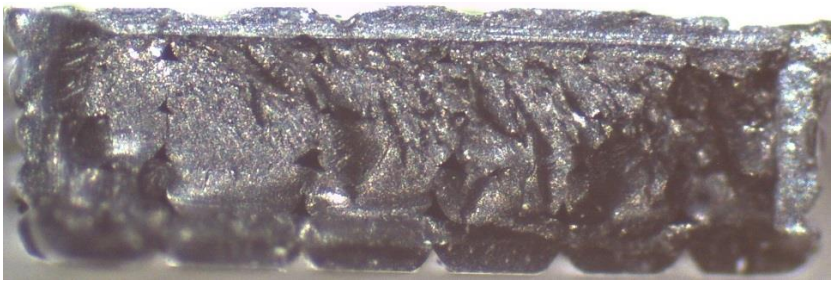

Figure 4.4: Fracture surface of a sample printed with 0.8 mm nozzle diameter and 0.53 mm line width

The size difference between 0.8 mm nozzle diameter and a 0.35 mm line width was too big. This meant that the extrudate should have been drawn more to reduce the width from 0.8 to 0.35 mm. This excessive drawing resulted in a bad adhesion between the layers, especially for the outline region. It only worked well within the infill where the bead was restricted on one side from a previously deposited bead. At reversal points of the infill lines, the extrudate got pulled back away from the outline creating a weak point in the structure. In Figure 4.5, the fracture surface of the gauge section is shown for this combination of nozzle diameter and line width.

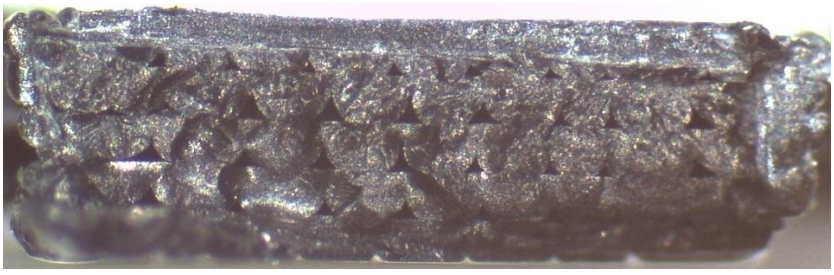

Figure 4.5: Fracture surface of a sample printed with 0.8 mm nozzle diameter and 0.35 mm line width

With 0.5 mm nozzle diameter and 0.35 mm line width, the print quality was the best. All the samples broke at the gauge length as shown in Figure 4.3. The number of infill lines was high enough to fill the area within the outline without any gap at the fillet section. In this case, the size difference between the nozzle diameter and the line width was small enough to enable a good layer adhesion. The print quality itself also looks better as shown in Figure 4.6. Compared to the sample

printed with a 0.8 nozzle and 0.35 mm line width (Figure 4.5), it is has less voids between the printing lines.

Figure 4.6: Fracture surface of a sample printed with 0.5 mm nozzle diameter and 0.35 mm line width

The mechanical properties of the samples printed with different nozzle size and line width combinations are shown in Figure 4.7. As seen, the samples printed with 0.8 mm nozzle diameter and 0.53 mm line width have a lower strength probably because of the gaps between the outline and the infill causing stress concentrations, as this is the failure location in all the tested samples of this type. The lower elongation at break of these samples can be attributed to the same reason. The samples printed with 0.8 mm nozzle diameter and 0.35 mm line width are stiffer than the other samples. This may not be a significant difference noting the imprecise measuring setup, but it could be because of the more significant drawing of the extrudate while printing, as this case provides the highest nozzle diameter to line width ratio, requiring the highest drawing ratio of the extrudate. The polymer molecular chains are aligned in the drawing direction, which increases the elastic modulus. The samples printed with 0.5 mm nozzle diameter and 0.35 mm line width showed a better strength and elongation before breakage, indicating less stress concentrations.

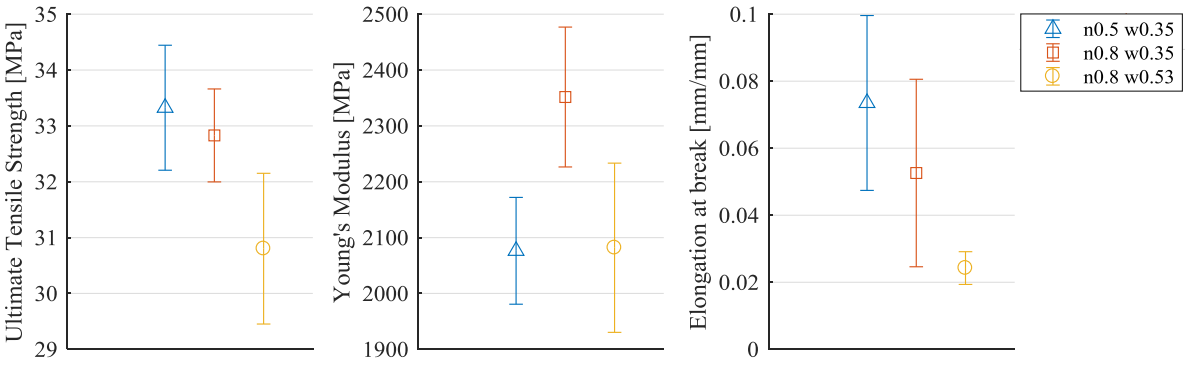

Figure 4.7: Comparison of the mechanical properties of ABS/1 wt% CNT samples printed using different combinations of nozzle diameter and line width

Combining the results of the mechanical properties and the quality of the print, the setup with the 0.5 mm nozzle diameter and the 0.35 mm line width was considered to be the best choice.

Compression molded pure ABS samples

The tensile test results of the pure ABS samples manufactured with compression molding are given in Figure 4.8. The stress-strain curves for the replications are close to one another and there is a low scatter. The samples exhibited considerable plastic deformation, with significant crazing easily visible with a naked eye. The strain at break reached up to 16 %.

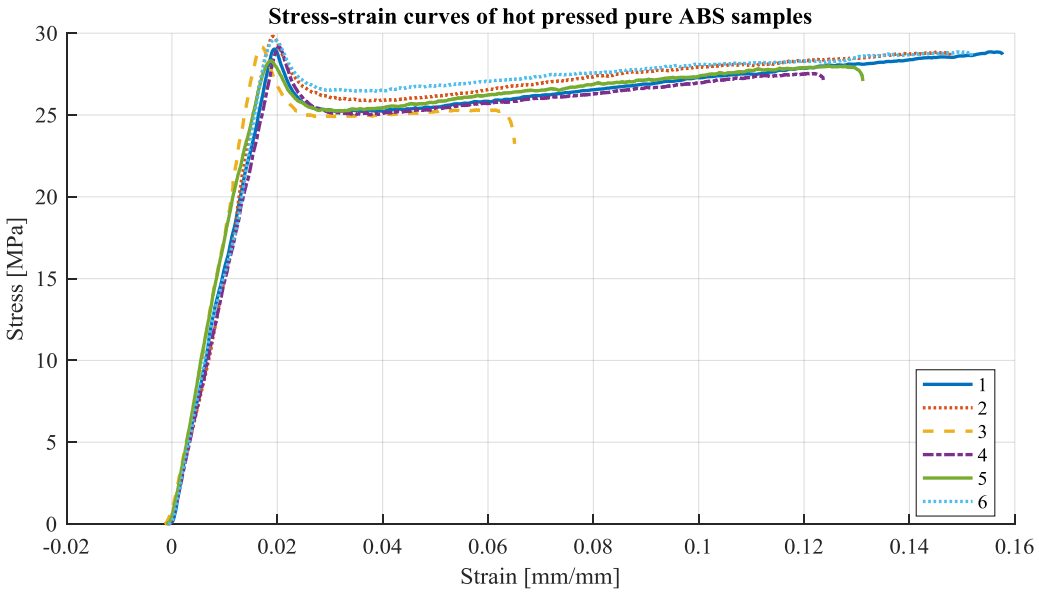

Figure 4.8: Stress-strain curves of the compression molded pure ABS samples

Printed pure ABS samples

The tensile test results of the printed pure ABS samples are shown in Figure 4.9. The scatter of these results is bigger. This is probably due to small imperfections from the printing process.

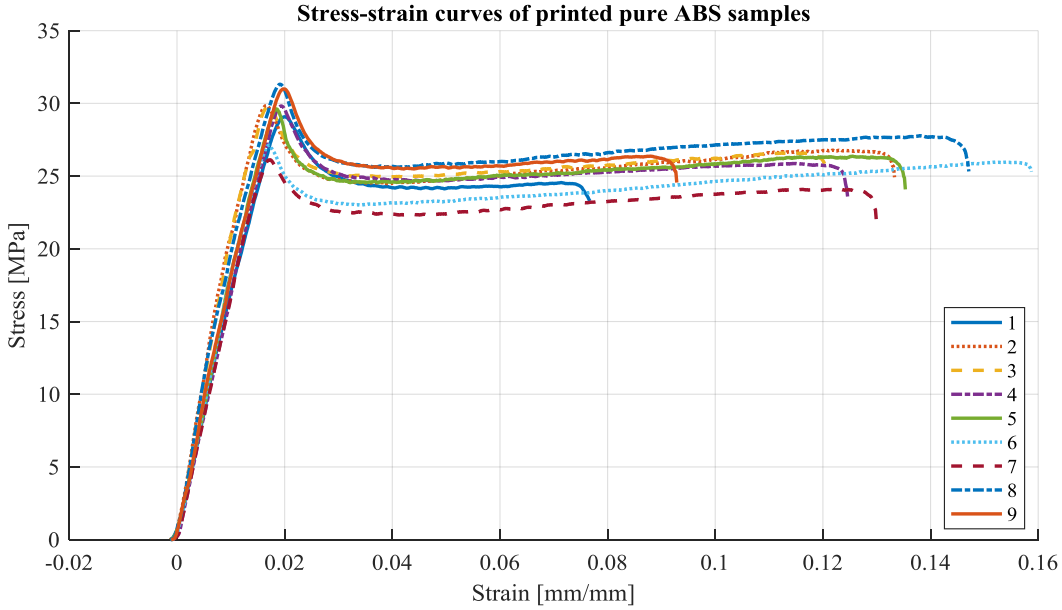

Figure 4.9: Stress-strain curves of printed pure ABS samples

Figure 4.10 shows the fracture surfaces of the first four printed pure ABS samples. The voids are relatively small and are visible only at the lower end of each layer. Since a line width of 0.35 mm is used together with a larger nozzle diameter (0.5 mm), a good level of line-to-line overlapping could be obtained.

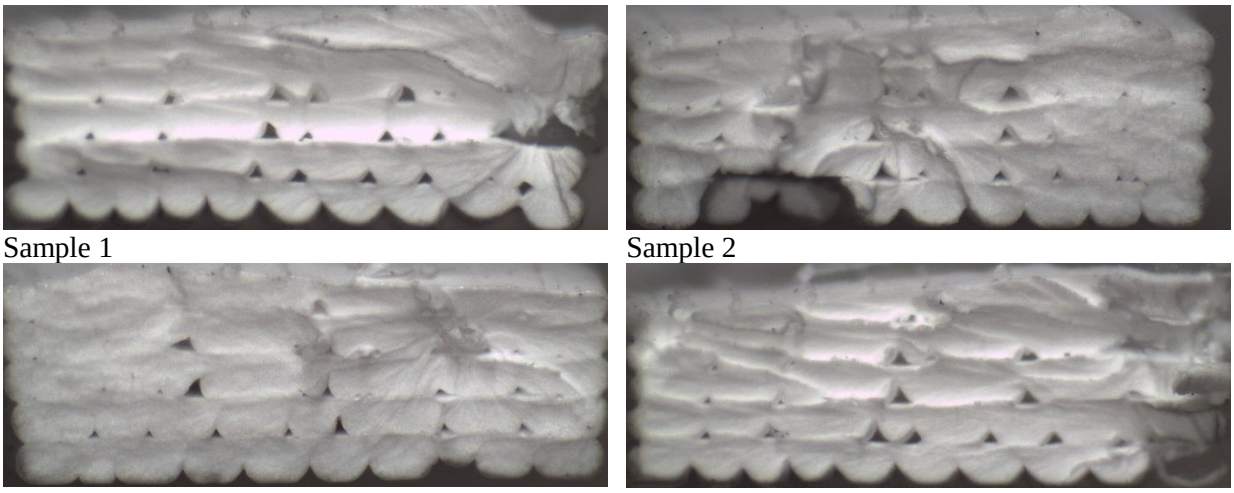

Sample 1 Sample 2

Sample 3 Sample 4

Figure 4.10: Fracture surface after tensile test for printed pure ABS samples

Comparison between compression molded and printed pure ABS samples

The mechanical properties of printed samples are usually reported to be inferior to those of the bulk counterparts. In this work, however, we report the strength, stiffness, and strain-at-break of the printed pure ABS to be very similar to those of the compression molded samples, if not better. This is considered a significant achievement. When comparing the ultimate tensile strength, it is apparent that the standard deviation of the printed samples is higher, but the strength is for both manufacturing methods are almost the same. More interestingly, the elastic moduli of the printed samples are even slightly higher than those of the compression molded ones. It is not a significant difference, but one reason could be that the molecular chains of the polymer are aligned during extrusion through the nozzle and drawn during the deposition of the lines. Aligned

molecular chains increase the stiffness in the alignment direction, when loaded axially. In the compression molded samples, the chains are more randomly oriented. The elongation at break is also about the same for the samples prepared using both manufacturing techniques. The reason for such good mechanical properties of the printed ABS samples can be attributed to a combination of the unusually high printing temperature (275 °C) for ABS, which led to better fusion of the layers as well as other optimized print conditions, especially the nozzle diameter and line width ratio. Recommended printing temperatures for ABS are typically between 220 °C and 240 °C.

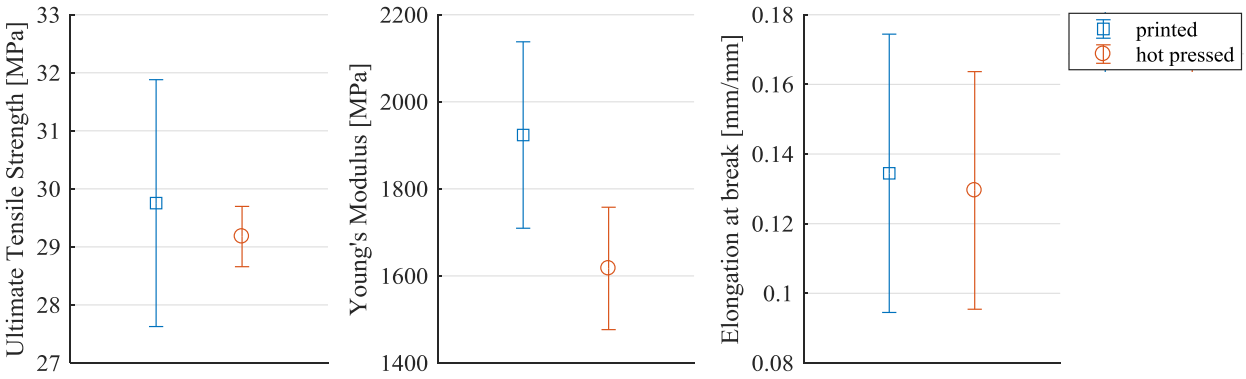

Figure 4.11: Comparison of the mechanical properties of pure ABS samples prepared using compression molding and 3D printing

Printed ABS with 1 wt% CNT

The tensile testing results for the nanocomposite with 1 wt% CNT are shown in Figure 4.12. Samples 1 and 2 were detected as outliers because they had a lot of initial slippage, which is already cut off in this graph. Sample 4 is also not valid because the first printing layer was bad and the sample broke too early.

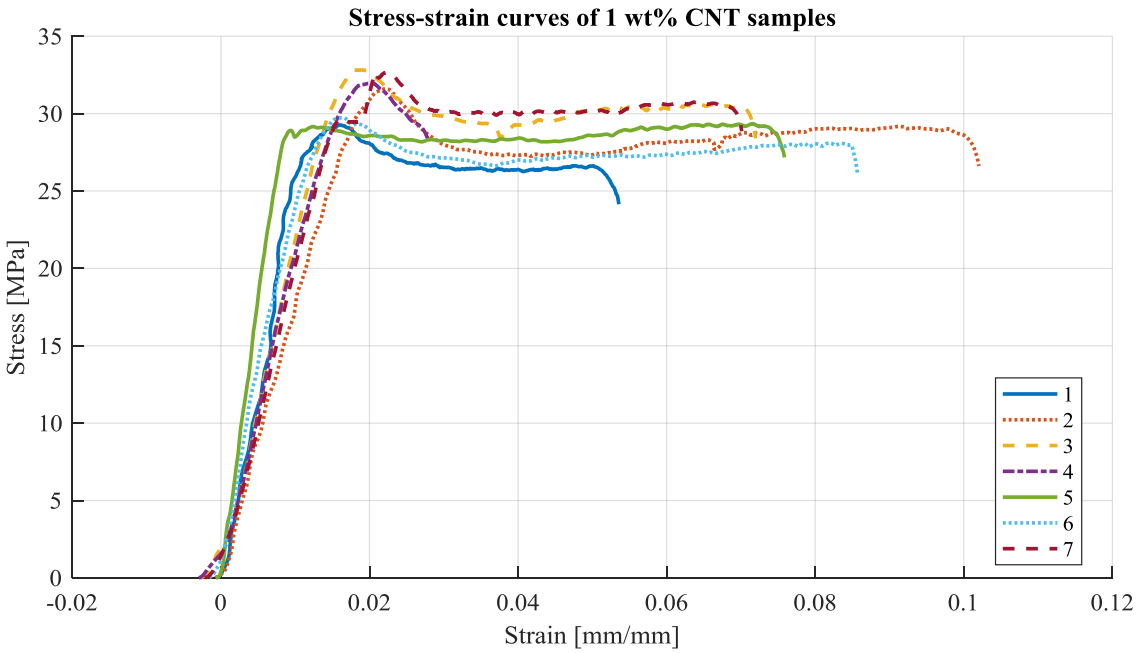

Figure 4.12: Stress-strain curves of printed ABS/1 wt% CNT samples

Figure 4.13 gives the fracture surfaces of the tensile test samples for ABS/ 1 wt% CNT. The printing quality and the density of the samples look very good. There are however some darker spots detectable within the beads, which are believed to be the small chunks of the masterbatch, which were not mixed well with pure ABS. In sample 5 image, a scale bar is introduced which shows the width and the height of one bead. The bigger masterbatch chunks have diameters of around 30 µm but the average size is below 10 µm. Even though there are these black dots, the strength has still increased compared to pure ABS, because most of the CNT were well dispersed.

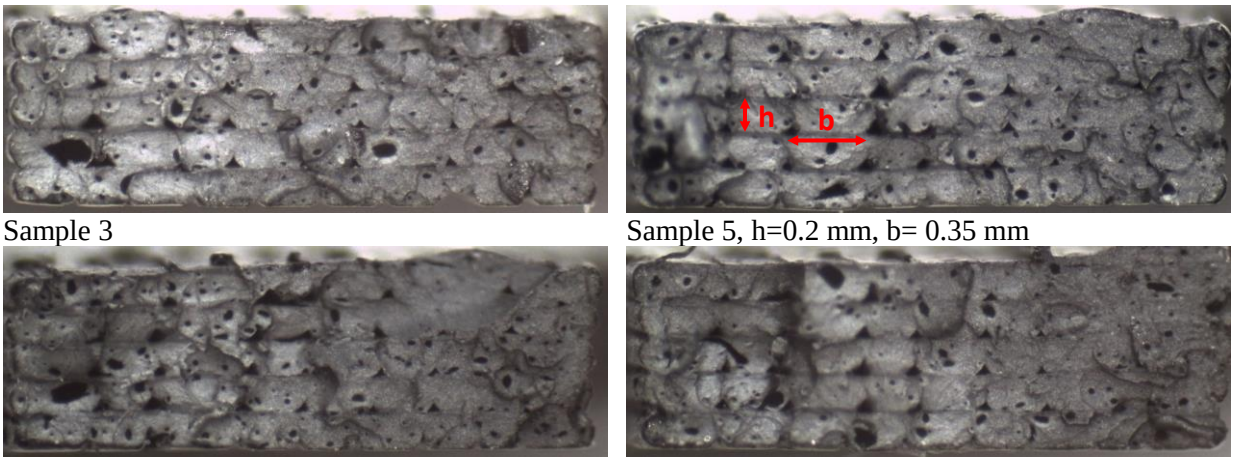

Sample 3 | Sample 5, h=0.2 mm, b= 0.35 mm

Sample 6 | Sample 7

Figure 4.13: Fracture surface of printed tensile test samples, ABS/1 wt% CNT

Printed ABS with 2 wt% CNT

The results of 2 wt% CNT nanocomposite are shown in Figure 4.14. Sample 6 is not valid because it slipped in the grips. Sample 7 did not break within the gauge length and is therefore not valid.

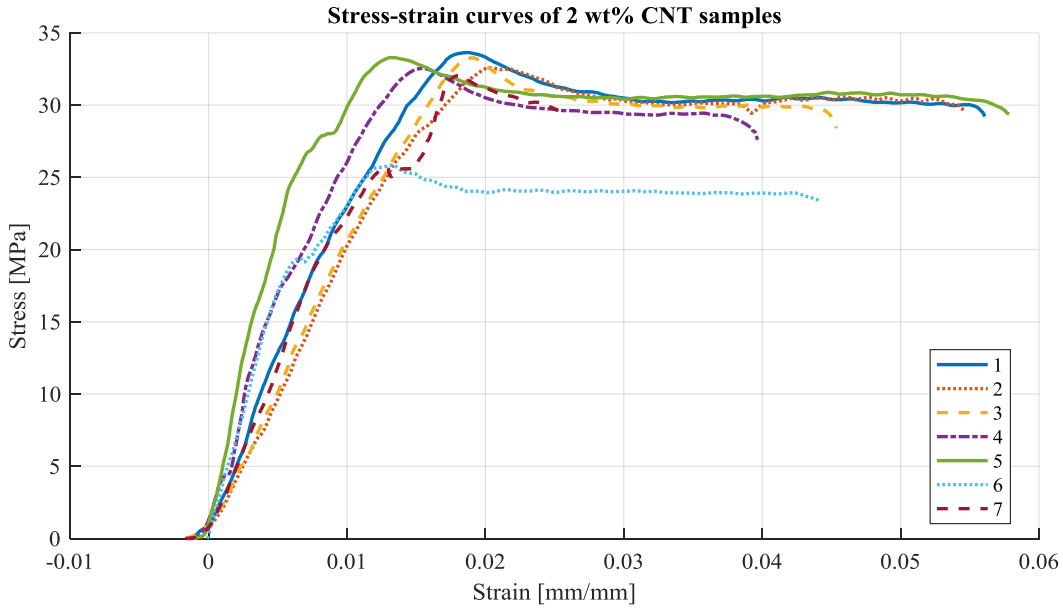

Figure 4.14: Stress-strain curves of printed ABS/2 wt% CNT samples

Figure 4.15 shows the fracture surfaces of the tensile test samples for printed ABS/2 wt% CNT. Compared to 1 wt% CNT, they appear a bit darker. This can either be because of the higher concentration of CNT or because there was less plastic deformation and thus less crazing which whitens the material. The elongation at break is about half of the ABS samples with 1 wt% CNT. Less dark spots or phases of the masterbatch are visible in this nanocomposite, compared to those in Figure 4.13. The print quality and density of the beads looked also good.

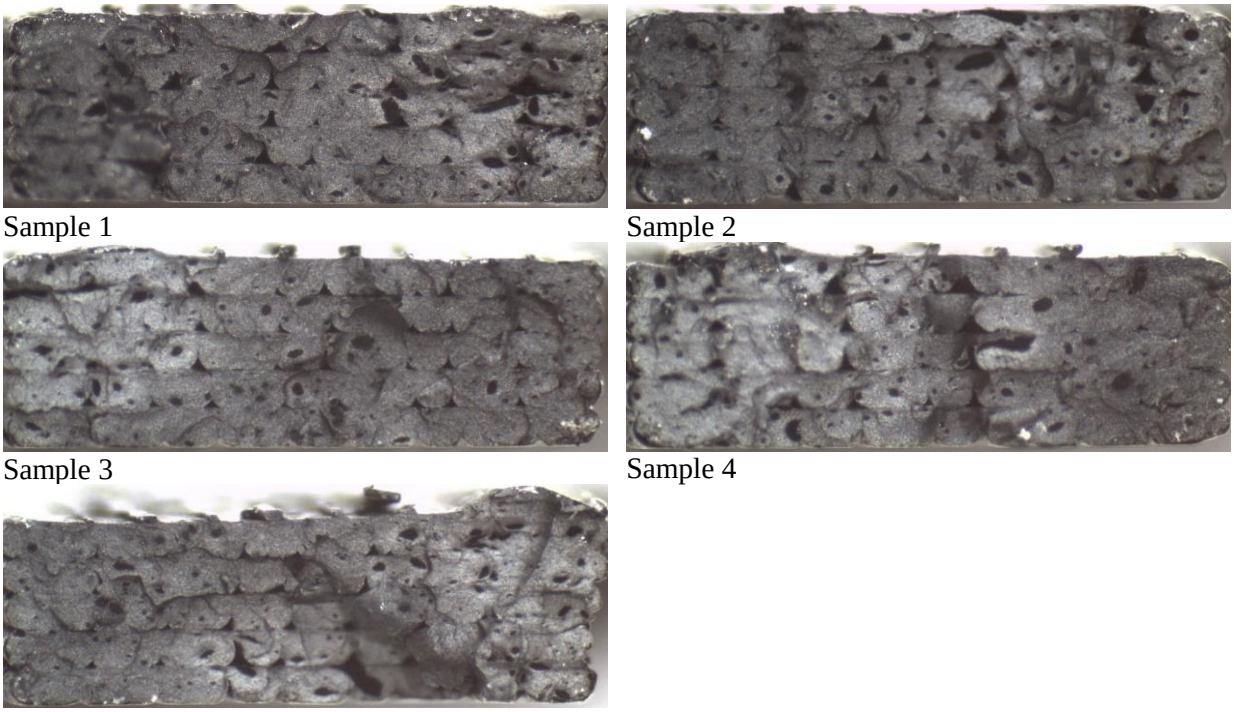

Sample 1 Sample 2

Sample 3 Sample 4

Sample 5

Figure 4.15: Fracture surface of printed tensile test samples, ABS/2 wt% CNT

Printed ABS with 3 wt% CNT

The tensile test results for ABS with 3 wt% CNT are presented in Figure 4.16. The results from samples 5, 8, and 9 were not used because they had massive slippage. Also with sample 7, something was wrong. It has a large deviation to the other samples and was therefore not counted. More replication for the future investigating are suggested.

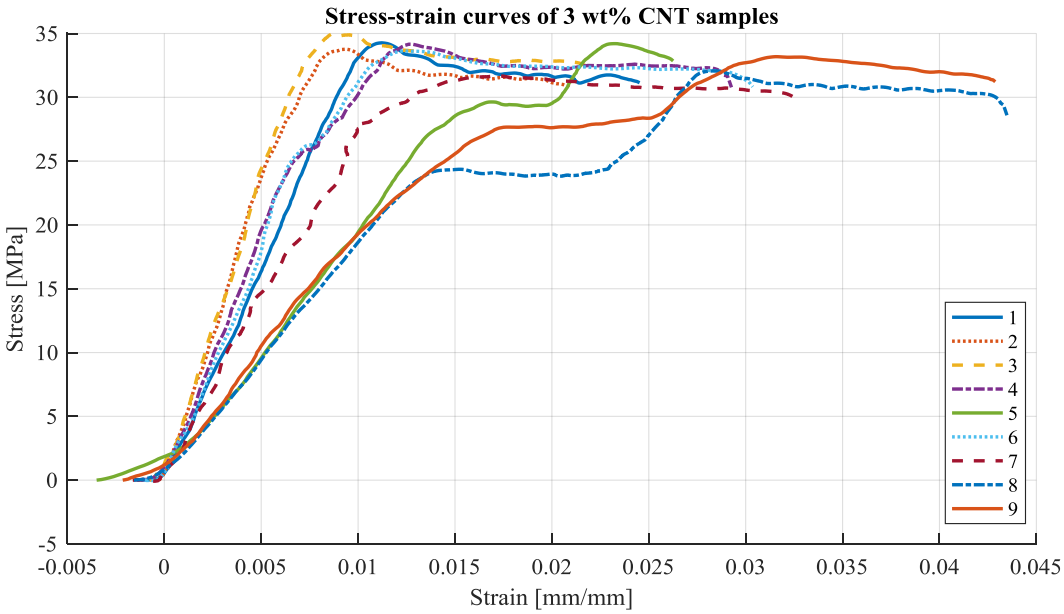

Figure 4.16: Stress-strain curves of printed ABS/3 wt% CNT samples

The fracture surfaces of the tensile test samples with 3 wt% CNT are shown in Figure 4.17. These samples look again darker than the previous ones with 2 wt% CNT, because of the same reason. There are still phases of the masterbatch visible, but the strength did increase regardless of that. The printing quality of these samples does not look much different from the previous samples and is good.

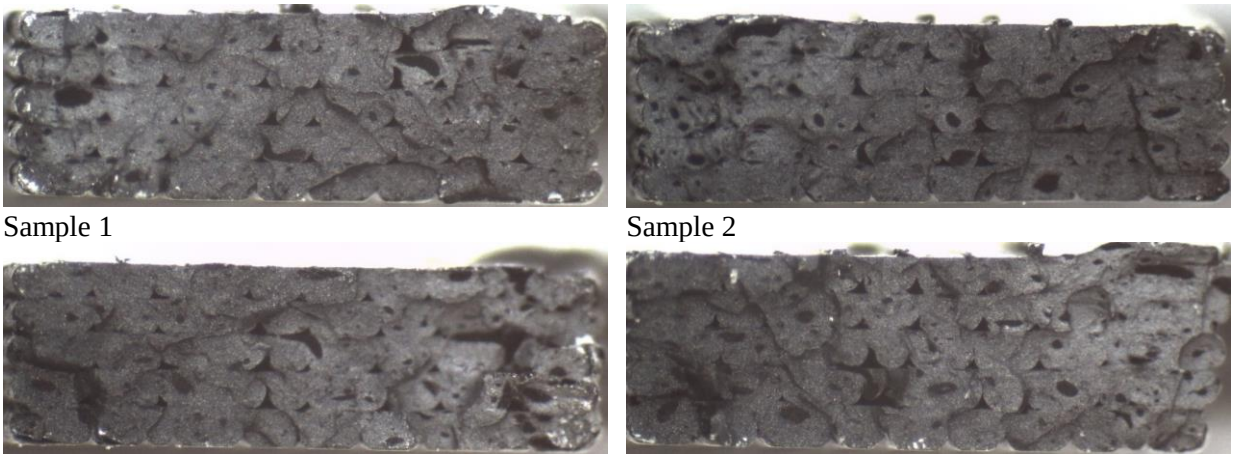
Sample 1 Sample 2

Sample 3 Sample 6

Figure 4.17: Fracture surface of printed tensile test samples, ABS/3 wt% CNT

Printed ABS with 5 wt% CNT

The tensile test results of the ABS samples with 5 wt% CNT are presented in Figure 4.18. Samples 1 and 10 were not used for further comparison because they broke too early. Samples 6, 7, and 8 had slippage and are not counted too. Sample 5 looks very good although the stiffness seems unreasonable because the deviation from the other samples was big. However, because it is not likely to measure a too high stiffness, this sample was included.

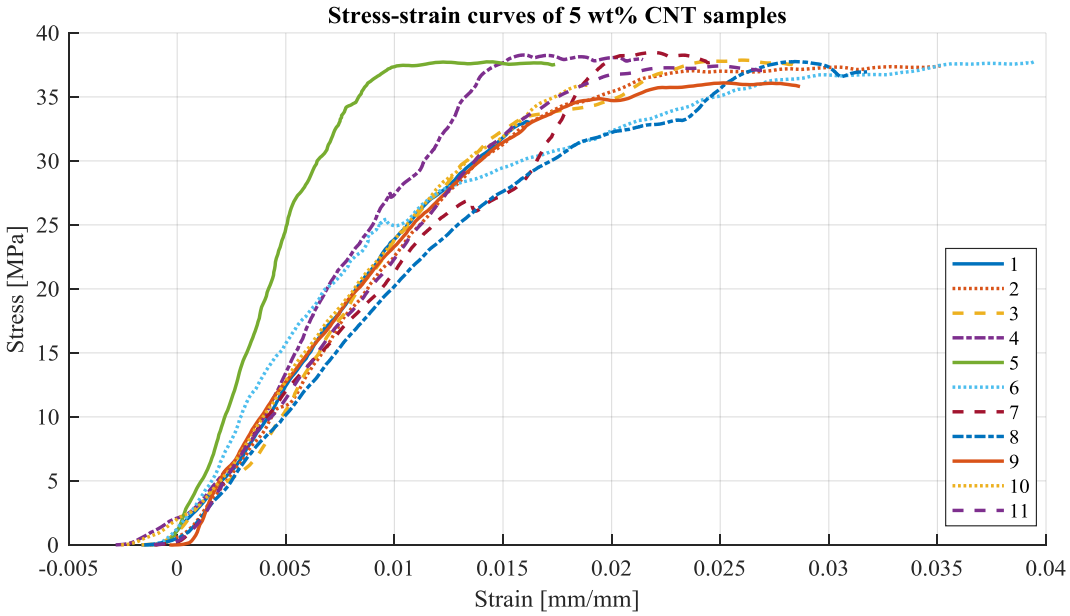

Figure 4.18: Stress-strain curves of printed ABS/5 wt% CNT samples

Figure 4.19 shows the tensile test sample fracture surfaces of ABS with 5 wt% CNT. Darker phases of the masterbatch are much rarer within this nanocomposite. The printing quality and the voids between the printed lines is about the same as for the previous samples. The fracture surface color is darker because of the higher concentration of CNT.

Sample 2

Sample 3

Sample 4

Sample 5

Figure 4.19: Fracture surface of printed tensile test samples, ABS/5 wt% CNT

Printed ABS with 10 wt% CNT

The results of 10 wt% CNT nanocomposite are shown in Figure 4.20. With this CNT concentration, the material is very brittle and difficult to print. The nozzle of the printer clogged many times. Only sample 3 is not included for further comparison. These samples showed higher ultimate tensile strength than the nanocomposites with lower CNT concentrations, but their brittleness limits their strengths.

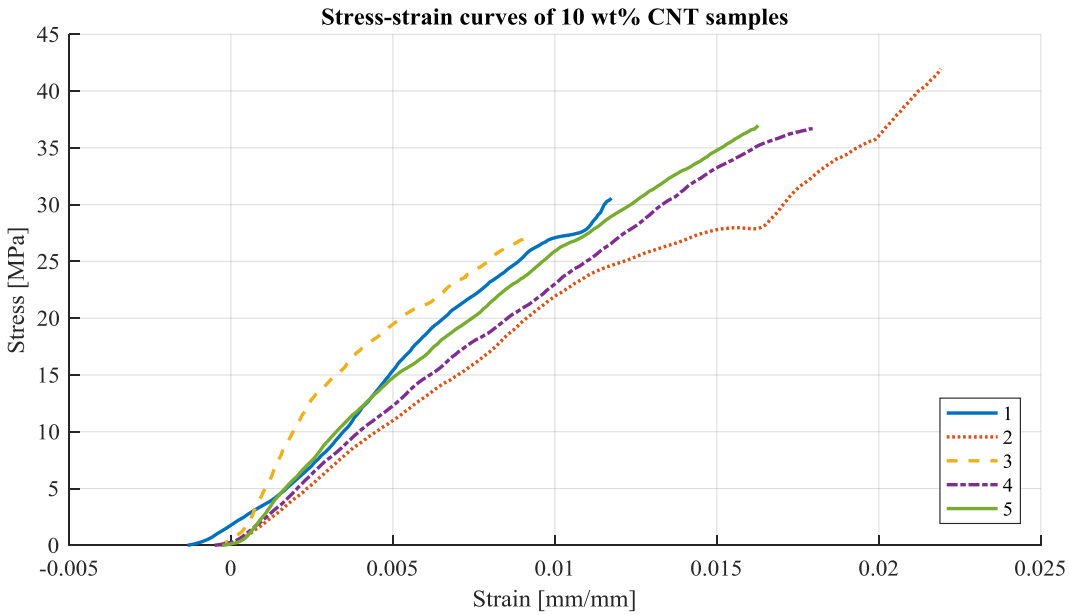

Figure 4.20: Stress-strain curves of printed ABS/10 wt% CNT samples

None of the samples broke in the gauge section although the quality of the prints looks good as visible in Figure 4.21. Sample 5 was only four layers high because the nozzle clogged but it was still tested. No phases of the masterbatch are visible. That is probably due to the very long residence time during the filament fabrication for ABS/10 wt% CNT nanocomposite.

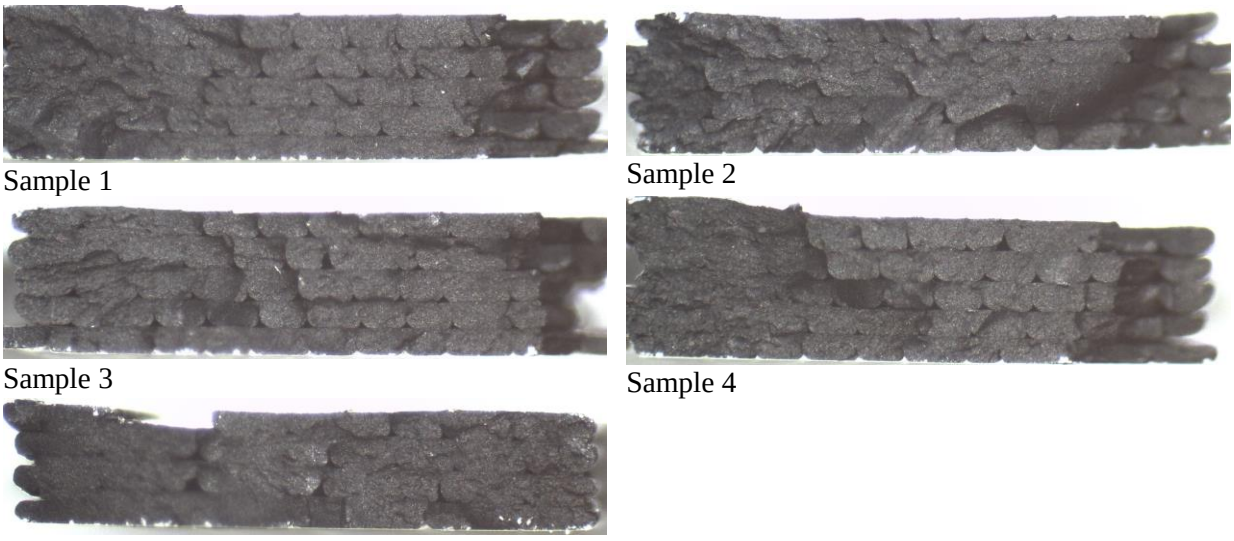

Sample 1

Sample 2

Sample 3

Sample 4

Sample 5

Figure 4.21: Fracture surface of printed tensile test samples, ABS/10 wt% CNT

4.4. Comparison

Figure 4.22 compares all the tensile test results of the printed samples. The ultimate tensile strength increases linearly with increase in CNT concentration. Up to 5 wt% CNT, the percentage increase in the ultimate tensile strength is about 5 times of the weight percentage of the filler. If the samples with 10 wt% CNT wouldn't have broken too early due to brittleness, they could have reached 50% increase in strength which is 45 MPa. If the adhesion between the ABS matrix and the CNT is good, they strengthen the material by preventing molecular chains from moving.

The Young's Modulus could not be measured very accurately as described earlier, but there is a clear trend that it increases quite drastically until 3 wt% CNT. The nanocomposite with 3 wt% CNT content has double the stiffness of pure ABS. At 5 wt% and 10 wt% CNT content, the stiffness is about the same as for 1 wt% CNT. The stiffness increases when CNTs have good adhesion to the ABS matrix and are aligned in loading direction. Because they are very stiff, they themselves and the surrounding polymer do not elongate as much as the overall matrix and thus enhances the stiffness of the composite.

As the CNT content increases, the material becomes more brittle and it allows less plastic deformation. The CNTs prevent the molecular chains from moving so that they rupture earlier. Another reason can be that there are agglomerations of CNT, which do not deform plastically and form voids during tension, causing stress concentrations, which lead to earlier fracture of the samples.

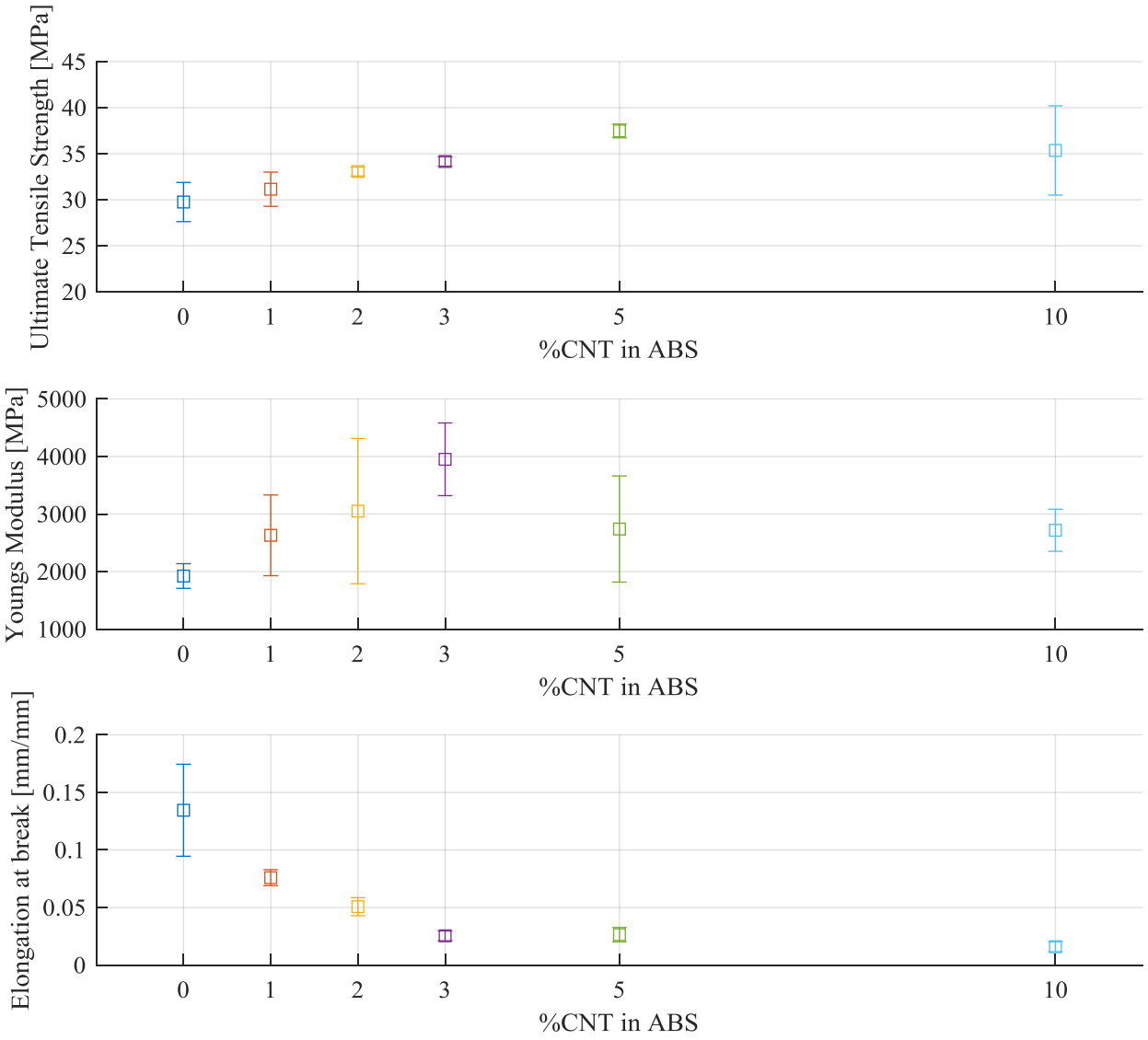

Figure 4.22: Comparison of the tensile test results of all printed ABS/CNT samples

4.5. Further experiments

Temperature analysis for pure ABS

Different nozzle temperatures for printing (p) and plate temperatures for the hot press (HP) were analyzed. The tensile test results are summarized in Figure 4.23. Because a printing temperature of 275 °C is very high for pure ABS, 240 °C was also tried. The strength is higher

with the lower temperature. This could be because some of the molecular chains already separated and the molecular weight dropped because of slight degradation at high temperatrue. With shorter chains, the entanglement of the molecules is lower and therefore the strength of the material decreases. If the higher stiffness of the ABS printed at 275 °C is not due to measurement inaccuracy, it could be because in a hotter nozzle the molecular chains can more easily orient themselves and align in flow direction. This would cause a higher stiffness. In general, the difference is not significant also regarding the overlapping error bars.

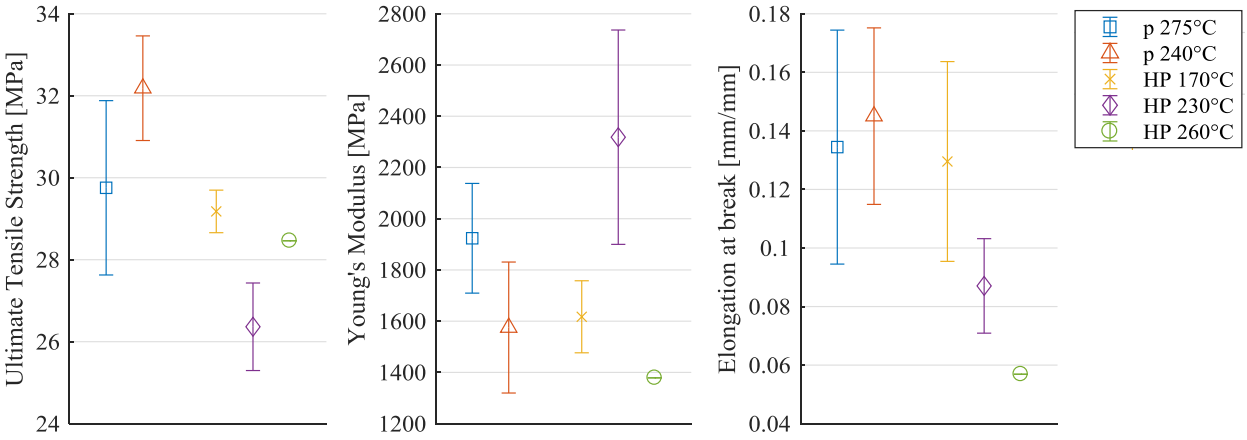

Figure 4.23: Comparison of different processing temperatures of pure ABS samples

The strength results of the hot-pressed samples can have the same reasons as for the printed ones. With higher temperature, more degradation and chain shortening can happen. At 260 °C, only one sample was tested, because most of these samples had bubbles caused by outgassing, and even the color changed a little from white to yellow because of degradation. Maybe it has a higher strength because the cross section is bigger than for the other two hot-pressed samples. I could not find another explanation why the stiffness of the samples at 230 °C is so much higher other than measurement inaccuracy.

5. PIEZORESISTIVITY

5.1. Introduction

In this chapter, the piezoresistive performance of ABS/CNT nanocomposite is analyzed. The resistance of the samples was measured with a voltage divider circuit while stretching them in the tensile test machine.

Voltage divider

To measure the resistance change in the samples during strain loadings, a standard voltage divider circuit was used as shown in Figure 5.1. The resistance R_1 is the sample whose resistance is unknown. R_2 is a resistor whose resistance is known. When applying a voltage V_{in} over the circuit of both resistors, the voltage is divided in the ratio of the two resistances. The sensitivity is the best if the value of R_2 is chosen as close to the resistance value of the sample as possible. The voltage V_{out} over R_2 can be measured and recorded and the resistance of the sample can then be calculated with the following formula: $R_1 = R_2 \left(\frac{V_{in}}{V_{out}} - 1\right)$.

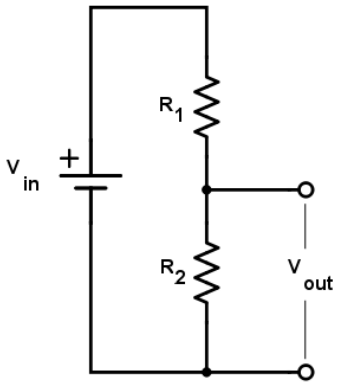

Figure 5.1: Voltage divider circuit

Gauge factor

To express the sensitivity of a strain sensing material, the gauge factor is often used. It is calculated by the resistance change ΔR over the initial resistance R_0 divided by the strain ε as below:

$$Gauge\ factor = \frac{\Delta R / R_0}{\varepsilon}$$

5.2. Experimental

A voltage divider circuit was built. Copper sheets were soldered on wires. One coming from one pole of the power supply and the other one leading to the next resistor. These copper sheets were clamped between the grips and the sample at the upper and lower clamps in the loadframe. The diamond surface coating of the grips was proven to be insulating, assuring no conduction within the tooling. The copper plates experienced slippage issue during loading. Grinding the copper plates to make them rougher did not help to prevent slippage. After that, a thick aluminum foil with a thickness of 0.08 mm was used. It did not penetrate the sample enough so that the clamping surface was limited to the foil surface area and thus not large enough to prevent slippage. The best solution was then to use a very thin aluminum foil of 0.01 mm thickness. With this foil, the sample was pressed over the entire surface area of the samples' grip section. With this setup, satisfactory stress-strain plots for the tensile tests could be obtained while measuring the resistance chance at the same time. The output voltage over the known resistor needed to be changed to get as close to half of the input voltage of 12 V as possible. This was done by changing the value of the known resistor. With the help of a breadboard, they could be switched in series to summarize the value of multiple resistors, or in parallel to divide the value.

5.3. Results and Discussion

The resistances of the printed tensile test samples with 1 and 2 wt% CNT were too high to be measured with the voltage divider circuit. At 3 wt% CNT, the resistance of some samples was low enough to measure. Measurements of nanocomposites with 5 and 10 wt% worked fine.

ABS with 3 wt% CNT

Figure 5.2 show the piezoresistivity results of the printed ABS/3 wt% CNT samples. The results showed a lot of noise. To be able to better analyze the resistance, a Savitzky-Golay filter was applied in Matlab software. Only samples below resistances of 10^8 Ω gave satisfactory results with a trend of increasing resistance. The change in resistance had the same magnitude as the noise of the signal itself. Because of that, the results need to be treated with caution for this composition.

Sample 1	Sample 2	Sample 3
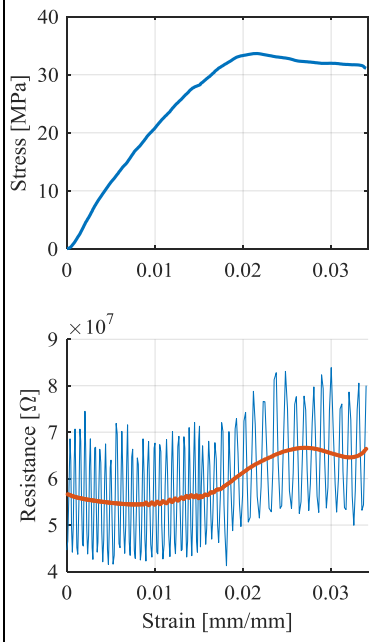	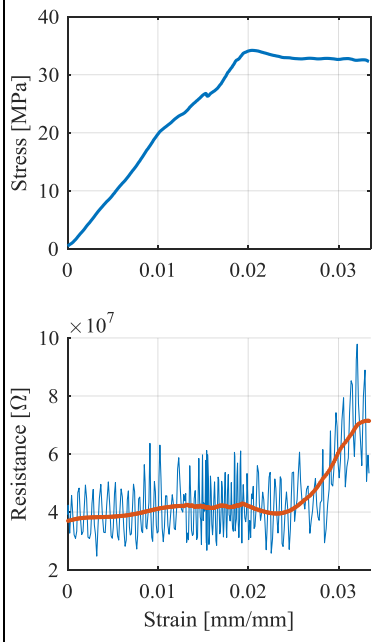	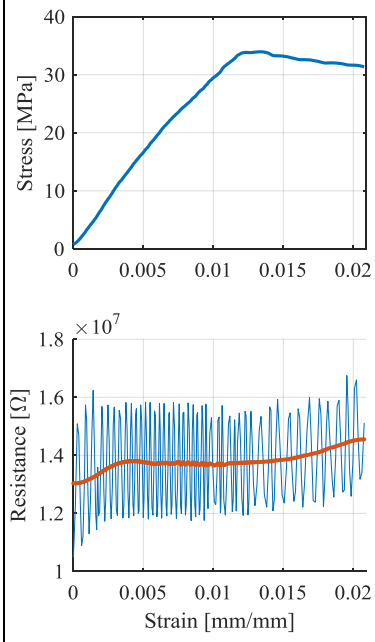
Absolute resistance change: 12.3 MΩ Gauge factor: 6.64	Absolute resistance change: 36 MΩ Gauge factor: 30.27	Absolute resistance change: 1.5 MΩ Gauge factor: 5.55

Figure 5.2: Piezoresistivity measurements of printed ABS/3 wt% CNT samples

ABS with 5 wt% CNT

Figure 5.3 shows the piezoresistivity measurements of printed ABS/5 wt% CNT samples. The resistance of the ABS/5 wt% CNT samples was significantly lower than that of ABS/3 wt% CNT samples (about three orders of magnitude). In this case, a proper electrical network was formed within the nanocomposite. The piezoresistivity of first three samples was measured with the thick aluminum foil as contact between the grips and the samples. The highest increase in resistance is when the samples start to deform plastically after reaching the ultimate tensile strength. The mechanism behind this is that the electrical paths are interrupted when the polymer matrix permanently deforms and the CNTs lose the connection to one another. This mechanism is more pronounced close to the percolation threshold. The lower increase in resistance in the elastic region can be explained through the tunneling effect. Electrons can flow from one CNT to another one through the polymer matrix if the CNT-to-CNT distance is small enough. With increasing the strain, the CNT-to-CNT distance increases and the tunneling effect is reduced and therefore the resistance increases. The piezoresistivity effect of the CNT themselves is assumed to be very small because they are very stiff.

Sample 1	Sample 2	Sample 3
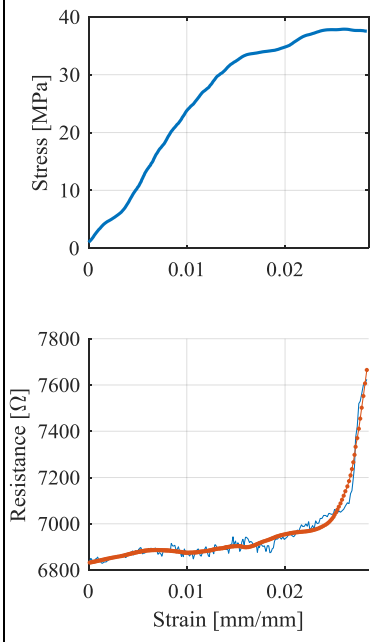	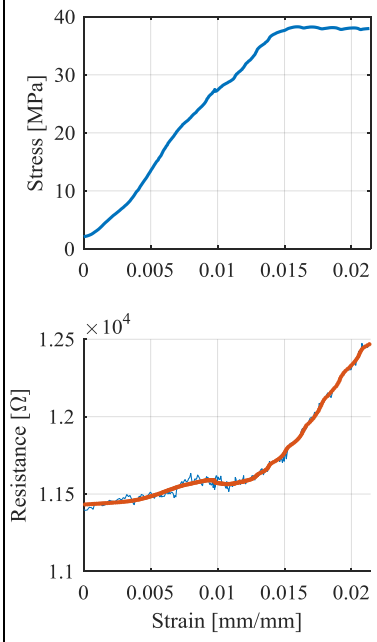	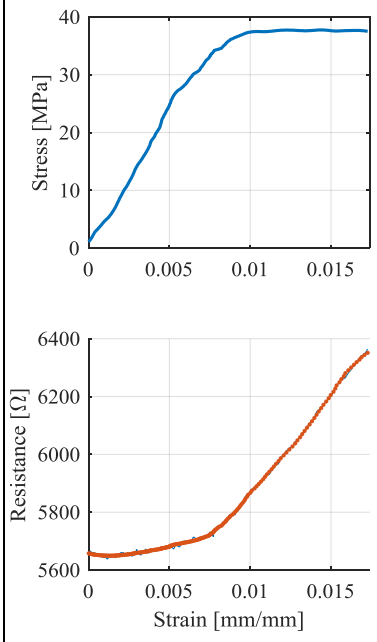
Absolute resistance change: 840.9 Ω Gauge factor: 4.32	Absolute resistance change: 1069 Ω Gauge factor: 4.37	Absolute resistance change: 701.6 Ω Gauge factor: 7.14

Figure 5.3: Piezoresistivity measurements of printed ABS/5 wt% CNT samples with thick aluminum foil

Samples 4 to 6 were printed a few days later than the first 3, but with the same parameters and they were tested using the thin aluminum foil as electrical contact. It is hard to say if this had an influence on the piezoresistivity measurement. It looks like the gauge factor of these samples is slightly lower.

Sample 4	Sample 5	Sample 6
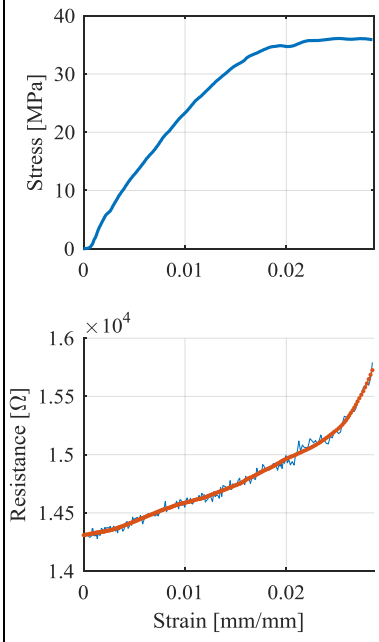	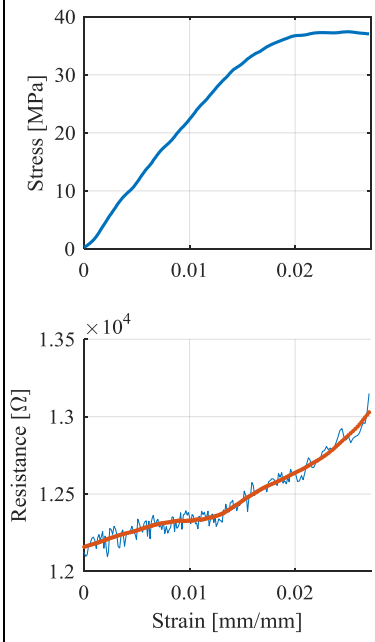	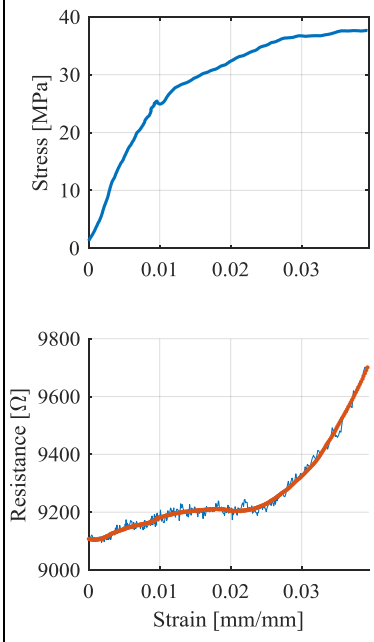
Absolute resistance change: 1426 Ω Gauge factor: 3.48	Absolute resistance change: 895.5 Ω Gauge factor: 2.72	Absolute resistance change: 595.6 Ω Gauge factor: 1.66

Figure 5.4: Piezoresistivity measurements of printed ABS/5 wt% CNT samples with thin aluminum foil

The repeatability of the piezoresistivity tests showed a relatively high scatter, although the mechanical properties of the samples did not change as much. Every sample had its own specific gauge factor. For a better application of this material for sensing purposes, it would need a more stable gauge factor. Further studies would be required to optimize the gauge factor with varying printing conditions.

ABS with 10 wt% CNT

Figure 5.5 gives the piezoresistivity results of the printed ABS/10 wt% CNT samples. The resistance of these samples was below 10 Ω. The change in resistance was quite low for all the samples because they only deformed elastically. No plastic deformation in ABS samples loaded with 10 wt% CNT occurred, as they became brittle. Therefore, the gauge factor was much lower than that for the previous CNT contents. However, the repeatability of measured gauge factor was increased, due to the formation of more robust conductive paths. For some samples, the change in resistance was also not as linear as the deformation of the material.

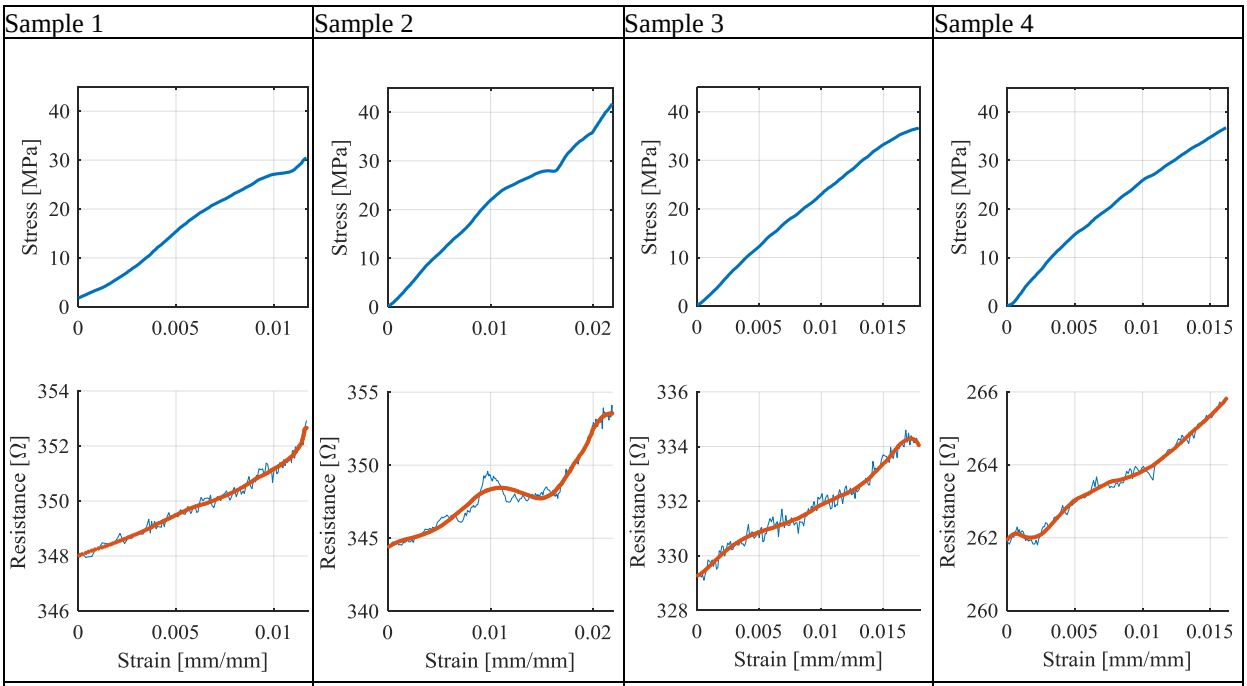

Figure 5.5: Piezoresistivity measurements of printed ABS/10 wt% CNT samples

5.4. Comparison

When comparing the gauge factor results for different ABS/CNT nanocomposites (Figure 5.6), it is apparent that the sensitivity decreases with increasing CNT content. In printed samples with low CNT content, it is difficult to have conductive samples, but they have a better gauge factor. This is because there are fewer conductive paths within the nanocomposite and if a few of them are interrupted during sample stretching, the increase in resistance becomes more significant.

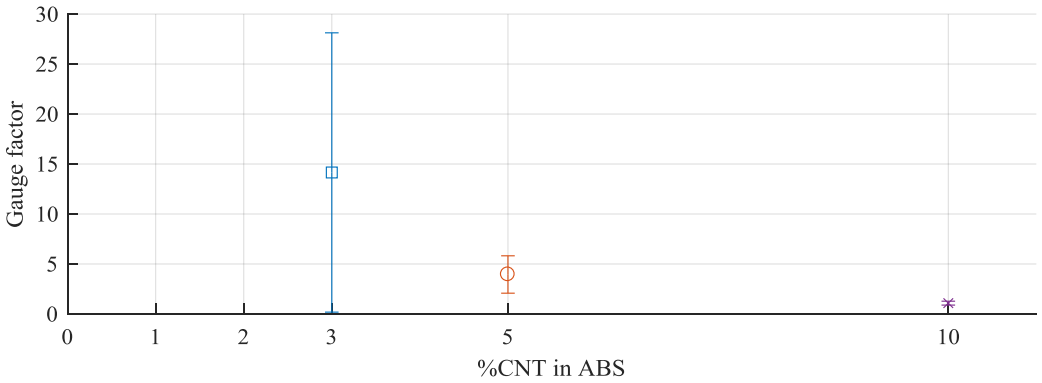

Figure 5.6: Comparison of the gauge factor for samples with 3, 5, and 10 wt% CNT

These results show that by simply measuring the resistance in a component out of ABS/CNT nanocomposite, a change in the loading of the part can be sensed without additional strain gauges. Also, as the slope of the resistance-strain curve increases when the sample starts to deform plastically, the start of plastic deformation can also be detected, which could be helpful to trigger an alarm before a part fails. Therefore, these nanocomposites may be used as a self-sensing material, which makes structural health monitoring possible without big efforts.

However, for strain sensing applications, the elastic part is most important, before the ultimate tensile strength is reached, because the sensors are not meant to be damaged during application. In the elastic region, the resistance change rate is much lower which is unfavorable.

6. FRACTURE TESTS

6.1. Introduction

This chapter covers the investigation of the influence of CNT on the fracture behavior of FFF printed ABS parts. To the best of the authors' knowledge, no studies have yet been conducted about this topic. Because the inter-layer bonding is the weakness of the FFF process, research about this matter is needed and important.

6.2. Experimental

The fracture tests were performed according to the standard ASTM D5045-14 (Standard Test Methods for Plane-Strain Fracture Toughness and Strain Energy Release Rate of Plastic Materials). This method is designed to characterize the toughness of plastics in terms of the critical-stress-intensity factor, K_{Ic}, and the energy per unit area of crack surface or critical strain energy release rate, G_{Ic}, at fracture initiation. Compact Tension (CT) specimens were fabricated using a FFF 3D printer (printer specification in appendix). Because a plane strain state is required by the standard, the specimen thickness must be sufficient to ensure this stress state is satisfied. The tested material was pure ABS and ABS/CNT nanocomposites filled with 1 wt%, 2 wt%, 3 wt%, and 5 wt% CNT content.

Sample preparation

The compact tension samples were designed according to the ASTM standard. The configuration of the specimen is presented in Figure 6.1. B is the thickness of the specimen, W is the width and $W=2B$, and a is the crack length and shall be selected such that $0.45 < a/W < 0.55$. Two sizes were initially designed one with B=10 mm and one with B=15 mm.

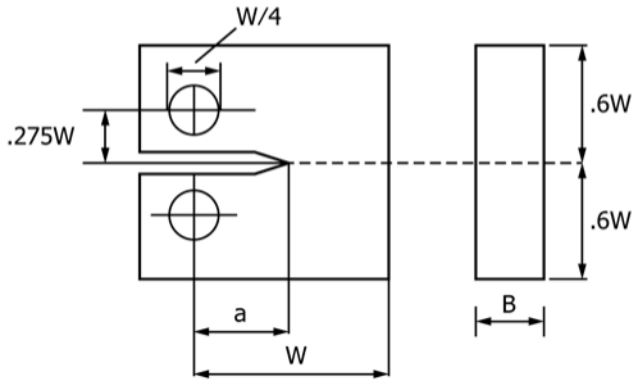

Figure 6.1: Compact Tension Specimen configuration

The samples were printed with a rectilinear infill without perimeter. The line direction was selected parallel to the crack growth direction. A 0.5 mm nozzle diameter was used with a line width of 0.35 mm and a layer height of 0.2 mm (same as the conditions for the tensile test samples). The temperature of the nozzle was set to 275 °C and the printing bed temperature was kept at 105 °C. The printing speed was 50 mm/s. The notches were already included in the design of the printable samples. A support structure was printed within the notch. After removal of the support structure, a sharp precrack was initiated by inserting a fresh cutter blade and tapping for all the thin samples (B=10 mm). For the thick samples (B=15 mm), another longer cutter blade was used to saw across the notch root, which was less sharp than the cutter for B=10 mm samples.

Fracture testing

The samples were tested at 24 °C with a loading rate of 10 mm/min (0.167 mm/s) with the same machine as used for the tensile testing. Four bent sheet metal strips of 0.6 mm thickness were clamped between the grips and two steel rods were used as the loading pins, which could be slid through them and the holes of the samples as shown in Figure 6.2. For the samples with 10 mm thickness, steel nails with 2.7 mm diameter were used. The 15 mm thick samples used steel rods

of 6.33 mm diameter. During testing, the load and the displacement were recorded. After fracture, the crack length including the cutter notch, the width, and the thickness were measured.

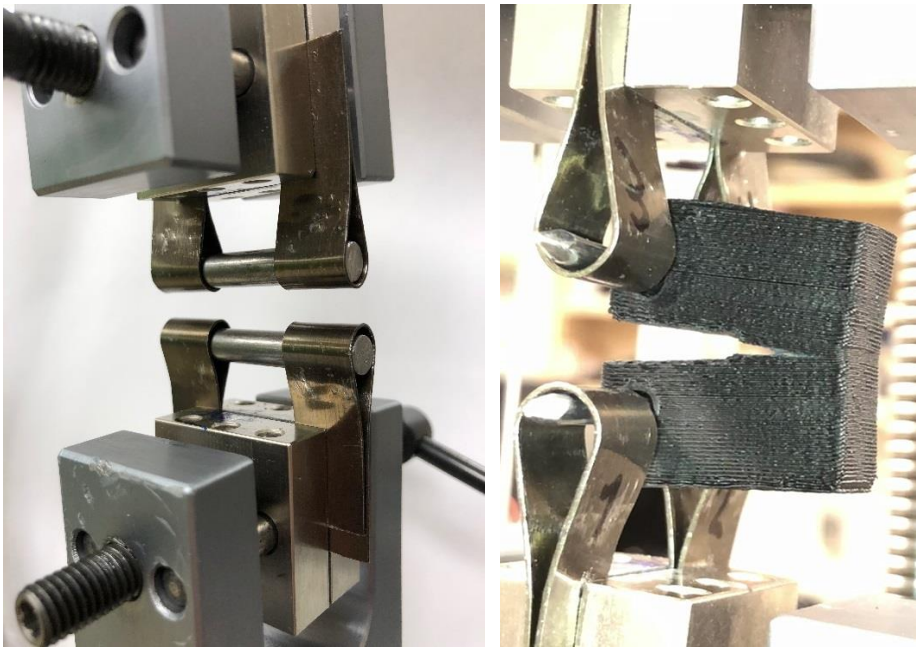

Figure 6.2: Compact tension sample holding set-up for fracture tests

Calculation of K_{Ic}

The data, load and displacement, was analyzed with Matlab. The Matlab script can be found in the appendix. The maximum load P_{max} was deduced and a line was fitted to the straight section in the beginning to determine the initial compliance, C. C is the reciprocal of the slope of this line. A second line with a compliance 5% greater is drawn on the same graph. If P_{max} falls within these two lines, then this value is used for further calculations. If P_{max} is outside, the intersection of the second line with the curve is P_Q and used for further calculations. P_{max}/P_Q should be smaller than 1.1. Otherwise, the test is invalid.

After the load was analyzed, the critical stress intensity factor K_Q is calculated with

$$K_Q = \left(P_Q / BW^{1/2}\right) f$$

where f is a function of *x*, *x=a/W*.

$$f = \frac{(2+x)\cdot(0.886 + 4.64\cdot x - 13.32\cdot x^2 + 14.72\cdot x^3 - 5.6\cdot x^4)}{(1-x)^{3/2}}$$

K_Q needs to be checked for validity with the following formula

$$2.5\left(K_Q/\sigma_y\right)^2$$

where σ_y is the yield stress obtained from a uniaxial tensile test. In this thesis, the tensile test results from chapter 4.3 were used, which are 29.75 MPa for pure ABS, 31.14 MPa for ABS/1 wt% CNT, 33.07 MPa for ABS/2 wt% CNT, 34.16 MPa for ABS/3 wt% CNT, and 37.47 MPa for ABS/5 wt% CNT nanocomposites, tested at a speed of 0.02 mm/s. The value obtained from this equation should be smaller than *B*, *a*, and (*W*-*a*).

Calculation of G_{Ic}

There are two ways to calculate the critical strain energy release rate G_{Ic}. The first one is via the energy derived from the integration of the load versus load-point displacement curve. A displacement correction for the system compliance is required. It accounts for the loading-pin penetration and the specimen compression. An un-cracked specimen prepared from the same material and tested under the same condition and with the same testing parameters is loaded to higher force values than that for the cracked samples. The area under the load-displacement curve until P_Q is the energy, U_Q. The indentation energy U_i is calculated from the load-displacement curve of the un-cracked sample up to the load P_Q of the respective sample. The indentation energy is subtracted from the energy of the sample to get the net strain energy as:

$$U = U_Q - U_i.$$

With the energy U, the strain energy release rate G_Q can be calculated as follows:

$$G_Q = U/(B \cdot W \cdot \varphi),$$

where φ is an energy calibration factor computed from:

$$\varphi = \frac{(1.9118 + 19.118x - 2.5122x^2 - 23.226x^3 + 20.54x^4)(1-x)}{(19.118 - 5.0244x - 69.678x^2 + 82.16x^3)(1-x) + 2(1.9118 + 19.118x - 2.5122x^2 - 23.226x^3 + 20.54x^4)}$$

The other way to calculate G_{Ic} is with the following formula:

$$G_{Ic} = \frac{(1-\nu^2) \cdot {K_{Ic}}^2}{E}$$

In this method, the difficulty is to obtain a precise Young's modulus E. It must be obtained at the same temperature and strain rate conditions as those of the fracture test because of the viscoelastic effects of plastics. In the case of this thesis, the E values were taken from the tensile tests in chapter 4.3, which are 1924 MPa for pure ABS, 2630 MPa for ABS/1 wt% CNT, 3051 MPa for ABS/2 wt% CNT, 3951 MPa for ABS/3 wt% CNT, and 2740 MPa for ABS/5 wt% CNT nanocomposites. The printing conditions of the fracture samples were not exactly the same as those of the tensile samples because the fracture samples were larger. In addition, the used tensile test machine could not provide repeatable stiffness measurements at different load levels. Because of these uncertainties of this procedure, it is preferable to determine G_{Ic} directly from the energy, which is G_Q here.

To cross check the accuracy of the second method, the tensile modulus E and Poisson's ratio ν can be calculated from the corrected compliance C_c, using the following equation:

$$[E/(1-\nu^2)] = \frac{2f^2\varphi}{B \cdot C_c}$$

The corrected compliance C_c is obtained from the measured compliance C_Q in the fracture test minus the compliance from the indentation test C_i. $[E/(1-\nu^2)]$ can also be calculated from

K_{Ic}^2/G_{Ic}. When calculated with the corrected compliance, it should be larger but not more than 15 %.

6.3. Results and Discussion

Pure ABS samples with *B*=15

The results of the 15 mm thick pure ABS samples are presented in Table 6.1. The fracture toughness of sample 1 and 2 is much higher than that of sample 3 and 4. The last two samples were printed later and the actual filament diameter was smaller than the diameter entered into the slicer software. This resulted in a lower extrusion flow rate, less pressure at the nozzle output and worse adhesion of the layers as visible in Figure 6.3.

Table 6.1: Fracture results of pure ABS with 15 mm thickness

	Sample number	1	2	3	4
Fracture Test Parameters	W [mm]	29.76	30.04	30.03	29.92
	a [mm]	14.54	15.24	14.73	14.70
	B [mm]	14.5	14.5	14.6	14.5
	P_{max} [N]	765.3	677.6	336.2	418.7
	P_Q [N]	732.0	674.0	336.2	404.0
	Crack growth	Stable	Stable	Unstable	Unstable
	K_{Ic} [MPa$\sqrt{m}$]	**2.73**	**2.65**	**1.25**	**1.52**
	U_Q [J]	0.6434	0.6202	0.1669	0.2249
	U [J]	0.4378	0.4425	0.1091	0.1517
	G_{Ic} [kJ/m^2]	**3.3991**	**3.2028**	**0.7091**	**1.0470**
	G_Q [kJ/m^2]	**5.0379**	**5.1475**	**1.2383**	**1.7409**
Validity Checks	P_{max}/P_Q	1.05	1.01	1.00	1.04
	$2.5(K_Q/\sigma_y)^2$	21.05	19.84	4.39	6.48
	$E/(1-\nu^2)$ via C [MPa]	1892.5	1649.6	1248.1	1403.3
	$E/(1-\nu^2)$ via K_Q^2/G_{Ic} [MPa]	2192.6	2192.6	2192.6	2192.6

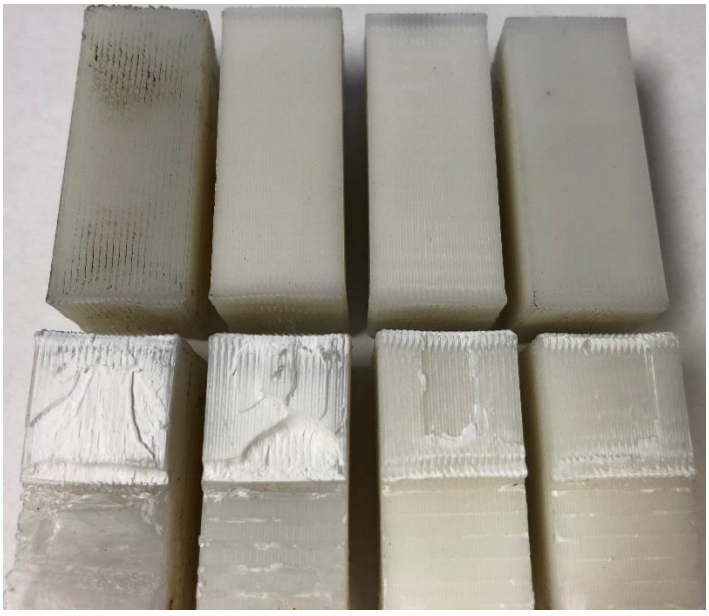

Figure 6.3: Fracture- and top-surfaces of pure ABS samples with 15 mm thickness

The order of the fracture samples in Figure 6.3 and in all the coming figures of the fracture samples is the same. Starting on the left side is sample number 1. The sample number increases when going to the right side. When looking at the samples in Figure 6.3, it is apparent that in sample 1 and 2 crazing happened and the crack formed stably and plastically. In samples 3 and 4, the individual printing lines are clearly visible and they didn't stick to each other as well. The top surfaces and the sides of sample 1 and 2 are not as smooth, an indication of over-extrusion.

Pure ABS samples with *B*=10

The fracture results of pure ABS samples with a thickness of 10 mm are presented in Table 6.2. Sample 1 and 4 have lower K_{Ic} and G_Q values than the other samples. The reason is the same as for the thicker samples. The extrusion flow rate was lower because of the inconsistent filament diameter. These differences are more pronounced in the strain energy release rate.

Table 6.2: Fracture results of pure ABS with 10 mm thickness

	Sample number	1	2	3	4	5	6
Fracture Test Parameters	W [mm]	19.30	19.38	19.48	19.45	19.50	19.60
	a [mm]	10.18	10.13	9.90	10.03	10.05	9.93
	B [mm]	9.5	9.6	9.7	9.6	9.6	9.7
	P_{max} [N]	209.0	326.7	349.1	282.4	299.8	356.5
	P_Q [N]	208.9	324.3	348.5	282.4	299.8	356.1
	Crack growth	Unstable	Stable	Stable	Stable	Stable	Stable
	K_{Ic} [MPa$\sqrt{m}$]	**1.67**	**2.52**	**2.55**	**2.14**	**2.27**	**2.59**
	U_Q [J]	0.1384	0.2906	0.3438	0.2263	0.2560	0.3452
	U [J]	0.0778	0.1734	0.2112	0.1330	0.1539	0.2072
	G_{Ic} [kJ/m^2]	**1.2687**	**2.8912**	**2.9671**	**2.0883**	**2.3431**	**3.0487**
	G_Q [kJ/m^2]	**2.2056**	**4.8117**	**5.6693**	**3.6454**	**4.2060**	**5.5189**
Validity Checks	P_{max}/P_Q	1.00	1.01	1.00	1.00	1.00	1.00
	$2.5(K_Q/\sigma_y)^2$	7.86	17.91	18.38	12.93	14.51	18.88
	$E/(1-\nu^2)$ via C [MPa]	1146.8	1473.6	1287.9	1353.1	1316.3	1374.0
	$E/(1-\nu^2)$ via K_Q^2/G_{Ic} [MPa]	2192.6	2192.6	2192.6	2192.6	2192.6	2192.6

Figure 6.4: Fracture- and top-surfaces of pure ABS samples with 10 mm thickness

When looking at Figure 6.4, especially sample 1 does not show crazing at all and the crack growth was unstable, indicating that the layers became separated from one another quite easily, before the stress levels reached for plastic deformation.

Comparison of the thickness *B*=15 with *B*=10

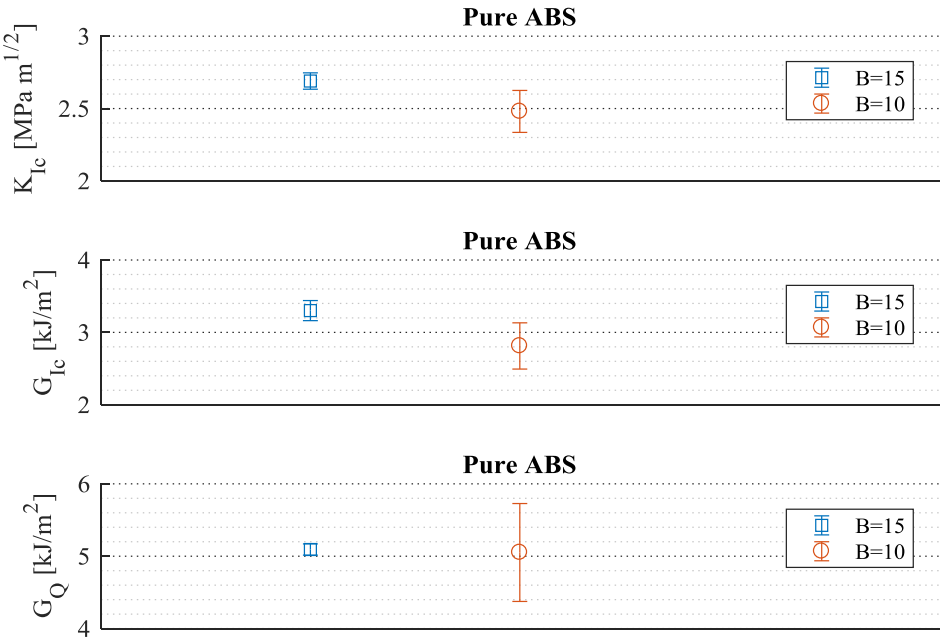

Figure 6.5: Comparison of the fracture toughness of ABS samples with 10 and 15 mm thickness

The critical stress intensity factor and critical strain energy release values of pure ABS samples with different thicknesses are compared in Figure 6.5. Not much attention was paid to the G_{Ic} values because their calculation procedure is less accurate. Only two of the 15 mm thick pure ABS samples were taken for this comparison because the fracture of the other samples were not stable. The two thicker pure ABS samples reached slightly higher K_{Ic} values than the ABS samples with *B*=10. Interestingly, this trend is not observable when looking at the G_Q values, which seem to be independent of the thickness. K_{Ic}, G_{Ic}, and G_Q should be geometry independent, which was the case in this experiment.

With the validity criteria, a plain strain condition should be assured, but also a sharp-crack condition at the tip of the crack and an adequate size of the specimen are important to give a linear elastic behavior. The criteria P_{max}/P_Q was always satisfied. The reason for this can be found when

looking at the load-displacement curves. Once the crack opened, the load dropped quite quickly and there was not a long plastic opening of the crack. In most of the cases, the criteria $2.5(K_Q/\sigma_y)^2$ was not met no matter how thick the samples were. It was met only for the samples with the low K_{Ic} values, which had bad layer adhesion and unstable crack growth resulting in unreasonably low K_{Ic} values. The reason is that even with a large thickness of 15 mm, a plain strain condition cannot be assured in the printed samples, because there are always voids between the printing lines, which give room for out-of-plane deformation and therefore the strain is not zero in the out-of-plane direction. The validity criterion with the calculation of $E/(1-\nu^2)$ with the corrected compliance should be bigger than the one calculated with K_Q. This was not the case for all the samples tested, meaning that the calculation of the critical strain energy release rate G_{Ic} with the Young's modulus and the Poisson's ration is not very accurate. Therefore, not much attention is spent on this value.

The pure ABS samples were the first ones printed. With the results of these samples, a decision needed to be made with which thickness the rest of the samples should be printed. The small samples only needed 2.5 m of filament whereas the big ones needed about 8 m. Also, the printing time was much longer for thicker samples. The first few samples have shown that the extrusion flow rate of the printer has a much bigger influence than the sample size. Because the plane strain condition can anyway not be guaranteed in the printed samples, the sample size of 10 mm and 15 mm would not provide a difference, as both of them give sufficiently large number of lines, which is the characteristic of the printed structures. In addition, a paper was found stating that the fracture toughness of ABS is independent of the thickness between 10 and 15 mm [71]. Therefore, a thickness of 10 mm was used for most of the samples for the rest of the study. If the filament diameter varies, samples with different extrusion flow rates can be tested and analyzed.

ABS with 1 wt% CNT, *B*=15

The only nanocomposite which was also produced with a thickness of 15 mm was ABS with 1 wt% CNT. The fracture results of this nanocomposite are presented in Table 6.3. Only sample 4 had a smaller extrusion flow rate, resulting in unstable crack growth and a lower fracture toughness value. The others resulted in relatively repeatable fracture toughness values.

Table 6.3: Fracture results of ABS with 1 wt% CNT and 15 mm thickness

	Sample number	1	2	3	4	5
Fracture Test Parameters	W [mm]	30.09	30.17	30.32	30.14	30.12
	a [mm]	14.22	14.39	14.72	14.94	14.44
	B [mm]	15.2	15.2	14.9	14.8	15.2
	P_{max} [N]	869.2	901.4	818.8	530.4	880.2
	P_Q [N]	824.3	850.4	766.6	530.4	799.0
	Crack growth	Stable	Stable	Stable	Unstable	Stable
	K_{Ic} [MPa$\sqrt{m}$]	**2.78**	**2.90**	**2.73**	**1.97**	**2.75**
	U_Q [J]	0.7154	0.7541	0.6537	0.3637	0.7045
	U [J]	0.5009	0.5233	0.4673	0.2576	0.5037
	G_{Ic} [kJ/m^2]	**2.5814**	**2.8115**	**2.4886**	**1.2919**	**2.5222**
	G_Q [kJ/m^2]	**5.3572**	**5.6040**	**5.1207**	**2.8887**	**5.4149**
Validity Checks	P_{max}/P_Q	1.05	1.06	1.07	1.00	1.10
	$2.5(K_Q/\sigma_y)^2$	19.95	21.72	19.23	9.98	19.49
	$E/(1-\nu^2)$ via C [MPa]	1826.0	1873.2	1800.0	1423.2	1754.5
	$E/(1-\nu^2)$ via K_Q^2/G_{Ic} [MPa]	2997.2	2997.2	2997.2	2997.2	2997.2

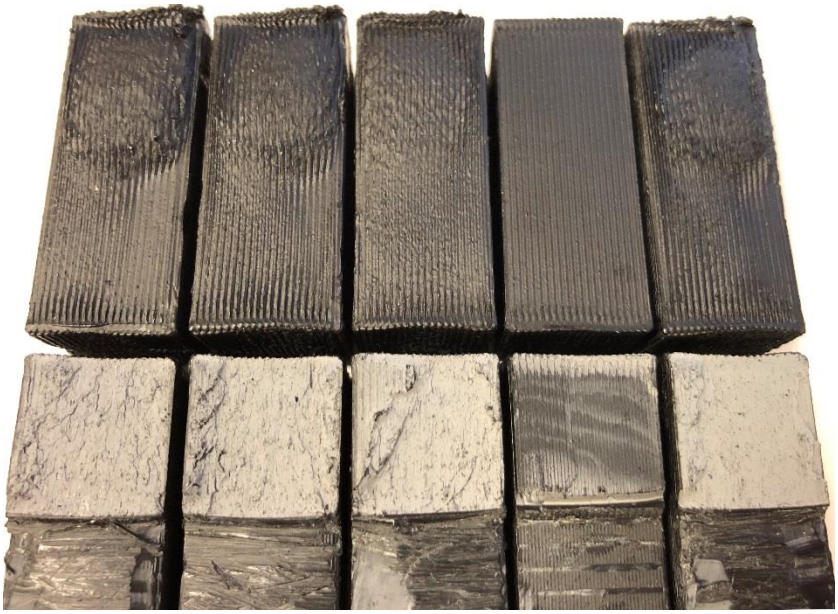

Figure 6.6: Fracture- and top-surfaces of ABS samples with 1 wt% CNT and 15 mm thickness

It is clearly visible in Figure 6.6 that the fracture and top surface of the printed sample 4 is different from the others. The top surface is flat and the printing lines on the fracture surface are well visible with minimal crazing. When examining the fracture surfaces of the other samples, it is almost not possible to see the individual printing lines, indicating that the fusion of the beads during the FFF process was very good. It almost looks like a surface of fractured bulk material. However, the geometry of the sample is quite far off the CAD model. Although the fracture toughness can be increased with over-extrusion (higher flow rates), the geometrical tolerances are likely exceeded. The bumps which are visible on the top surface of the samples are located above the notch and the holes for the loading pins. At these locations, the extrudate had more space and was not contained from the neighboring beads as mush. Therefore, this was the place where the over-extruded material built up. The printing layer after the hole which would be consistent again (continuous printing lines), was not, because material was already there. If the nozzle moves over this section, it still extrudes material which doesn't have space and it gets squished to the sides

(not continuous printing lines). Because the printer extrudes a consistent amount of polymer, this bump does not disappear on higher layers unless the filament diameter would decrease.

ABS with 0 wt% CNT, *B*=10

Pure ABS samples with a thickness of 10 mm were produced again and a sharper cutter blade was used to initiate a natural crack by inserting a fresh cutter blade and tapping. This pre-crack condition was then also used for all the thin nanocomposite samples. For sample 1 and 2, the actual filament diameter was too small and not enough material was extruded to achieve a good layer adhesion.

Table 6.4: Fracture results of pure ABS with 10 mm thickness and sharp pre-crack

	Sample number	1	2	3	4
Fracture Test Parameters	W [mm]	19.73	19.53	19.80	19.65
	a [mm]	10.40	10.63	10.43	10.50
	B [mm]	9.9	9.6	9.7	10.1
	P_{max} [N]	280.0	139.2	326.3	313.0
	P_Q [N]	274.4	139.2	300.2	297.5
	Crack growth	Unstable	Unstable	Stable	Stable
	K_{Ic} [MPa$\sqrt{m}$]	**2.08**	**1.16**	**2.31**	**2.26**
	U_Q [J]	0.1768	0.0566	0.2002	0.2211
	U [J]	0.0888	0.0257	0.0973	0.1202
	G_{Ic} [kJ/m^2]	**1.9674**	**0.6098**	**2.4386**	**2.3397**
	G_Q [kJ/m^2]	**2.3608**	**0.7303**	**2.6297**	**3.1762**
Validity Checks	P_{max}/P_Q	1.02	1.00	1.09	1.05
	$2.5(K_Q/\sigma_y)^2$	12.18	3.78	15.10	14.49
	$E/(1-\nu^2)$ via C [MPa]	2604.8	1536.3	2968.8	2272.2
	$E/(1-\nu^2)$ via K_Q^2/G_{Ic} [MPa]	2192.6	2192.6	2192.6	2192.6

The change in layer adhesion quality from sample 1 and 2 to sample 3 and 4 can be seen in Figure 6.7. The individual printing lines are visible for samples 1 and 2. The fracture surfaces

of sample 3 and 4 are much whiter and show more crazing and a plastic stable crack growth occurred. This was the reason why they achieved better fracture toughness results.

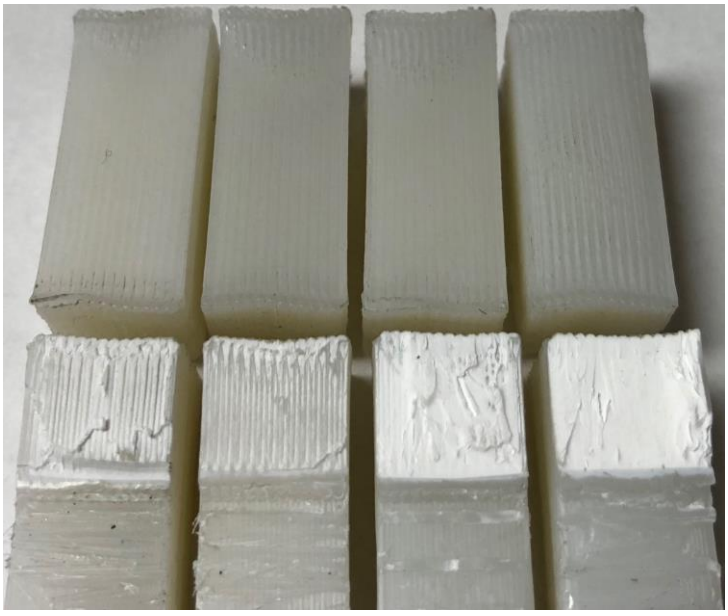

Figure 6.7: Fracture- and top-surfaces of pure ABS samples with *B*=10 mm and sharp pre-crack

ABS with 1 wt% CNT, *B*=10

Table 6.5 contains the results of the thin nanocomposite samples with 1 wt% CNT. Sample 1 and 3 were probably printed with a thinner section of the filament because their fracture toughness values are lower.

Table 6.5: Fracture results of ABS with 1 wt% CNT and 10 mm thickness

	Sample number	1	2	3	4	5
Fracture Test Parameters	W [mm]	19.85	19.85	19.95	20.20	20.35
	a [mm]	10.43	10.20	10.40	10.43	10.33
	B [mm]	9.6	9.9	9.9	10.3	10.2
	P_{max} [N]	266.0	323.9	292.0	352.9	376.9
	P_Q [N]	262.4	320.3	287.6	340.3	362.7
	Crack growth	stable	stable	unstable	stable	stable
	K_{Ic} [MPa$\sqrt{m}$]	**2.03**	**2.32**	**2.12**	**2.36**	**2.47**
	U_Q [J]	0.1686	0.2210	0.1913	0.2344	0.2516

	U [J]	0.0997	0.1228	0.1103	0.1267	0.1311
	G_{Ic} [kJ/m^2]	**1.3761**	**1.7899**	**1.5058**	**1.8633**	**2.0278**
	G_Q [kJ/m^2]	**2.7118**	**3.1924**	**2.8777**	**3.1204**	**3.2015**
Validity Checks	P_{max}/P_Q	1.01	1.01	1.02	1.04	1.04
	$2.5(K_Q/\sigma_y)^2$	10.63	13.83	11.64	14.40	15.67
	$E/(1-\nu^2)$ via C [MPa]	1686.0	1833.3	1659.9	1960.2	2104.3
	$E/(1-\nu^2)$ via K_Q^2/G_{Ic} [MPa]	2997.2	2997.2	2997.2	2997.2	2997.2

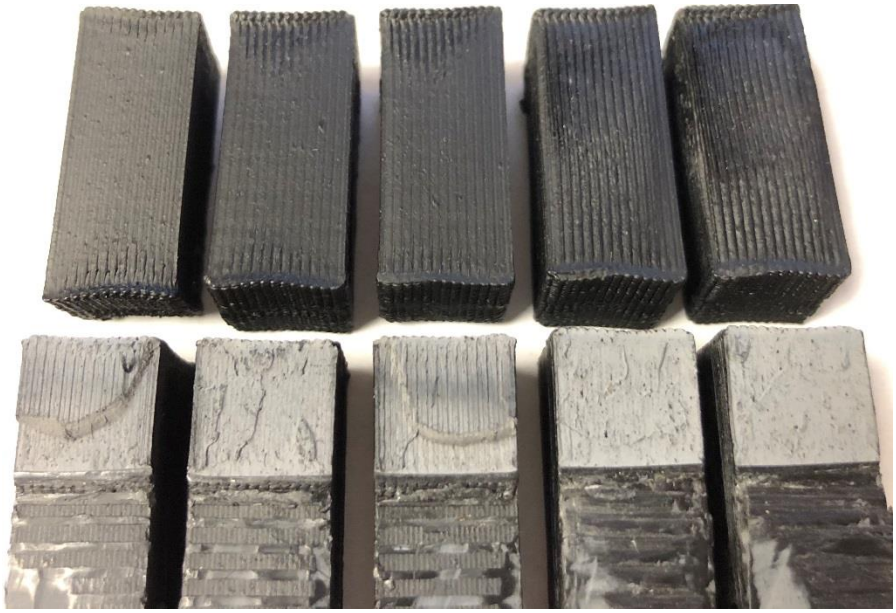

Figure 6.8: Fracture- and top-surfaces of ABS samples with 1 wt% CNT and 10 mm thickness

When examining the fracture surface of sample 1 in Figure 6.8, a stable crack growth in the beginning followed by an unstable growth is visible. Sample 3 started a partial unstable crack on the left side. Sample 4 and 5 with the most over-extrusion visible on the top layer achieved the best fracture toughness results. When looking at the strain energy release rate, the difference between sample 2, 4, and 5 are less pronounced.

ABS with 2 wt% CNT, *B*=10

The fracture tests results of ABS/2 wt% CNT samples are presented in Table 6.6. All the samples showed a stable crack growth and the K_{Ic} values are close to one another. There is more variation noticeable in the G_Q values.

Table 6.6: Fracture results of ABS with 2 wt% CNT and 10 mm thickness

	Sample number	1	2	3	4	5	6
Fracture Test Parameters	W [mm]	20.15	20.03	20.08	20.05	20.13	19.90
	a [mm]	10.28	10.23	10.25	10.40	10.38	10.40
	B [mm]	9.7	10.0	10.1	10.0	10.1	10.2
	P_{max} [N]	339.1	334.7	341.7	321.9	341.1	325.2
	P_Q [N]	338.3	327.4	336.0	318.0	327.6	312.3
	Crack growth	Stable	Stable	Stable	Stable	Stable	Stable
	K_{Ic} [MPa$\sqrt{m}$]	**2.45**	**2.31**	**2.34**	**2.30**	**2.32**	**2.25**
	U_Q [J]	0.2466	0.2094	0.2005	0.2199	0.2105	0.1796
	U [J]	0.1560	0.1235	0.1109	0.1379	0.1245	0.1000
	G_{Ic} [kJ/m^2]	**1.7256**	**1.5352**	**1.5784**	**1.5220**	**1.5467**	**1.4577**
	G_Q [kJ/m^2]	**4.0576**	**3.1369**	**2.7813**	**3.5337**	**3.1343**	**2.5428**
Validity Checks	P_{max}/P_Q	1.00	1.02	1.02	1.01	1.04	1.04
	$2.5(K_Q/\sigma_y)^2$	13.72	12.20	12.55	12.10	12.29	11.59
	$E/(1-\nu^2)$ via C [MPa]	1580.8	1860.3	2110.4	1640.4	1878.6	2087.0
	$E/(1-\nu^2)$ via K_Q^2/G_{Ic} [MPa]	3476.9	3476.9	3476.9	3476.9	3476.9	3476.9

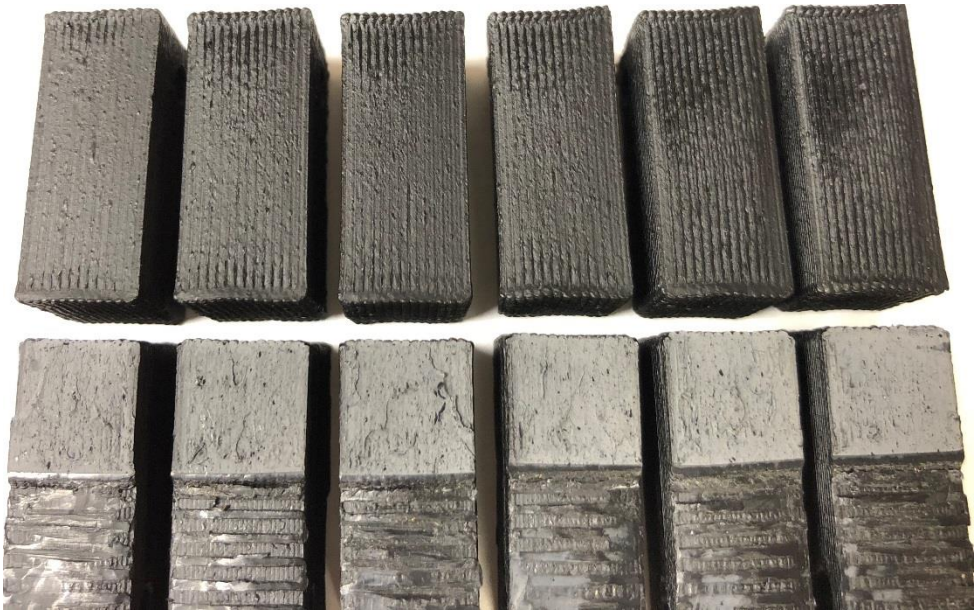

Figure 6.9: Fracture- and top-surfaces of ABS samples with 2 wt% CNT and *B*=10 mm

When comparing the fracture surfaces in Figure 6.9, no big differences can be seen. All the samples fractured plastically with stable crack growth. Although a slight difference can be seen from the extrusion flow rate effect on the top surface, it seems not to have a big effect on the fracture toughness results. Interestingly, sample 1 achieved the highest toughness values. This cannot be explained with over-extrusion. The extrusion flow rate was already on a good level with enough pressure at the nozzle leading to a proper adhesion between the layers.

ABS with 3 wt% CNT, *B*=10

Table 6.7 contains the results of the nanocomposite samples with 3 wt% CNT. Samples 1, 2, and 7 show lower fracture toughness values than the others. The reasons can be found when looking at the fracture surfaces.

Table 6.7: Fracture results of ABS with 3 wt% CNT and 10 mm thickness

	Sample number	1	2	3	4	5	6	7	8
Fracture Test Parameters	W [mm]	19.98	20.00	20.18	20.23	20.18	20.23	20.35	20.33
	a [mm]	10.35	10.15	10.08	10.23	9.95	10.18	10.33	10.33
	B [mm]	9.9	10.0	10.2	10.2	10.3	10.3	10.3	10.3
	P_{max} [N]	280.5	303.6	344.5	332.5	357.2	345.3	302.5	338.5
	P_Q [N]	280.5	302.3	343.8	332.5	350.2	342.3	302.5	338.0
	Crack growth	Unstable	Stable	Unstable	Stable	Unstable	Stable	Unstable	Stable
	K_{Ic} [MPa$\sqrt{m}$]	**2.05**	**2.11**	**2.29**	**2.25**	**2.26**	**2.28**	**2.04**	**2.28**
	U_Q [J]	0.1517	0.1717	0.2063	0.2144	0.2145	0.2110	0.1688	0.2293
	U [J]	0.0878	0.0997	0.1223	0.1335	0.1276	0.1277	0.0966	0.1478
	G_{Ic} [kJ/m^2]	**0.9322**	**0.9919**	**1.1630**	**1.1274**	**1.1377**	**1.1539**	**0.9208**	**1.1543**
	G_Q [kJ/m^2]	**2.2776**	**2.5253**	**2.9830**	**3.2714**	**3.0618**	**3.0897**	**2.3370**	**3.5790**
Validity Checks	P_{max}/P_Q	1.00	1.00	1.00	1.00	1.02	1.01	1.00	1.00
	$2.5(K_Q/\sigma_y)^2$	8.99	9.57	11.22	10.88	10.97	11.13	8.88	11.13
	$E/(1-\nu^2)$ via C [MPa]	1842.6	1881.4	2042.8	1713.3	1929.5	1937.7	1782.4	1752.0
	$E/(1-\nu^2)$ via K_Q^2/G_{Ic} [MPa]	4502.6	4502.6	4502.6	4502.6	4502.6	4502.6	4502.6	4502.6

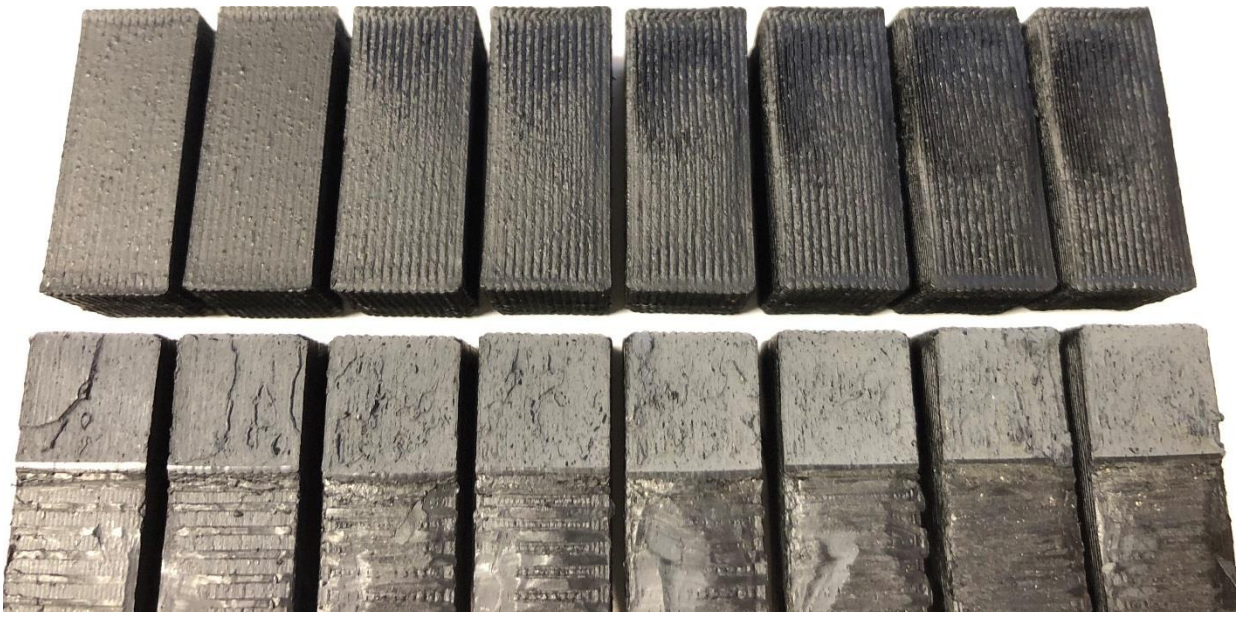

Figure 6.10: Fracture- and top-surfaces of ABS samples with 3 wt% CNT and *B*=10 mm

Figure 6.10 shows the top surface and the fracture surface of the ABS samples with 3 wt% CNT. The slightly lower K_{Ic} values for samples 1 and 2 are most likely due to the lower extrusion

flow rate visible on the top surface. Sample 7 shows a flaw on the right side, which is probably the cause for the slightly lower fracture toughness.

ABS with 5 wt% CNT, *B*=10

The fracture results of the ABS samples with 5 wt% CNT are presented in Table 6.8. These samples all showed unstable crack growth and broke suddenly. With this amount of CNT, the nanocomposite becomes quite brittle and not as tough anymore. The K_{Ic} values were all close to one another.

Table 6.8: Fracture results of ABS with 5 wt% CNT and 10 mm thickness

	Sample number	1	2	3	4	5	6
Fracture Test Parameters	W [mm]	20.15	20.43	20.33	20.30	20.35	20.40
	a [mm]	10.38	10.28	10.23	10.23	10.20	10.28
	B [mm]	10.0	10.7	10.2	10.3	10.2	10.4
	P_{max} [N]	266.9	296.7	280.4	301.6	284.5	295.2
	P_Q [N]	266.9	296.7	280.4	301.6	284.5	295.2
	Crack growth	Unstable	Unstable	Unstable	Unstable	Unstable	Unstable
	K_{Ic} [MPa$\sqrt{m}$]	**1.90**	**1.89**	**1.88**	**2.01**	**1.90**	**1.94**
	U_Q [J]	0.1242	0.1428	0.1393	0.1422	0.1457	0.1438
	U [J]	0.0613	0.0683	0.0715	0.0655	0.0762	0.0696
	G_{Ic} [kJ/m^2]	**1.1612**	**1.1468**	**1.1328**	**1.2931**	**1.1509**	**1.2090**
	G_Q [kJ/m^2]	**1.5564**	**1.5748**	**1.7391**	**1.5806**	**1.8464**	**1.6567**
Validity Checks	P_{max}/P_Q	1.00	1.00	1.00	1.00	1.00	1.00
	$2.5(K_Q/\sigma_y)^2$	6.46	6.38	6.30	7.19	6.40	6.72
	$E/(1-\nu^2)$ via C [MPa]	2119.0	2298.9	2056.3	2736.6	1607.9	2335.2
	$E/(1-\nu^2)$ via K_Q^2/G_{Ic} [MPa]	3122.5	3122.5	3122.5	3122.5	3122.5	3122.5

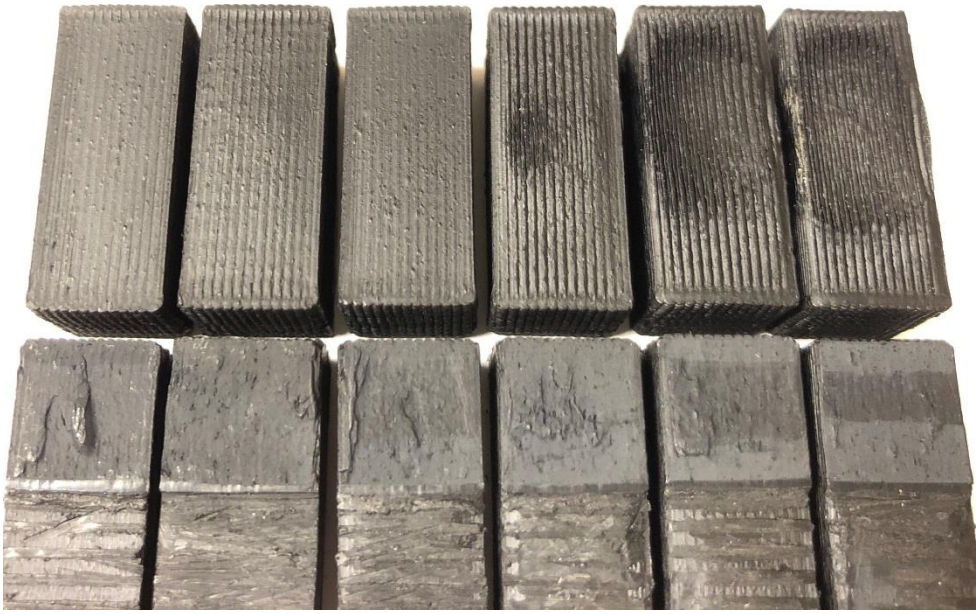

Figure 6.11: Fracture- and top-surfaces of ABS samples with 5 wt% CNT and *B*=10 mm

Figure 6.11 shows the top- and fracture- surfaces of the ABS samples with 5 wt% CNT. Although there is minimal crazing visible at the early stages of crack growth, the samples broke suddenly which is visible in the darker area in the middle of the fracture surface. Even though there was clearly some over extrusion happening for sample 4, 5, and 6, they did not show higher fracture toughness than the other three samples.

6.4. Comparison

The fracture toughness comparison of all the nanocomposites including pure ABS was done using the samples with a thickness 10 mm. Only the samples with enough extrusion flow rate and the higher fracture toughness values were used for the comparison, as they were repeatable and reliable in each nanocomposite case. The K_{Ic}, G_{Ic}, and G_Q values for all the composites are compared in Figure 6.12.

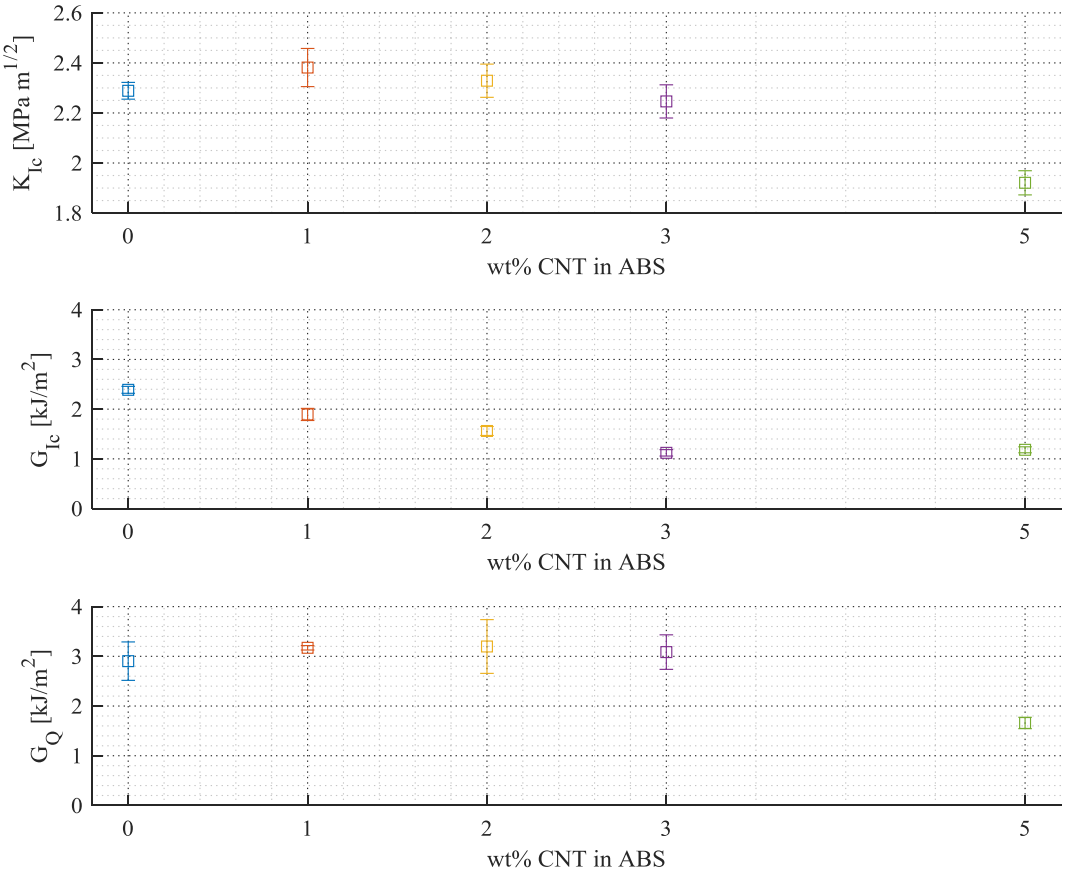

Figure 6.12: Comparison of the fracture toughness of all the samples with *B*=10

When looking at K_{Ic} and G_Q results of this graph, it is apparent that the fracture toughness does not depend much on the CNT content at concentrations up to 3 wt%. The fracture toughness increases slightly with 1 wt% CNT. After that, it very slowly decreases with increasing CNT content up to 3 wt%. Only at a CNT content of 5 wt%, the fracture toughness of the ABS/CNT nanocomposite becomes lower than that of the pure ABS. This is probably due to the increased brittleness of the nanocomposites at this CNT content. The reason could be the formation of agglomeration of CNT with higher filler content. These weakening points cause stress concentrations and lead to a lower fracture toughness.

For pure ABS, it could be observed that over-extrusion increased the fracture toughness. Starting from 2 wt% CNT, increasing the flow rate did not increase the K_{Ic} value anymore. The

extrusion flow rate only needs to be sufficiently high to have enough pressure at the nozzle tip, which enables proper adhesion between the layers and decreases the voids between the printing lines.

Comparison of pure ABS with 1 wt% CNT samples at 15 mm thickness

Only pure ABS and 1 wt% CNT samples were printed and tested at a thickness of 15 mm. In Figure 6.13, the comparison of the results is presented. As for the thin samples, the fracture toughness increases from pure ABS to ABS with 1 wt% CNT. Therefore, independent of the sample size, the fracture toughness increases as 1 wt% CNT is introduced to ABS. Some of the CNT might have served as bridges, connecting the two sides of the opening crack, improving the fracture resistance.

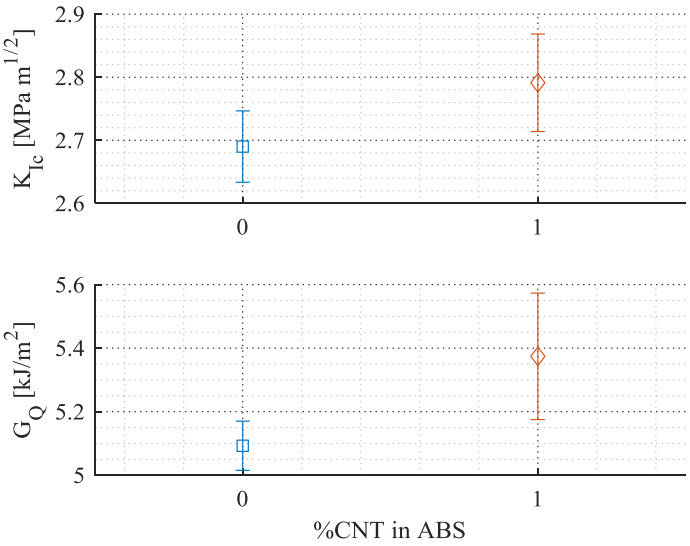

Figure 6.13: Comparison of the fracture toughness of samples with *B*=15

7. CONCLUSION

Acrylonitrile-Butadiene-Styrene (ABS) is a commonly used engineering plastic and its fused filament fabrication (FFF) is gaining importance to produce functional and complex parts. With the introduction of carbon nanotubes (CNT), ABS can be functionalized and its properties can be enhanced. Due to the capability of FFF in printing nanocomposites and multi-material structures, interesting engineering solutions can be created with this method. Research has been done about ABS/CNT nanocomposite but not as much in concern of 3D printing. In this thesis, the influences of the FFF process on various properties of ABS/CNT nanocomposite were investigated.

ABS/CNT nanocomposite filaments were produced with a twin-screw extruder. The filament was used as feedstock for a FFF 3D printer. To better understand how the material properties change during the printing process, different samples were printed. With thin plate and cuboid samples, the through-layer and in-line conductivities were measured. Dumbbell-shaped specimen were printed for uniaxial tensile tests and were also used to analyze the piezoresistive behavior. At the end, compact tension specimens were printed to analyze the fracture toughness of the nanocomposites. A particular attention was paid on the effect of CNT content on the inter-layer bonding in printed nanocomposites.

During the electrical conductivity tests of ABS/CNT, it was observed that printed samples have a higher percolation threshold, compared to the hot pressed counterparts, resulting in a conductivity of the printed samples that is at least one order of magnitude lower. Moreover, the in-layer conductivity of printed samples was almost two orders of magnitudes higher than that in the through-layer direction, at CNT concentrations up to 5 wt%. The conductivity in through-layer direction at 3 wt% CNT decreased by two orders of magnitudes when the nozzle diameter was

changed from 0.8 mm to 0.35 mm. These variations in the electrical conductivity can be explained in terms of the CNT alignment, caused by the extrusion process during printing. In further experiments, it would be interesting to analyze what the influence of the printing temperatures is and if better conductivity results can be achieved.

With the tensile tests, it was observed that up to 5 wt% CNT, the percentage increase in ultimate tensile strength is 5 times the weight percentage of the filler. The samples with 10 wt% CNT broke early and didn't reach much higher values of strength. The Young's modulus increases quite drastically until 3 wt% CNT where the increase is 100%. At 5 wt% and 10 wt% CNT contents, the stiffness is about the same as for 1 wt% CNT. As the CNT content increases, the material becomes more brittle with less plastic deformation.

To the best of the authors knowledge no papers were published about the piezoresistive behavior as well as the fracture toughness of ABS/CNT. Therefore, the results of this work are new and will help to better understand the properties and potential applications of ABS/CNT.

The piezoresistive tests have shown that the resistance of ABS/CNT nanocomposite changes when strained. Gauge factors were calculated for different CNT concentrations. The sensitivity decreases with increasing CNT content. In printed samples with low CNT concentration, it is difficult to form conductive networks, but once the networks are formed, they show a better sensitivity. These results show that the strain in this nanocomposite can simply be measured via the resistance. In addition, the start of the plastic deformation can potentially be detected. This nanocomposite is self-sensing and enables structural health monitoring.

The most important information about the mechanical properties of printed ABS/CNT nanocomposite was obtained from the fracture toughness tests and analysis. The tests showed that the interlayer bonding (adhesion between the layers) is not significantly influenced by CNT at

concentrations up to 3 wt%. There is even a small increase in the toughness observable with 1 wt% CNT. Because most of the times, 3D printed parts fail between the layers, the inter-layer fracture toughness is the most important criterion for the structural integrity of FFF printed parts. The stiffness and strength of printed ABS can be increased by adding CNT without a decrease in the fracture toughness at low CNT concentrations. In further experiments, printing parameters can be changed to assess what the influences of layer orientation, line width, nozzle size, printing temperature and speed, or infill pattern are.

The key to achieve good properties in all categories is a good CNT dispersion. Further research would be necessary to evaluate optimal processing parameters for the melt mixing process with a twin-screw extruder to produce quality filament with a masterbatch as feedstock. Even after secondary extrusion, there were still phases of masterbatch visible in the fracture surfaces of the tensile test specimen. The most promising CNT concentration is around 3 percent, where the electrical conductivity is on a good value, especially for printed parts, piezoresistive measurements are possible and the mechanical properties have a decent increase without decrease in fracture toughness. At higher CNT concentrations, the material becomes brittle with low fracture resistance and low strain measuring sensitivity. With lower CNT content, even though the mechanical properties are better, the nanocomposite is not conductive enough.

REFERENCES

[1] J. N. Coleman, U. Khan, W. J. Blau and Y. K. Gun'ko, "Small but strong: A review of the mechanical properties of carbon nanotube–polymer composites," *Elsevier-Carbon 44,* pp. 1625-1652, 23 February 2006.

[2] M. M. Shokrieh und R. Rafiee, «A REVIEW OF THE MECHANICAL PROPERTIES OF ISOLATED CARBON NANOTUBES AND CARBON NANOTUBE COMPOSITES,» *Mechanics of Composite Materials,* 2010.

[3] K. Rupesh und B. Suryasarathi, «Carbon Nanotube Based Composites- A Review,» *Journal of Minerals & Materials Characterization & Engineering,* pp. 31-46, 2005.

[4] "Wikipedia," [Online]. Available: https://en.wikipedia.org/wiki/Acrylonitrile_butadiene_styrene. [Accessed 09 04 2018].

[5] M. H. Al-Saleh, B. A. Al-Saidi und R. M. Al-Zoubi, «Experimental and theoretical analysis of the mechanical and thermal properties of carbon nanotube/acrylonitrile-styrene-buradiene nanocomposites,» *Elsevier-Polymer 89,* pp. 12-17, 27 January 2016.

[6] B. E. Tiganis, L. S. Burn, P. Davis und A. J. Hill, «Thermal degradation of acrylonitrile–butadiene–styrene (ABS) blends,» *Elsevier, Polymer Degradation and Stability 76,* pp. 425-434, 27 January 2002.

[7] T. Villmow, P. Pötschke, S. Pegel, L. Häussler und B. Kretzschmar, «Influence of twin-screw extrusion conditions on the dispersion of multi-walled carbon nanotubes in a poly(lactic acid) matrix,» *Elsevier, Polymer 49,* pp. 3500-3509, 13 June 2008.

[8] S. Kapoor, G. Meenakshi und J. Prashant, «Effect of Multi-Walled Carbon Nanotubes (MWCNT) on Mechanical Properties of Acrylonitrile Butadiene Styrene (ABS) Nano-Composite,» *Indian Journal of Science and Technology,* May 2017.

[9] M. H. Al-Saleh, H. K. Al-Anid und Y. A. Hussain, «CNT/ABS nanocomposites by solution processing: Proper dispersion and selective localization for low percolation threshold,» *Elsevier-Composites: Part A,* pp. 53-59, 7 November 2013.

[10] P. Jindal, J. Jyoti und N. Kumar, «Mechanical characterisation of ABS/MWCNT composites under static and dynamic loading conditions,» *Journal of Mechanical Engineering and Sciences (JMES),* pp. 2288-2299, December 2016.

[11] A. Dorigato, V. Moretti, S. Dul, S. Unterberger und A. Pegoretti, «Electrically conductive nanocomposites for fused deposition modelling,» *Elsevier-Synthetic Metals*, pp. 7-14, 1 February 2017.

[12] J. Jyoti, B. P. Singh, S. Rajput, V. N. Singh und S. R. Dhakate, «Detailed dynamic rheological studies of multiwall carbon nanotube-reinforced acrylonitrile butadiene styrene composite,» Springer Science+Business Media, New York, 2015.

[13] D. Mari und R. Schaller, «Mechanical spectroscopy in carbon nanotube reinforced ABS,» *Elsevier, Materials Science and Engineering A*, pp. 255-258, 22 September 2008.

[14] N. K. Shrivastava, S. Suin, S. Maiti und B. B. Khatua, «An approach to reduce the percolation threshold of MWCNT in ABS/MWCNT nanocomposites through selective distribution of CNT in ABS matrix,» *Royal Society of Chemistry,* 23 April 2014.

[15] B. Brenken, E. Barocio, A. Favaloro, V. Kunc und R. B. Pipes, «Fused filament fabrication of fiber-reinforced polymers: A review,» *Elsevier, Additive Manufacturing,* pp. 1-16, 02 February 2018.

[16] "Kul3D," 25 August 2014. [Online]. Available: http://www.kul3d.com/what-is-fdm-3d-printing/. [Accessed 09 April 2018].

[17] S. Dul, L. Fambri und A. Pegoretti, «Filaments Production and Fused Deposition Modelling of ABS/Carbon Nanotubes Composites,» *Nanomaterials*, 18 January 2018.

[18] D. J. Thomas, «Developing nanocomposite 3D printing filaments for enhanced integrated device fabrication,» *The International Journal of Advanced Manufacturing Technology,* 12 December 2017.

[19] D. Thomas, "Developing enhanced carbon nanotube reinforced composites for full-scale 3D printed components," *Elsevier, Reinforced Plastics,* July 2017.

[20] F. Gardea, D. Cole, B. Glaz und J. Riddick, «Strain Energy Dissipation Mechanisms in Carbon Nanotube Composites Fabricated by Additive Manufacturing,» in *Mechanics of Additive and Advanced Manufacturing, Volume 9, Proceedings of the 2017 Annual Conference on Experimental and Applied Mechanics*, Bethel, 2017.

[21] W. Zhang, A. S. Wu, J. Sun, Z. Quan, B. Gu, B. Sun, C. Cotton, D. Heider und T.-W. Chou, «Characterization of residual stress and deformation in additively manufactured ABS polymer and composite specimens,» *Elsevier, Composites Science and Technology,* pp. 102-110, 16 July 2017.

[22] F. Ning, W. Cong, Z. Hu und K. Huang, «Additive manufacturing of thermoplastic matrix composites using fused deposition modeling: A comparison of two reinforcements,» *Journal of Composite Materials*, 2017.

[23] S. Dul, L. Fambri und A. Pegoretti, «Fused deposition modelling with ABS–graphene nanocomposites,» *Elsevier, Composites: Part A*, pp. 181-191, 21 March 2016.

[24] M. H. Al-Saleh and U. Sundararaj, "Microstructure, Electrical, and Electromagnetic Interference Shielding Properties of Carbon Nanotube/Acrylonitrile–Butadiene–Styrene Nanocomposites," *Journal of Polymer Science,* 3 August 2012.

[25] M. H. Al-Saleh, H. K. Al-Anid, Y. A. Husain, H. M. El-Ghanem und S. A. Jawad, «Impedance characteristics and conductivity of CNT/ABS nanocomposites,» *J. Phys. D: Appl. Phys. 46 385305*, 5 September 2013.

[26] W.-Y. Wang, G.-H. Luo, F. Wei and J. Luo, "Electrical Conductivity and Thermal Properties of Acrylonitrile-Butadiene-Styrene Filled With Multiwall Carbon Nanotubes," *Polymer Engineering and Science 49*, pp. 2144-2149, 24 August 2009.

[27] M. H. Al-Saleh, W. H. Saadeh und U. Sundararaj, «EMI shielding effectiveness of carbon based nanostructured polymeric materials: A comparative study,» *Elsevier, Caron 60*, pp. 146-156, 10 April 2013.

[28] J. Jyoti, S. Basu, B. P. Singh und S. Dhakate, «Superior mechanical and electrical properties of multiwall carbon nanotube reinforced acrylonitrile butadiene styrene high performance composites,» *Elsevier, Composites Part B*, pp. 58-65, 20 August 2015.

[29] H. M. El Ghanem, S. A. Jawad, M. H. Al-Saleh, Y. A. Hussain und W. Salah, «Effect of dc-bias on the dielectric behavior of CNT/ABS nanocomposites,» *Elsevier, Physica B*, pp. 41-46, 14 March 2013.

[30] I.-S. Han, Y. K. Lee, H. S. Lee, H. G. Yoon und W. N. Kim, «Effects of multi-walled carbon nanotube (MWCNT) dispersion and compatibilizer on the electrical and rheological properties of polycarbonate/poly(acrylonitrile–butadiene–styrene)/MWCNT composites,» *Springer Science+Business Media, J Mater Sci*, pp. 4522-4529, 25 March 2014.

[31] S. Monemian, S. H. Jafari, H. A. Khonakdar, V. Goodarzi, U. Reuter und P. Pötschke, «MWNT-Filled PC/ABS Blends: Correlation of Morphology with Rheological and Electrical Response,» *Journal of Applied Polymer Science*, pp. 739-784, 2 April 2013.

[32] S. K. Sharma, R. P. Tandon und V. K. Sachdev, «Pre-localized MWCNT network for a low percolation threshold in MWCNT/ABS nanocomposites: experiment and theory,» *Royal Society of Chemistry,* pp. 60733-60740, 20 October 2014.

[33] L. Xie and Y. Zhu, "Tune the Phase Morphology to Design Conductive Polymer Composites: A Review," *Polymer Composites,* 15 March 2017.

[34] F. Du, J. E. Fischer und K. I. Winey, «Effect of nanotube alignment on percolation conductivity in carbon nanotube/polymer composites,» *Physical Review B 72,* 19 September 2005.

[35] E. Chang, A. Ameli, L. H. Mark and C. B. Park, "Effects of uniaxial and biaxial orientation on fiber percolation in conductive polymer composites," in *AIP Conference Proceedings, Volume 1695,* Salerno, 2015.

[36] J. C. Riddick, M. A. Haile, R. Von Wahlde, D. P. Cole, O. Bamiduro und T. E. Johnson, «Fractographic analysis of tensile failure of acrylonitrile-butadiene-styrene fabricated by fused deposition modeling,» *Elsevier, Additive Manufacturing,* 26 April 2016.

[37] P. A. Menchhofer, J. E. Johnson and J. Lindahl, "Carbon nanotube chopped fiber for enhanced properties in additive manufacturing," Oak Ridge National Laboratory, Tennessee, 2016.

[38] G. Tsiakatouras, E. Tsellou and C. Stergiou, "Comparative study on nanotubes reinforced with carbon filaments for the 3D printing of mechanical parts," *World Transactions on Engineering and Technology Education,* 2014.

[39] A. N. Khan, Q. Waheed, R. Jan, K. Yaqoob, Z. Ali und I. H. Gul, «Experimental and Theoretical Correlation of Reinforcement Trends in Acrylonitrile Butadiene Styrene/Single-Walled Carbon Nanotubes Hybrid Composites,» *Polymer Composites,* 2017.

[40] S. Zhong, H. J. Q. Lin, C. Y. T. Chor and G. Tan, "Synthesis Of A Conductive Polymer For Potential Use In Printing Prosthetic Hands Using FDM Technique," in *Proceedings of the 2nd International Conference on Progress in Additive Manufacturing,* 2016.

[41] Q. Waheed, A. N. Khan und R. Jan, «Investigating the reinforcement effect of few layer graphene and multi-walled carbon nanotubes in acrylonitrile-butadiene-styrene,» *Elsevier, Polymer,* pp. 496-503, 27 May 2016.

[42] F.-R. F. Javier, R.-R. J. Luis, C.-C. Fernando and E.-B. F. Javier, "Resonance Tracking Atomic Force Acoustic Microscopy Quantitative Modulus Mapping of Carbon Nanotubes-Reinforced Acrylonitrile–Butadiene–Styrene Polymer," *Journal of Applied Polymer Science,* 19 February 2014.

[43] J. Jyoti, A. S. Babal, S. Sharma, S. R. Dhakete und B. P. Singh, «Significant improvement in static and dynamic mechanical properties of graphene oxide–carbon nanotube acrylonitrile butadiene styrene hybrid composites,» *Springer Science+Business Media,* pp. 2520-2536, 20 November 2017.

[44] Alamusi, N. Hu, H. Fukunaga, S. Atobe, Y. Liu und J. Li, «Piezoresistive Strain Sensors Made from Carbon Nanotubes Based Polymer Nanocomposites,» *Sensors, 11,* pp. 10691-10723, 11 November 2011.

[45] N. Hu, Y. Karube, C. Yan, Z. Masuda und H. Fukunaga, «Tunneling effect in a polymer/carbon nanotube nanocomposite strain sensor,» *Elsevier, Acta Materialia 56,* pp. 2929-2936, 24 March 2008.

[46] C. Li, E. T. Thostenson und T.-W. Chou, «Sensors and actuators based on carbon nanotubes and their composites: A review,» *Elsevier, Composites Science and Technology 68,* pp. 1227-1249, 26 January 2008.

[47] F. Avilés, A. I. Olivia-Avilés and M. Cen-Puc, "Piezoresistivity, Strain, and Damage Self-Sensing of Polymer Composites Filled with Carbon Nanostructures," *Advanced Engineering Materials*, 22 March 2018.

[48] A. Gbaguidi, M. Anees, S. Namilae und D. Kim, «Dynamic piezoresistive response of hybrid nanocomposites,» in *Proceedings of Spie 10168*, Portland, 2017.

[49] E. Bilotti, R. Zhang, H. Deng, M. Baxendale und T. Peijs, «Fabrication and property prediction of conductive and strain sensing TPU/CNT nanocomposite fibres,» *Royal Society of Chemistry,* pp. 9449-9455, 10 September 2010.

[50] R. Zhang, H. Deng, R. Valenca, J. Jin, Q. Fu, E. Bilotti und T. Peijs, «Strain sensing behaviour of elastomeric composite films containing carbon nanotubes under cyclic loading,» *Elsevier, Composites Science and Technology 74,* pp. 1-5, 3 October 2012.

[51] J. R. Bautista-Quijano, P. Pötschke, H. Brünig and G. Heinrich, "Strain sensing, electrical and mechanical properties of polycarbonate/multiwall carbon nanotube monofilament fibers fabricated by melt spinning," *Elsevier, Polymer 82,* pp. 181-189, 1 December 2015.

[52] K. Kim, J. Park, J.-h. Suh, M. Kim, Y. Jeong und I. Park, «3D printing of multiaxial force sensors using carbon nanotube (CNT)/thermoplastic polyurethane (TPU) filaments,» *Elsevier, Sensors and Actuators A 263,* pp. 493-500, 15 August 2017.

[53] J. F. Christ, N. Aliheidari, A. Ameli und P. Pötschke, «3D printed highly elastic strain sensors of multiwalled carbon nanotube/thermoplastic polyurethane nanocomposites,» *Elsevier, Materials and Design 131,* pp. 394-401, 13 June 2017.

[54] C. J. Hohimer, G. Petrossian, A. Ameli, M. Changki und P. Pötschke, «Electrical conductivity and piezoresistive response of 3D printed thermoplastic polyurethane/multiwalled carbon nanotube composites,» in *Proceedings of Spie 105960J,* Denver, 2018.

[55] X. Wang, J. Li, H. Song, H. Huang und J. Gou, «Highly Stretchable and Wearable Strain Sensor Based on Printable Carbon Nanotube Layers/Polydimethylsiloxane Composites with Adjustable Sensitivity,» *ACS Applied Materials & Interfaces,* pp. 7371-7380, 12 February 2018.

[56] Y. Ni, R. Ji, K. Long, T. Bu, K. Chen und S. Zhuang, «A review of 3D-printed sensors,» *Applied Spectroscopy Reviews 52,* pp. 623-652, 26 February 2017.

[57] M. S. Prasad, C. Venkatesha and T. Jayaraju, "Experimental Methods of Determining Fracture Toughness of Fiber Reinforced Polymer Composites under Various Loading Conditions," *Journal of Minerals & Materials Characterization & Engineering, Vol. 10,* pp. 1263-1275, 2011.

[58] A. E. Oskui, N. Choupani und E. Haddadi, «Experimental investigation of acrylonitrile butadiene styrene fracture,» *Society of Plastics Engineers, Plastics Research Online,* 20 November 2013.

[59] P. C. Ma, J.-K. Kim und B. Z. Tang, «Effects of silane functionalization on the properties of carbon nanotube/epoxy nanocomposites,» *Elsevier, Composites Science and Technology 67,* pp. 2965-2972, 13 May 2007.

[60] P. Zhao, K. Wang, H. Yang, Q. Zhang, R. Du and Q. Fu, "Excellent tensile ductility in highly oriented injection-molded bars of polypropylene/carbon nanotubes composites," *Elsevier, Polymer 48,* pp. 5688-5695, 18 July 2007.

[61] L. Liu, Y. Wang, Y. Li, J. Wu, Z. Zhou and C. Jiang, "Improved fracture toughness of immiscible polypropylene/ethylene-co-vinyl acetate blends with multiwalled carbon nanotubes," *Elsevier, Polymer 50,* pp. 3072-3078, 8 May 2009.

[62] R. E. Gorga and R. E. Cohen, "Toughness enhancements in poly(methyl methacrylate) by addition of oriented multiwall carbon nanotubes," *Polymer Physics 42,* pp. 2690-2702, 15 July 2004.

[63] C. S. Grimmer und C. Dharan, «Enhancement of delamination fatigue resistance in carbon nanotube reinforced glass fiber/polymer composites,» *Elsevier, Composites Science and Technology 70,* pp. 901-908, 6 February 2010.

[64] P.-Y. B. Jar, T. Shinmura and K. Konishi, "A study of rubber particle cavitation in poly(acrylonitrile-butadiene-styrene) (ABS) using a freeze fracture technique," *Journal of Materials Science Letters, Volume 19,* pp. 73-75, January 2000.

[65] S. Ramaswamy and A. Lesser, "Microscopic damage and macroscopic yield in acrylonitrile–butadiene–styrene (ABS) resins tested under multi-axial stress states," *Elsevier, Polymer 43*, pp. 3743-3752, 11 February 2002.

[66] P.-Y. B. Jar, R. Lee, T. Shinmura und K. Konishi, «Rubber particle cavitation on toughness enhancement of SMI-modified poly(acrylonitrile-butadiene-styrene),» *Polymer Physics 37*, pp. 1739-1748, 15 July 1999.

[67] K. R. Hart and E. D. Wetzel, "Fracture behavior of additively manufactured acrylonitrile butadiene styrene (ABS) materials," *Elsevier, Engineering Fracture Mechanics 177*, pp. 1-13, 29 March 2017.

[68] J. Gardan, A. Makke and N. Recho, "A Method to Improve the Fracture Toughness Using 3D Printing by Extrusion Deposition," *Elsevier, Procedia Structural Integrity 2*, pp. 144-151, 20 June 2016.

[69] N. Aliheidari, R. Tripuraneni, A. Ameli and S. Nadimpalli, "Fracture resistance measurement of fused deposition modeling 3D printed polymers," *Elsevier, Polymer Testing 60*, pp. 94-101, 16 March 2017.

[70] D. Young, J. Kessler and M. Czabaj, "Interlayer Fracture Toughness of Additively Manufactured Unreinforced and Carbon-Fiber-Reinforced Acrylonitrile Butadiene Styrene," in *31st Annual Technical Conference of the American Society for Composites*, Williamsburg, 2016.

[71] M.-L. Lu, C.-B. Lee und F.-C. Chang, «Fracture Toughness of Acrylonitrile-Butadiene-Styrene by J-Integral Methods,» *Polymer Engineering and Science*, September 1995.

APPENDIX

Summary of used equipment

Extruder

Scientific 16 mm Benchtop Twin-Screw Extruder Type LTE16-40 from Labtech Engineering Co., Ltd., Serial No. 1506-LTE16-40

Screw configuration:

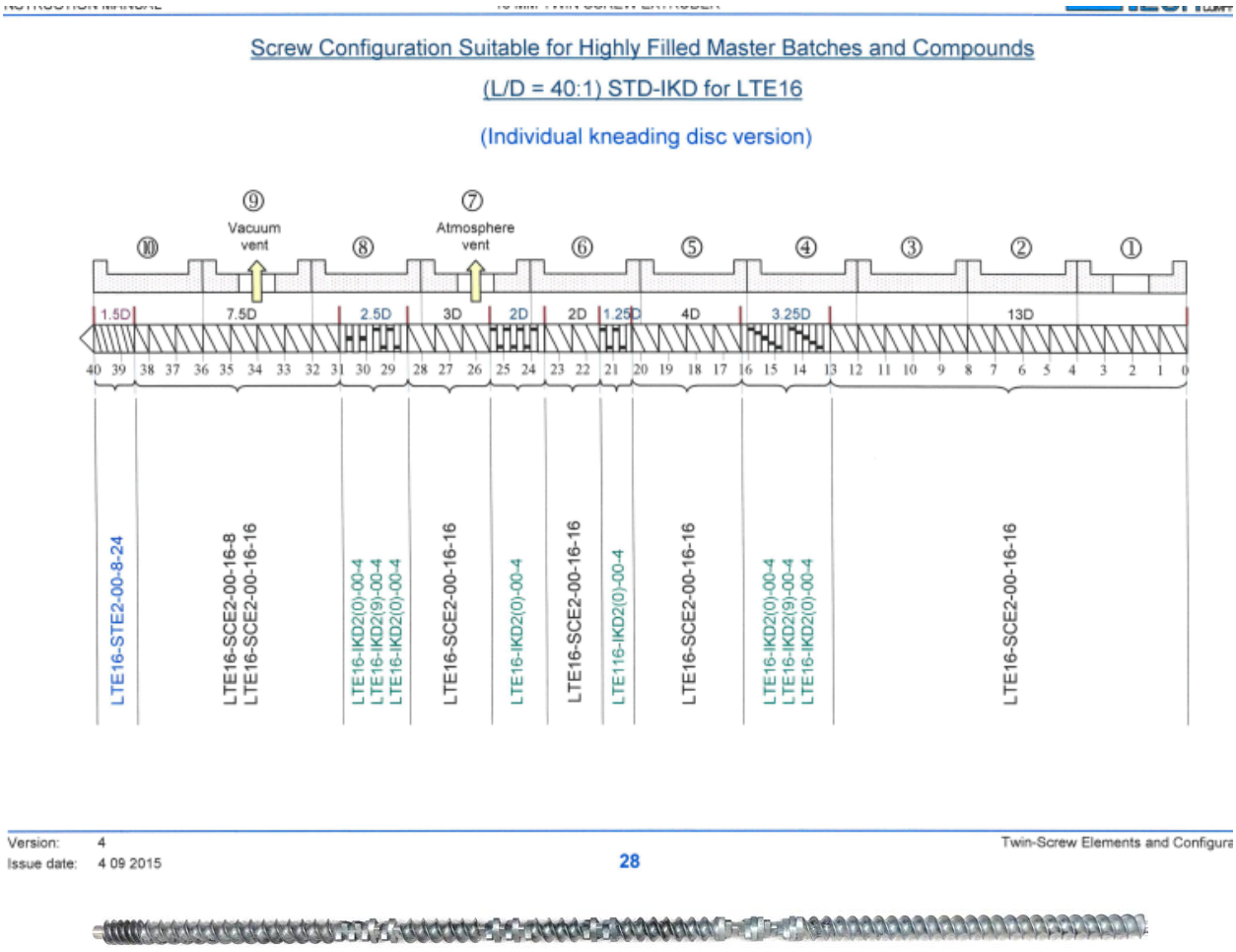

Vacuum Oven

Isotemp Vacuum Oven Model 281 from Fisher

Filament winder

Filabot Spooler from Triex LLC

3D printer

Felix Pro 1 with Pro 2 head part from FELIX printers, Serial No. 101 011.0266

with Simplify3D slicing software, Version 4.0.0

Hot press

Hotpress Model 3851-0 from Carver with hydraulic unit model 3912, Serial No. 150130

Impedance analyzer

Impedance analyzer 4192A LF (5Hz – 13MHz) from Hewlett Packard with Electrode B (∅5 mm Guarded/Guard Electrode), Serial No. 2514J04411

Load cell of tensile test machine

Load Cell Model MLP-750 with a capacity of 750 lbs from Transducer Techniques, Serial No. 239940

Displacement sensor of tensile test machine

Linear variable differential transformer (LVDT) Model 0244-000 from Trans-Tek Inc.

Data acquisition for tensile test machine

Personal Daq/55 from iQtech, Part No. 195295A-01, Serial No. 380424

Stereo Microscope

EZ4HD from Leica Microsystems

Matlab code for tensile and piezoresistivity tests

```
clear all; clc; close all;
format long;

% Load displacement data import, width, and thickness of specimen:
import{1}='CNT3_1.txt';
Width(1)=[3.34];
Thickness(1)=[1.09];

import{2}='CNT3_2.txt';
Width(2)=[3.44];
Thickness(2)=[1.11];

import{3}='CNT3_3.txt';
Width(3)=[3.39];
Thickness(3)=[1.09];

import{4}='CNT3_4.txt';
Width(4)=[3.30];
Thickness(4)=[1.10];

import{5}='CNT3_5.txt';
Width(5)=[3.32];
Thickness(5)=[1.13];

import{6}='CNT3_6.txt';
Width(6)=[3.30];
Thickness(6)=[1.10];

% resistances used for voltage divider:
R2=[30000000,30000000,20000000,30000000,10000000,30000000];

% number of specimen:
K=length(import);

for k=1:K % loop to do it for all the specimens
    clear -regexp ^Stress ^Strain ^Load ^Distance ^a ^b ^c ^n ^slope ^R1 ^Vout;
    A(k)=Width(k)*Thickness(k); % calculate crosssection area
    a=importdata(import{k});
    b=a.data(:,1);  % voltage of displacement measurement
    c=a.data(:,2);  % voltage of load measurement
    Vout=a.data(:,3);  % voltage of voltage divider
    n=length(b);    % number of data points
    Loadlb=-(37.744*c-7.0388); % calculate load [lb] out of voltage
    Loadlb1=Loadlb-min(Loadlb(1:5)); % set first load measurement to 0
    LoadN=Loadlb1*4.44822; % convert load to [N]
    Displacement=6.6119*b+30.137; % calculate displacement [mm] out of voltage
    Stress=LoadN/A(k); % [MPa]
    Vin=12.114; % Voltage of power supply
```

```
    for i=1:n % calculate strain out of displacement
        Strain(i,1)=(Displacement(i)-Displacement(1))/Displacement(1);
        R1(i,1)=(Vin/Vout(i)-1)*R2(k); % Resistance in sample [Ohm]
    end

    % modifying the plot:
    % 2nd cut:
    for i=1:n-1
        if  Stress(i)-Stress(i+1)>1 % cut off end, if difference of two follwing stress
                                    values is bigger than 1 MPa
            d=i; % d is the new number of datapoints
        break
        end
    end

    Stress1=Stress(1:d); % stress,strain,resistance, and voltage with cut-off end
    Strain1=Strain(1:d);
    R1_1=R1(1:d);
    Vout1=Vout(1:d);
    n=d; % update number of data points

    % Smoothening: mean over 5 points (2 before, 2 after)
    for i=1:n-4
        Stress1(i+2,1)=mean(Stress(i:i+4));
    end

    for i=60:n-20 % calculate the slope over 20 datapoints (10 before, 10 after)
        slope(i+10,1) = (Stress1(i+20)-Stress1(i))/(Strain1(i+20)-Strain1(i));
    end

    % 1st cut:
    for i=1:length(slope) % finds the point when the slope increases suddenly and the sample
                            is loaded
        if  slope(i)>300  % if slope exceeds 300 MPa
            e(k)=i;       % datapoint where slope exceeds 300
        break
        end
    end

    % for the plot with the cut marks:
    Strainp=Strain;
    Strainp(d+1)=Strainp(d);Strainp(e(k)-1)=Strainp(e(k));
    Stressp=Stress1;
    Stressp(1:e(k)-1)=0; % sets stress before 1st cut to 0
    Stressp(d+1:length(b))=0; % sets stress after 2nd cut to 0

%%%%%%%%%% uncomment if modification should be shown %%%%%%%%%%%%%%%%%%%%
% figure(k)
% plot(Strain,Stress,'LineWidth',1.5)
% grid on
% hold on
```

```
% plot(Strainp,Stressp); % plot with the cut marks
% hold off

    Stress2=Stress1(e(k):end); % 1st cut
    Strain2=Strain1(e(k):end); % 1st cut
    R1_2=R1_1(e(k):end);
    Vout2=Vout1(e(k):end);

    Strain2=Strain2-Strain2(1); % subtraction of the first new data point
    Stress2=Stress2-Stress2(1); % subtraction of the first new data point

    % fitting of a line to the elastic region:
    Y1=3;    % between Y1 and Y2 a line gets fitted
    Y2=15;   % the slope of this line is the Young's Modulus
    [minDistance, indexOfMin] = min(abs(Stress2-Y1));
    [minDistance2, indexOfMin2] = min(abs(Stress2-Y2));
    P = polyfit(Strain2(indexOfMin:indexOfMin2),Stress2(indexOfMin:indexOfMin2),1);
    yfit = P(1)*Strain2+P(2);
    YoungsModulus(k)=P(1); % [MPa]

%%%%%%%%%% uncomment if modification should be shown %%%%%%%%%%%%%%%%%%%%
% figure(k+100)  % graph after 1st cut and 2nd cut
% hold on
% plot(Strain2,Stress2)
% plot(Strain2,yfit,'k:');
% hold off
% ylim([0 50]);

    % 3rd cut:
    % set the zero-strain point to the intersection of the line with the zero-stress axis
    Strain3=Strain2-(-P(2)/P(1)); % subtraction of the first new data point

%%%%%%%%%% uncomment if final stress-strain plot should be shown %%%%%%%%%%
figure(k+200)  % final Stress-Strain plot
mrk={'-',':','--','-.','-',':','--','-.'};
hold all
set(gca,'LineStyleOrder',mrk(k))
plot(Strain3,Stress2)
set(gcf,'defaultlinelinewidth',1.5)
grid on
title('Stress-Strain curves of ABS/CNT samples');
xlabel('Strain [mm/mm]'); ylabel('Stress [MPa]');
legend('1','2','3','4','5','6','Location','best');

    Strain4{k}=Strain3; % modified final Strain data points
    Stress4{k}=Stress2; % modified final Stress data points

    MaxStrain(k)=max(Strain3);
    UltStress(k)=max(Stress2);

%     % Wrtie modified strain-stress data to .txt file:
%         Data=[Strain4.';Stress4.'];
```

```
%         Name = sprintf('ABSCNT_3percent_%d.txt', k);
%         fileID = fopen(Name,'w');
%         fprintf(fileID,'%11.6f %13.8f\n',Data);
%         fclose(fileID);

% Filter for resistance plot with a Savitzky-Golay filter
order = 6;
framelen = length(Strain3)*4/order;
framelen = framelen-mod(framelen,2)+3;
R1_2f = sgolayfilt(R1_2(1:end-1),order,framelen);

% absolute increase in resistance with strain:
Rincr(k)=max(R1_2f)-min(R1_2f);
Rincrs(k)=Rincr(k)/(max(Strain3)*100);

% percentual increase in resistance with strain:
Rincrp(k)=100/min(R1_2f)*max(R1_2f)-100;
Rincrsp(k)=Rincrp(k)/(max(Strain3)*100);

% Gauge factor
GF(k)=(Rincr(k)/min(R1_2f))/max(Strain3);

%%%%%%%% uncomment if piezoresistivity plot should be shown %%%%%%%%%%%%%
% hold off
% figure(k+300)  % Piezoresistivity plot
% subplot(2,1,1);
% plot(Strain3(1:end-1),Stress2(1:end-1),'LineWidth',1.5);
% ylabel('Stress [MPa]');
% grid on
% xlim([0 max(Strain3)]);
% subplot(2,1,2);
% hold on
% plot(Strain3(1:end-1),R1_2(1:end-1));
% plot(Strain3(1:end-1),R1_2f,'.-')
% grid on
% hold off
% ylabel('Resistance [\Omega]');
% xlabel('Strain [mm/mm]');
% xlim([0 max(Strain3)]);
end

mRincr=mean(Rincr(1:5)); sRincr=std(Rincr(1:5));
mRincrp=mean(Rincrp(1:5)); sRincrp=std(Rincrp(1:5));
mGF=mean(GF); sGF=std(GF);
A               % [mm^2]
MaxStrain       % [-]
UltStress       % [MPa]
YoungsModulus   % [MPa]
GF              % [-]
```

Published with MATLAB® R2016b

Matlab code for fracture tests

```
clear all; clc; close all;
format long;

% Load displacement data import, thickness, crack length, and width of specimen:
import{1}='F2_1.txt';
B(1)=9.7;a(1)=10.28;W(1)=20.15;

import{2}='F2_2.txt'
B(2)=10;a(2)=10.23;W(2)=20.03;

import{3}='F2_3.txt';
B(3)=10.1;a(3)=10.25;W(3)=20.08;

import{4}='F2_4.txt';
B(4)=10.0;a(4)=10.40;W(4)=20.05;

import{5}='F2_5.txt';
B(5)=10.1;a(5)=10.38;W(5)=20.13;

import{6}='F2_6.txt';
B(6)=10.2;a(6)=10.40;W(6)=19.90;

import{7}='F2comp_1.txt'; % compliance
B(7)=1;a(7)=1;W(7)=1;PQ(7)=100;

% number of specimen:
K=length(import);

for k=1:K % loop to do it for all the specimens
    clear -regexp ^Load ^Disp ^Distance ^data ^b ^c ^n ^slope ^R1 ^Vout ^ZDist;
    data=importdata(import{k});
    b=data.data(:,1);  % voltage of displacement measurement
    c=data.data(:,2);  % voltage of load measurement
    n=length(b);    % number of data points
    Loadlb=-(37.744*c-7.0388); % calculate load [lb] out of voltage
    Loadlb1=Loadlb-min(Loadlb(1:5)); % set first load measurement to 0
    LoadN=Loadlb1*4.44822; % convert load to [N]
    Displacement=6.6119*b+30.137; % calculate displacement [mm] out of voltage
    Disp=Displacement-Displacement(1);

    for i=1:n-10 % calculate the slope over 10 datapoints (5 before, 5 after)
        slope(i+5,1) = (LoadN(i+10)-LoadN(i))/(Disp(i+10)-Disp(i));
    end

    % modifying the plot:
    % 1st cut (sample settling):
    for i=1:length(slope) % finds the point when the slope increases suddenly and the sample
                            is loaded
```

```
        if  slope(i)>50   % if slope exceeds value
            d(k)=i;       % datapoint where slope exceeds value
        break
        end
    end

    LoadN1=LoadN(d(k):end); % 1st cut
    Disp1=Disp(d(k):end); % 1st cut

    Disp1=Disp1-Disp1(1); % subtraction of the first new data point
    LoadN1=LoadN1-LoadN1(1); % subtraction of the first new data point

    % for the plot with the cut marks:
    Dispp=Disp;
    Dispp(d(k)-1)=Dispp(d(k));
    LoadNp=LoadN;
    LoadNp(1:d(k)-1)=0; % sets load before 1st cut to 0

%%%%%%%%%%% uncomment if modification should be shown %%%%%%%%%%%%%%%%%%%%%
% figure(k)
% plot(Disp,LoadN,'-x')
% grid on
% hold on
% plot(Dispp,LoadNp,'LineWidth',1.5); % plot with the cut marks
% hold off

    % fitting of a line to the elastic region:
    Y1=0.4;    % between the displacement Y1 and Y2 a line gets fitted
    Y2=1.2;
    [minDistance, indexOfMin] = min(abs(Disp1-Y1));
    [minDistance2, indexOfMin2] = min(abs(Disp1-Y2));
    P = polyfit(Disp1(indexOfMin:indexOfMin2),LoadN1(indexOfMin:indexOfMin2),1);
    yfit = P(1)*Disp1+P(2);
    CQ(k)=1/P(1);  % Compliance [mm/N]
    C2(k)=CQ(k)*1.05;  % 5% greater compliance
    yfit2 = (1/C2(k))*Disp1+P(2);

%%%%%%%%%%% uncomment if fitted lines should be shown %%%%%%%%%%%%%%%%%%%%%
% figure(k+100)  % graph after 1st cut
% hold on
% plot(Disp1,LoadN1)
% grid on
% plot(Disp1,yfit,'k:');
% plot(Disp1,yfit2,'r-.');
% hold off
% xlim([0 2]);

    Pmax(k)=max(LoadN1);
    PQ(1)=338.3;
    PQ(2)=327.4;
    PQ(3)=336.0;
    PQ(4)=318.0;
```

```
    PQ(5)=327.6;
    PQ(6)=312.3;

    PP(k)=(Pmax(k)/PQ(k));
    x(k)=a(k)/W(k);
    fx(k)=((2+x(k))*(0.886+4.64*x(k)-13.32*x(k)^2+14.72*x(k)^3-5.6*x(k)^4))/((1-
x(k))^(3/2));
    KQ(k)=((PQ(k)/(B(k)*W(k)^(1/2)))*fx(k))/sqrt(1000);  % [MPa.m^1/2]
    valid(k)=(2.5*(KQ(k)/33.07)^2)*1000; %[mm],this value must be smaller than B,a,and (W-a)

% figure(k+200)  % final Stress-Strain plot
    mrk={'-',':','--','-.','-',':','--','-.','-'};
    hold all
    set(gca,'LineStyleOrder',mrk(k))
    plot(Disp1,LoadN1)
    set(gca, 'FontName', 'times new roman')
    set(gca, 'FontSize', 10);
    set(gcf,'defaultlinelinewidth',1.5)
    grid on
    title('Load-displacement curves of 2 wt% CNT samples');
    xlabel('Displacement [mm]'); ylabel('Load [N]');
    legend('1','2','3','4','5','6','Compliance','Location','best');

    E=3051; % [MPa]
    nu=0.35;

    % find the data point closest to PQ on the load displacement curve
    for i=1:length(LoadN1)-1
        slope2(i+1,1) = (LoadN1(i+1)-LoadN1(i))/(Disp1(i+1)-Disp1(i));
        if slope2(i)>0 % PQ is either on the rising side of the load curve or at the top
        ZDistPQ(i)=abs(LoadN1(i)-PQ(k));
        else
            ZDistPQ(i)=1000;
        end
    end
    [minDistPQ(k), indexOfMinPQ(k)] = min(ZDistPQ);

    % integration of the load versus load-point displacement curve
    UQ_(k)=trapz(Disp1(1:indexOfMinPQ(k)),LoadN1(1:indexOfMinPQ(k)))/1000; % [Nm][J]
    UQ(k)=UQ_(k)+(((PQ(k)-
LoadN1(indexOfMinPQ(k)))*CQ(k))*abs(PQ(k)+LoadN1(indexOfMinPQ(k)))/2)/1000 ; %correction
    % correction if data points are too far away from one another

end

for k=1:K

    Ci=CQ(K); % last sample K=7 is compliance sample
    [minDistP(k), indexOfMinP(k)] = min(abs(LoadN1-PQ(k)));
    Ui_(k) = (trapz(Disp1(1:indexOfMinP(k)),LoadN1(1:indexOfMinP(k))))/1000; % [Nm][J]
    Ui(k)=Ui_(k)+(((PQ(k)-
LoadN1(indexOfMinP(k)))*Ci)*abs(PQ(k)+LoadN1(indexOfMinP(k)))/2)/1000 ; %correction
```

```
    U(k)=UQ(k)-Ui(k); % [Nm][J]

    GIC(k)=(1-nu^2)*KQ(k)^2/E*1000; % [kJ/m^2]

    phi(k)=((1.9118+19.118*x(k)-2.5122*x(k)^2-23.226*x(k)^3+20.54*x(k)^4)*(1-
x(k)))/((19.118-5.0244*x(k)-69.678*x(k)^2+82.16*x(k)^3)*(1-x(k))+2*(1.9118+19.118*x(k)-
2.5122*x(k)^2-23.226*x(k)^3+20.54*x(k)^4));
    GQ(k)=U(k)/(B(k)*W(k)*phi(k))*1000; % [kJ/m^2]

    Cc(k)=CQ(k)-Ci;  % [mm/N]
    valid2_bigger(k)=2*fx(k)^2*phi(k)/(B(k)*Cc(k));
    valid2_smaller(k)=KQ(k)^2/GIC(k)*1000;

end

Pmax           % [N]
x              % [-]
KQ             % [MPa.m^1/2]
valid          % [mm]
PP             % [-]
UQ             % [J]
U              % [J]
GIC            % [kJ/m^2]
phi            % [-]
GQ             % [kJ/m^2]
Cc             % [mm/N]
valid2_bigger  % [MPa]
valid2_smaller % [MPa]

    % gather all the values in one matrix:

Data=[W',a',B',Pmax',PQ',PQ',KQ',UQ',U',GIC',GQ',PP',valid',valid2_bigger',valid2_smaller']'
```

Published with MATLAB® R2016b